

# Neuroactive drug discovery in the larval zebrafish

Jessica Sabrina Burgstaller



Dissertation

at the Graduate School of Systemic Neurosciences

Ludwig-Maximilians-Universität München

May, 2019





Supervisor: Prof. Dr. Herwig Baier  
Max-Plank-Institute Neurobiology  
Department: Genes-Circuits-Behavior

First Reviewer: Prof. Dr. Herwig Baier  
Max-Plank-Institute Neurobiology

Second Reviewer: Dr. Jason Rihel  
University College London

External Reviewer: Prof. Dr. Geoffrey Goodhill  
Queensland Brain Institute

Date of Submission: May 3<sup>rd</sup>, 2019  
Date of Defense: September 2<sup>nd</sup>, 2019



*To Dorit Helene Burgstaller & Josef Paul Marschall*



## Summary

There is still an unmet need for the discovery and development of neuroactive drugs to treat psychiatric illness. The list of compounds used for treatment today is long, yet the often times reported lack of efficacy and the broad spectrum of unpleasant side effects are concerning. With my work presented in this thesis I aim to explore new routes of drug discovery using the zebrafish model system as valuable tool to bridge the gap between bench and bedside.

In the first and second study I exploit the transparency of zebrafish to test the utility of synthetic photochemical compounds to modify behavior in a targeted fashion. Small molecules that can be activated and inactivated by light are attractive targets for drug development since they offer spatiotemporal control and their dose can potentially be calibrated instantly and interactively during treatment. I explored remote optical control of neuronal activity and behavior and implemented a rapid behavioral assay that is designed to provide a readout of neurotropic effects in zebrafish larvae (Barber et al., 2016; Trads et al., 2017).

In the third project I studied the  $gr^{s357}$  zebrafish mutant as a tool for drug discovery. Dysregulation of the hypothalamic-pituitary-adrenal (HPA) axis is highly correlated with depression and is thought to contribute to the etiology and progression of the disease. The  $gr^{s357}$  zebrafish mutant has a missense mutation that abolishes glucocorticoid receptor transcriptional activity and results in a chronically elevated stress axis together with behavioral endophenotypes of depression. This mutant therefore provides an entry point for research into the pathogenesis of depression and for the development of potential drug treatments. To examine how known antidepressant compounds affect brain activity of larval zebrafish, I employed brain-wide, cellular-resolution light-sheet microscopy. With a graph-theoretical approach, I extracted network parameters of neuronal activity in both wildtype and  $gr^{s357}$  mutant fish, following treatment with fluoxetine, ketamine and cycloserine.

Consistent with broad expression of the glucocorticoid receptor throughout the brain, I showed that the mutant fish exhibit an altered correlational structure of resting-state brain activity. Antidepressants differentially affected particular metrics of

functional connectivity. Intriguingly, in *gr<sup>s357</sup>* mutant fish, an increased ‘modularity’, which represents the degree of segregation of the network into highly clustered modules, with fewer functional connections among them, was restored by fluoxetine to wildtype levels. With this project I showed that light-sheet imaging of zebrafish brain activity combined with graph-theoretical analysis of functional connectivity provides a content-rich and scalable approach for studying the neural consequences of drug x genotype interactions (Burgstaller et al., 2019).

In summary, the work presented here took advantage of cutting edge methods like photopharmacology and cellular-resolution light-sheet microscopy for drug discovery in the larval zebrafish. Importantly, apart from the biological findings, these methods can be applied to study various compounds and animal models of psychiatric disorders.



## Contents

1. Introduction	
1.1 Zebrafish as model organism.....	2
1.1.1 Stress and depression.....	3
1.1.2 Zebrafish and stress-related diseases.....	5
1.1.3 GIRK channels and their role in depression research.....	7
1.2 Methods for drug research in the zebrafish .....	10
1.2.1 Remote optical control of behavior with a photoswitchable neuroactive compound .....	10
1.2.2 Light-sheet microscopy .....	12
1.2.3 Graph-theoretical analysis of whole-brain functional connectivity .....	15
1.3 Aims of the thesis .....	18
2. Publications	
2.1 Optical control of neuronal activity using a light-operated GIRK channel opener (LOGO).....	21
2.2 Optical control of GIRK channels using visible light.....	36
2.3 Light-sheet imaging and graph analysis of antidepressant action in the larval zebrafish brain network .....	43
3. Discussion and outlook	
3.1 Photoswitchable neuroactive compounds in drug discovery.....	73
3.2 Emerging roles of light-sheet microscopy combined with graph-theoretical analysis in health and disease .....	75
3.3 Outlook .....	80
4. References	
5. Appendix	
Acknowledgements .....	94
Curriculum vitae .....	95
List of publications .....	96
Affidavit.....	97
Author contributions.....	98



### List of figures

Figure 1: HPA-axis

Figure 2: Hyperactivated HPA-axis in *gr<sup>s357</sup>* zebrafish mutants

Figure 3: Schematic of the custom-built light-sheet microscope

Figure 4: Light-sheet microscope and sample preparation

Figure 5: Network properties

Figure 6: Behavioral assay to test photoswitchable properties of the GIRK channel  
agonist LOGO

# 1 Introduction

## 1.1 Zebrafish as model organism

The zebrafish (*Danio rerio*) is an Indian freshwater teleost first introduced to laboratory research by Georg Streisinger (Streisinger et al., 1981). Due to the development of genetic and molecular techniques, the establishment of genetic mutant models of disease and advances in high-resolution functional imaging *in vivo* and pharmacological manipulation of neuronal activity, zebrafish have emerged as a promising vertebrate model to study the cellular network architecture in healthy and diseased brains.

Considering zebrafish for neuroscience research in the light of these advances, we should take into account the size of the brain and the number of neurons it contains. Ideally, the brain of a well-suited model organism should be functionally complex and conform to the basic organization of a vertebrate brain, yet it should comprise a small number of neurons. The zebrafish brain contains approximately 100.000 neurons (Naumann et al., 2010) with an average brain size of 300µm x 400µm x 800µm. Thus, compared to a human brain with its  $10^{11}$  neurons, the fish brain offers many advantages in order to study the functional connectivity in the whole-brain. Sophisticated imaging and light-induced manipulation in an intact, behaving animal is possible in larval zebrafish as they are transparent during early development (Ahrens et al., 2013; Kubo et al., 2014). Furthermore, with their rich behavioral repertoire (Burgess, Schoch, & Granato, 2010; Easter, Jr. & Nicola, 1996; Kubo et al., 2014, Orger, Smear, Anstis, & Baier, 2000), it is possible to identify mutant phenotypes and to investigate the underlying network properties of functional connectivity in the brain with cellular resolution.

### 1.1.1 Stress and depression

With 350 million people affected worldwide (Marcus et al., 2015), depression is listed as fourth leading cause of disease burden by the World Health Organisation (Ansorge et al., 2007; Ustun, 2004). It is a debilitating disorder of the central nervous system that causes severe social and economic impact to the patient and society (Simon, 2003). Affected individuals often experience persistent low mood, sadness, guilt, irritability, worthlessness and self-loathing as well as anhedonia, fatigue, weight changes, sleep abnormalities, attention deficits, and suicidal thoughts.

The broad spectrum of symptoms and the attempt to elucidate the etiology of depression led to a variety of theories concerning the causes of depression. The two major neurobiological theories are: a) the monoamine theory and b) the hypothalamus – anterior pituitary – adrenal medulla (HPA) axis theory. In the first theory, impaired signal transduction is attributed to an imbalance of monoamines (Urani et al., 2005). This hypothesis spurred the development of a plethora of antidepressants, like selective serotonin reuptake inhibitors (SSRIs), to increase and stabilise monoaminergic signalling (Ansorge et al., 2007). These drugs however, are slow in onset (several weeks) and often patients do not respond to them at all (Artigas, 2001). Because major depression is often associated with a hyperactivated neurobiological stress response and corresponding endocrine parameters (Holsboer, 2000; Pariante & Lightman, 2008), the second theory focuses on the HPA axis (Fig. 1).

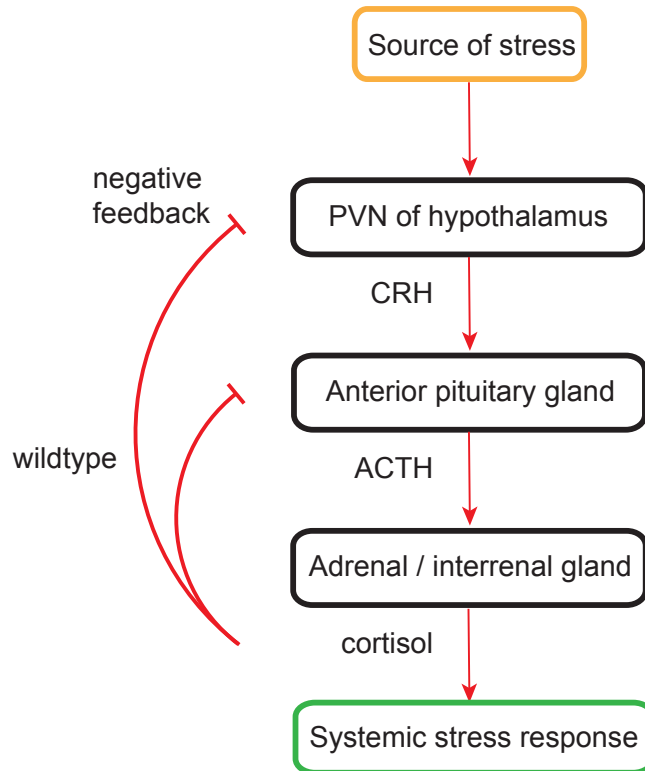


**Figure 1. HPA-axis.** The so-called ‘stress response’ is mediated by the HPA-axis. Increased synthesis and release of corticotropin-releasing hormone (CRH) in the hypothalamus promotes the release of adrenocorticotrophic hormone (encoded by the *pomc* gene) from the pituitary gland into the circulation. Adrenocorticotrophic hormone stimulates the production of glucocorticoids in the adrenal gland, whose fish homolog is named interrenal organ. In teleost fish and humans, the major glucocorticoid hormone is cortisol.

In response to stress, the paraventricular nucleus of the hypothalamus releases corticotropin releasing hormone (CRH), which in turn stimulates the anterior pituitary gland to secrete adrenocorticotrophic hormone (ACTH). This leads to a release of cortisol/corticosterone from the adrenal gland in humans (corresponding to the interrenal gland in teleosts). As part of a negative feedback loop, cortisol binds to the glucocorticoid receptor (GR) in the hypothalamus and anterior pituitary in order to terminate the stress response (Jeanneteau et al., 2012). When individuals are chronically exposed to stress, these receptors become desensitised and downregulated, which ultimately leads to disrupted negative feedback loops and a disinhibition of the HPA axis. As a result, the levels of cortisol, CRH and ACTH are increased together with the production of neurotoxic free radicals and a decrease in brain derived

neurotrophic factor. Neurobiological consequences may include atrophy of apical dendrites, granular cell death in the hippocampus, release of pro-inflammatory cytokines from macrophages and microglia, serotonergic dysregulation and an increase in monoamine oxidase-A (Meloni et al., 2008; Willner et al., 2013). Together with symptoms of memory problems and a disrupted immune system (Belmaker & Agam, 2008), depression is considered a heterogeneous disorder and our understanding of its etiology and neuropathology remains incomplete (Berton et al., 2012). There is an unmet need for effective treatment, but the development of successful therapeutics is extremely difficult.

### 1.1.2 Zebrafish and stress-related diseases

The aim to investigate the link between depression and an elevated HPA axis has led to the development of genetic animal models as vital instrument to dissect disease etiology and as a platform for therapeutic innovation. However, attempts to abolish glucocorticoid activity in mice turned out to be challenging because GR is expressed in lungs and disruption is lethal in 90% of new-borns due to respiratory failure. Methods like conventional knock-out of one allele, overexpression of antisense GR mRNA, central nervous system-specific knockouts, disrupted GR dimerization or GR overexpression gave rise to several heterozygous mouse models. Their behavioral phenotype however only becomes apparent when mice are exposed to stress, where it significantly differs compared to behaviors observed in control animals (Urani et al., 2005).

Zebrafish (*Danio rerio*) are small vertebrate teleosts with a high reproductive rate, fast embryonic development as well as a complex set of behaviors (Burgess, Schoch, & Granato, 2010; Easter, Jr. & Nicola, 1996; Kubo et al., 2014; Orger, Smear, Anstis, & Baier, 2000). Homologies to higher vertebrates, such as humans, in key genetic, physiological, and behavioral features (Griffiths et al., 2012; Randlett et al., 2015) have rendered them extremely useful as a model organism in neurobiology. Our lab identified an adult viable homozygous GR mutant *gr*<sup>s357</sup> in a genetic screen (Muto et al., 2005) with a single basepair change that disrupts transcriptional activity of the receptor. In these mutants, the HPA axis is chronically elevated due to a disrupted

negative feedback loop (Fig. 2). The receptor can still bind cortisol and translocate to the nucleus, but downstream regulation of target genes is impeded (Ziv et al., 2013).

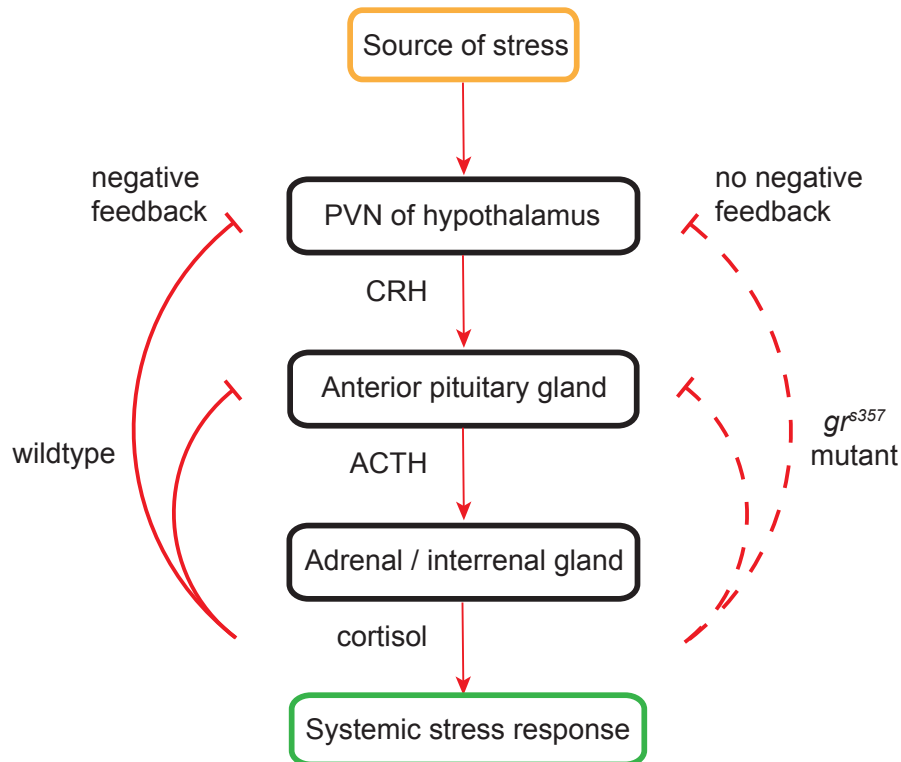


**Figure 2. Hyperactivated HPA-axis in *gr<sup>s357</sup>* zebrafish mutants.** The *gr<sup>s357</sup>* zebrafish mutant harbors a missense mutation that abolishes glucocorticoid receptor transcriptional activity and negative feedback on the stress response, which results in a chronically elevated stress axis together with endophenotypes of depression.

Morphologically the larval mutants cannot be distinguished from their heterozygous siblings, except for their inability to perform visual background adaptation (VBA) (Muto et al., 2005). This means that in response to a bright background the mutants are not able to contract their melanophores to hide from potential predators (Neuhauss et al., 1999). For experimental procedures, this is useful in the sense that mutants can be identified by color at the larval stage and no genetic sequence analysis needs to be performed. Homozygous GR mutation becomes apparent in the adult by elevated levels of CRH, ACTH and cortisol. Additionally, a blunted suppression of cortisol after application of the synthetic GR agonist dexamethasone has been described as well as less exploratory behavior, increased

periods of immobility, reduced tank wall preference (thigmotaxis) and lack of habituation when placed in an unfamiliar environment, like a novel tank (Ziv et al., 2013). In larval *gr<sup>s357</sup>* mutants, spontaneous locomotion over a period of 24 hours is reduced, but the startle response to unknown auditory stimuli is increased (Griffiths et al., 2012).

Heterozygous larvae display an intact VBA (Griffiths et al., 2012) and their cortisol level as adults is only marginally higher compared to wildtype fish (Ziv et al., 2013). The endocrine stress level in both, larval and adult fish could be normalized after treatment with the antidepressant SSRI fluoxetine. Cause and effect in the association of antidepressants and the HPA axis have not been fully disentangled. Changes in behavior of treated fish were evident almost immediately. But CRH, ACTH and cortisol levels were only reduced after continuous treatment for 2 weeks (Griffiths et al., 2012). A slow time course of drug action can also be observed in human patients, but the fast effect on fish behavior may be due to some other, yet unknown mechanism. Griffiths et al. (2012) suggest other targets of the SSRIs, for instance the serotonergic population of neurons in the raphe nucleus. With functional whole-brain imaging, I hope to gain further insight into the mechanism of antidepressant drug action.

### 1.1.3 GIRK channels and their role in depression research

For neurons to function normally, a well-balanced interplay between excitatory and inhibitory signals is necessary (Trevelyan & Watkinson, 2005). Ionotropic glutamate receptors like NMDARs (*N*-methyl-d-aspartate receptors) and AMPARs ( $\alpha$ -amino-3-hydroxy-5-methyl-4-isoxazole propionic acid receptors) are typically located in the postsynaptic density of dendritic spines and play a role in excitatory signal transmission. Ionotropic GABA ( $\gamma$ -aminobutyric acid type A) and glycine receptors that are located on the soma and dendritic shafts mediate fast inhibitory signals (Trevelyan & Watkinson, 2005). G protein-coupled inwardly rectifying potassium ( $K^+$ ) channels (GIRK) are expressed perisynaptically outside the postsynaptic density in the spine and on the shaft (Lujan et al., 2009), where they balance excitatory and inhibitory signals by mediating slow inhibitory postsynaptic currents (sIPSC).

GIRK channels are members of a large family of inwardly rectifying  $K^+$  channels. But what does inward rectification mean? At the channel's reversal potential, the equilibrium potential for  $K^+$  at which no current flows ( $E_K$ ), the slope of the current-voltage relationship changes. Rectification refers to the fact that the outward current is considerably smaller when the membrane potential of the cell is above  $E_K$  compared to the inward current when the membrane potential is below the channel's reversal potential. Intracellular  $Mg^{2+}$  and polyamines that occlude the central pore at potentials above  $E_K$  are responsible for this effect (Yamada et al., 1998). With the small outward  $K^+$  current, GIRK channels decrease excitability of neurons at physiological conditions because the resting membrane potential is typically positive to  $E_K$ . The channels are activated by stimulating their G protein-coupled receptors (GPCRs). This happens upon release of several neurotransmitters like acetylcholine, dopamine, opioids, serotonin, somatostatin, adenosine and GABA. The GPCRs are specifically coupled to pertussis toxin (PTX)-sensitive heterotrimeric G proteins. These proteins release  $G\beta\gamma$  dimers that bind to and thereby open GIRK channels (Huang et al., 1995; Inanobe et al., 1995; Logothetis et al., 1987; Pfaffinger et al., 1985; Reuveny et al., 1994; Wickman et al., 1994). There are four subunits, GIRK1-4 expressed throughout the body, that form homo- or heterotetramers. In the central nervous system (CNS), GIRK channels are comprised of GIRK1/2 heteromers (Lesage et al., 1994; Krapivinsky et al., 1996), whereby GIRK2 has been shown to play the primary role in generating GIRK currents in the hippocampus, cerebellum, substantia nigra, locus coeruleus and ventral tegmental area (Cruz et al., 2008; Koyrakh et al., 2005; Labouèbe et al., 2007; Lüscher et al., 1997; Marker et al., 2006; Slesinger et al., 1997; Torrecilla et al., 2002).

In order to understand the role of GIRK channels in disease, emphasizing their physiological role is indispensable. When GIRK channels function at basal activity, they shift the membrane voltage by -8mV and thereby hyperpolarize the resting membrane potential. This decrease in electrical excitability shapes the functionality of neuronal networks in several brain regions. Physiological activation of the channel leads to another level of inhibition in signal processing (Lüscher et al., 1997). The well-orchestrated interplay of membrane excitation and inhibition is disrupted when



GIRK channel function is altered. Without GIRK functioning, neurons show excessive excitability and produce symptoms of epilepsy (i.e. seizures). When selectivity of GIRK channels is lost, irregular ion fluxes, such as Na<sup>+</sup> influx, trigger cell death as it is observed in Parkinson's disease (Harkins et al., 2002; Mazarati et al., 2006; Siarey et al., 1999; Signorini et al., 1997).

The antidepressant SSRI fluoxetine causes inhibition of GIRK channels. Therefore, there might be a link to episodes of major depressive disorder (Hibino et al., 2009). SSRIs have a rapid effect on extracellular serotonin (5-HT) levels but why therapeutic drug action in patients is slow remains to be investigated. Some attempts have been made using cellular assays of 5-HT<sub>1A</sub> receptor responses in serotonergic neurons of the dorsal raphe nucleus (DRN). Using electrophysiological recordings, Cornelisse et al. (2007) could show that the 5-HT<sub>1A</sub> response is decreased in mice chronically treated with fluoxetine, but receptors were not downregulated. This class of receptors acts on G proteins that target GIRK channels and cause them to hyperpolarize the membrane potential and thereby decrease excitability. This effect seems to be independent of the animals' level of stress it is exposed to. Pharmacological treatment and the etiology of depression seem to diverge but because there is no evidence for changes in 5-HT<sub>1A</sub> expression in anhedonic mice the receptor might not directly affect the depressive phenotype. However, SSRIs seem to be involved in decreasing excitability by affecting GIRK channel expression in serotonergic neurons activated together with 5-HT<sub>1A</sub>. Excitability of dorsal raphe neurons and release of serotonin is then increased after treatment with fluoxetine, because inhibitory inputs from numerous metabotropic receptors are reduced due to a downregulation of GIRK (Cornelisse et al., 2007). The therapeutic effect of antidepressants as reuptake inhibitors of norepinephrine and/or serotonin in the brain may be complemented by inhibition of GIRK channels. This makes them an intriguing new therapeutic target and opens up the possibility to develop effective new drugs to treat depression and other psychiatric disorders (Kobayashi et al., 2004). Novel tools, such as photoswitchable compounds that selectively open or close GIRK channels may further increase our understanding of GIRK channel function in disease and help to establish the link between these cellular observations and brain function underlying behavior.

### 1.2 Methods for drug research in the zebrafish

In the present work, I introduce methods to advance the zebrafish system as a powerful model organism for innovative therapies to treat major depression and anxiety disorders. In my research, I exploit the transparency of zebrafish larvae's body to test the utility of synthetic photochemical compounds to modify behavior in a targeted fashion. Using a photoswitchable GIRK channel agonist, I aim to explore remote optical control of neuronal activity and behavior and implement a rapid behavioral assay that is designed to provide a readout of neurotropic effects in zebrafish larvae. Small molecules that can be activated and inactivated by light are attractive targets for drug development (Luján et al., 2014; Velema et al., 2014) since they offer spatiotemporal control and their dose can potentially be calibrated instantly and interactively during treatment.

Whole-brain light-sheet imaging is another powerful tool to study different genotypes and drugs in the larval zebrafish. Screening of drug x genotype interactions using *gr<sup>s357</sup>* mutants is opening up the possibility of identifying novel therapeutic avenues for the treatment of stress-related disorders. Together with a sophisticated analysis of brain network structure using a graph-theoretical approach, I hope to accelerate our understanding about the effects of neuroactive compounds on the nervous system and implement a methodological pipeline to use the zebrafish as model organism for drug discovery. Together, these fundamental studies are designed to fulfil the criteria to establish the zebrafish as a powerful neuropsychiatric model system.

#### 1.2.1 Remote optical control of behavior with a photoswitchable neuroactive compound

Light is impressive in its temporal and spatial precision when transferring information and ties together chemistry, physics and biology as one of the most fascinating phenomena. Nature and its ancient biochemical pathways gave rise to numerous photoreceptive systems, e.g. human vision which use molecular photoswitches, like retinal, that exist in different states of isomerization depending on irradiation. In evolution, these so called chromophores proved to be useful tools in

biological systems and thus remained unaltered. They absorb wavelengths from UV to near-infrared, are involved in building up ionic gradients and act on enzymes, ion channels or proteins. They control many biological functions, yet only a few natural chromophores exist. A new branch of chemistry, photopharmacology, gave rise to a variety of highly tunable synthetic photoswitches that are either covalently attached to or noncovalently interactive with a target structures. Thereby, they put proteins, G protein coupled receptors (GPCRs), ion channels, membranes, transporters, enzymes, parts of the cytoskeleton, lipids, and other native biopolymers under optical control (Broichhagen et al., 2015; Fehrentz et al., 2011; Kramer et al., 2013; Velema et al., 2014).

Designing such photoswitches is quite complex since switching needs to be reliable over many cycles without being associated with phototoxicity. Initial isomerization of a bistable switch by irradiation at a certain wavelength needs to be reversible at another wavelength to turn it on and off, unless a thermally unstable photoswitch is designed that spontaneously turns itself off when irradiation stops. The most suitable technique can be determined by the biological question to be tackled. The photoswitch then needs to be incorporated into the biological structure of interest to act as agonist, antagonist or blocker in one state and be inactive in the other configuration. Development of these tools requires skills in protein engineering and know-how about solubility and stability of these molecules. When targeting intracellular structures one has to ensure permeability of the molecule or design it in a way so it can actively be transported across the membrane or be microinjected. Additionally, synthesizing these photopharmaceuticals should be low in cost and time consumption. The wavelength of a photoswitch has to be compatible with the biological sample and the methods used in research, e.g. when performing fluorescence imaging experiments in neurobiology the switching wavelengths and fluorophore excitation/emission wavelengths should be orthogonal (Broichhagen et al., 2015; Fehrentz et al., 2011; Velema et al., 2014).

Taking all these criteria into account, synthetic photoswitches that are properly designed and made available through well-planned and efficient syntheses, provide a powerful tool to study drugs or drug targets and to infer causality when switching the compounds on and off.

### 1.2.2 Light-sheet microscopy

While a myriad of techniques allow the recording of single neurons or proximal populations of neurons, distal connections can be easily missed (Ahrens et al., 2013). To grasp the whole complexity of neuronal interaction that drives behavior it is key to record as many single units as possible, irrespective of their location in the brain (Ahrens & Engert, 2015). Combined with genetically encoded calcium sensors, the transparent and small-sized brains of larval zebrafish (800 x 500 x 300  $\mu\text{m}$ , approximately 100 000 neurons) enable whole-brain, functional, non-invasive *in vivo* imaging at cellular and millisecond resolution (Orger & Portugues, 2016). In general, 2-photon microscopy is the gold-standard however, its single point scanning mechanism is a double-edged sword. On the one hand, it only excites one point in space, thereby reducing photobleaching and increasing depth penetration. On the other hand, it becomes increasingly slow in larger volumes, where an increase in speed would result in fewer collected photons and thus a higher signal-to-noise ratio (Bennett & Ahrens, 2016). Light-sheet microscopy overcomes this issue by illuminating an entire plane by means of a sheet of light, generated for instance by a galvanometer scanning system. For good coverage of the brain and avoidance of the eyes, 1-2 excitation objectives are placed orthogonally to the detection objective. This allows vertical scanning of the sample (again via a galvanometer system) at a speed of 1-2 orders of magnitude faster than conventional 2-photon microscopy (Ahrens et al., 2013).

The microscope was custom-built (Fig. 3) by several laboratory members and had not yet reached completion at the start of this project. One major task was thus to optimise acquisition and develop a user protocol. The light-sheet microscope consists of two orthogonal excitation arms for frontal and lateral scanning, and a detection arm imaging from above. A laser beam (473nm wavelength, 3-5mW power) is split by a dichroic mirror and guided to the excitation arms by six di-electric mirrors. There, two pairs of mirror galvanometers oscillate horizontally and vertically, to create a sheet of light and scan the sample in the z plane, respectively. Two serial lenses act as a pinhole and focus the sheet into the back aperture of a 4x objective. The detection arm consists of a 20x detection objective, a piezoelectric component to adjust the focus (10V displacement, corresponds to a 400 $\mu\text{m}$  range in z), a tube lens, fluorescence

## INTRODUCTION

filter, and an Orcaflash 4.0 sCMOS camera. The chamber containing the sample sits on a lab jack stage, which is brought into the field of view of the camera by x, y, and z actuators (Fig. 4).

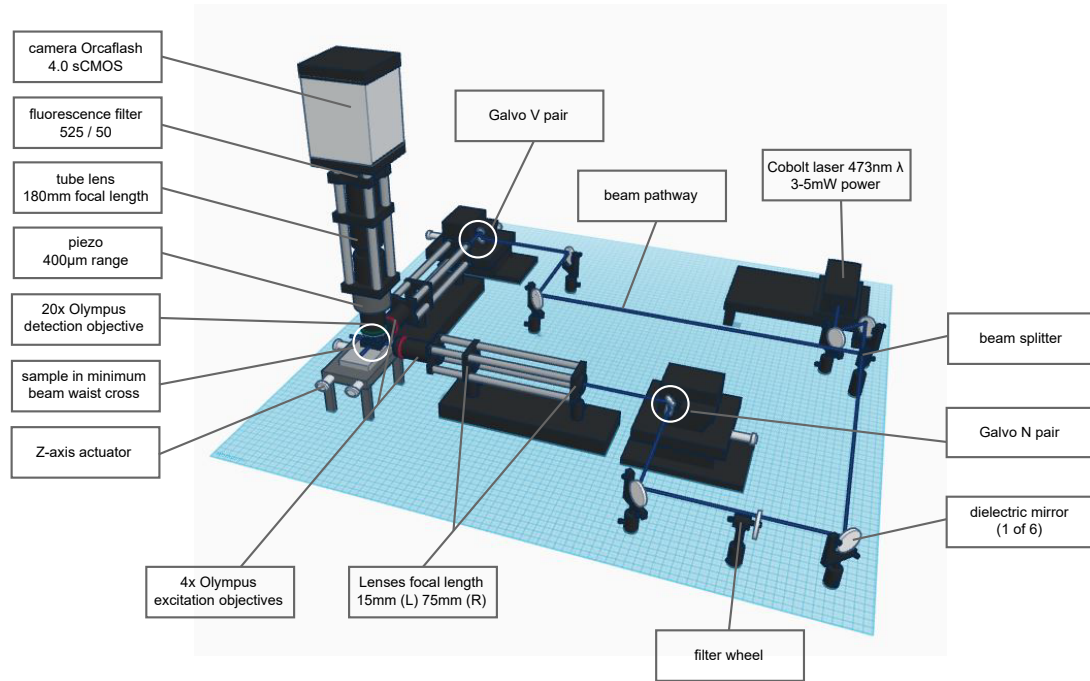


**Figure 3. Schematic of the custom-built light-sheet microscope.**

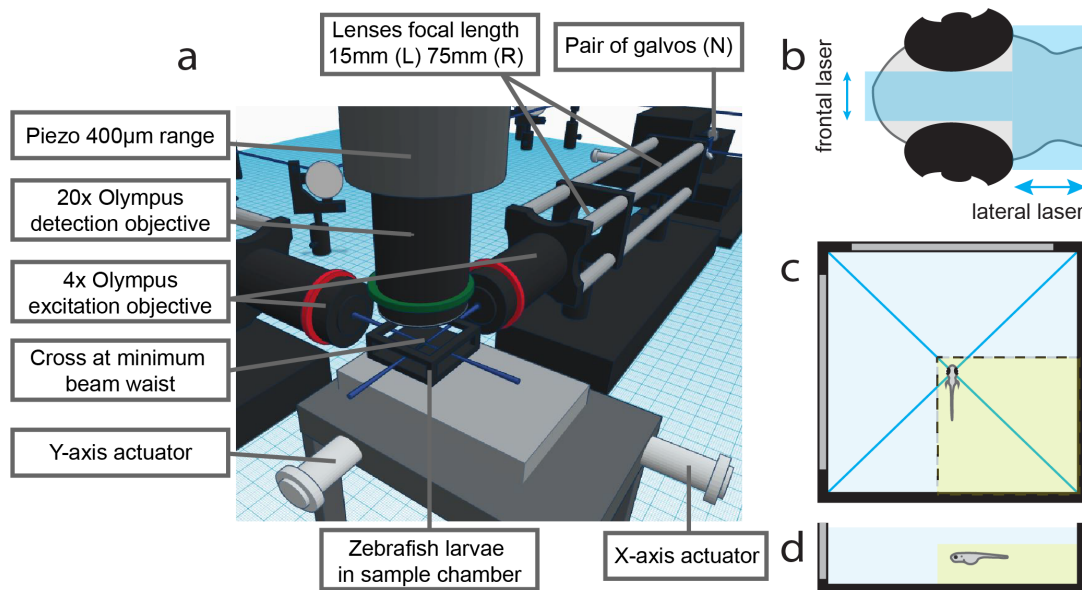


**Figure 4. Light-sheet microscope and sample preparation.** (a) Close-up view of stage, sample, excitation and detection objectives. (b) beam cross on head of larva (c) dorsal view of embedded larva in a custom chamber (d) side view of location in z of larva in chamber. For a and b, blue indicates laser beams. For c and d, yellow indicates a block of agarose cut along dashed lines, immersed in Danieau's solution (blue).

The experimental approach in my studies consisted of 5 min recordings of spontaneous whole-brain activity in *gr<sup>s357</sup>* mutants and wildtype fish at baseline and after 1.5h and 3h incubation with drugs (i.e. fluoxetine, ketamine, cycloserine) to evaluate their effect on functional connectivity in the neuronal network. When not locked to the temporal sequence of a stimulus or behavior, analysis of functional whole-brain imaging data is still constrained. Firstly, collected data files are of a vast size, requiring highly efficient data storage and processing facilities. Secondly, an issue in neural network research using brain-wide single-cell-resolution functional imaging is its complex representation in high-dimensional space. In order to extract functionally relevant features comprehensively and uncover major patterns in the data, I applied the graph theory, which I will explain in further detail in the next chapter of this thesis.

To examine functional connectivity, four-dimensional imaging stacks (dimensions being: time, z- , y- and x- plane) were split into time series of single planes and corrected for motion artefacts using an adapted version of the CaImAn package (Pnevmatikakis et al., 2017; Giovannucci et al., 2019). In brief, this consists of a rigid transformation, which grossly rotates the images in the x- and y- plane, followed by an optic flow transformation for finer features. This was followed by the first steps of data analysis, which include segmentation of the brain and extraction of regions of interest (ROIs). Voxelization is one method that is simple to implement, and reduces the number of features significantly, however, it may not separate neighbouring cells perfectly and thus create a bias in the temporal activity of that voxel. Manual neuron segmentation is usually region-of-interest selection based and outdated due to its time-consuming and heuristic nature (Mukamel et al., 2009). Therefore, the method used in this project was automated neuron segmentation that is more computationally demanding, but can be achieved for instance based on local time series correlations of pixels (Portugues et al., 2014). Extracting the activity traces of selected neurons is the first step to explore changes taking place within the neuronal

network in response to drug treatment and leads the way to using zebrafish as a valuable tool for drug discovery.

### 1.2.3 Graph-theoretical analysis of whole-brain functional connectivity

Exploring the activity of single cells over time by looking at their activity traces is crucial, yet not sufficient when facing the challenge of actually quantifying changes happening on a whole-brain level. To use the zebrafish as a tool to study drug effects on the neuronal network, I chose graph theory as a method to describe and explore the topological organization of functional connectivity. It was further applied to extract and quantify differences between zebrafish genotypes and changes taking place in response to treatment with neuroactive compounds.

Graph theory first appeared in the literature in 1736, when Leonhard Euler used this theoretical concept, which describes the pairwise relationship between objects to solve the “Königsberg Bridge Problem” (Euler, 1736). By representing the map of the city of Königsberg and its topographic structure as a topological graph with four nodes and seven edges (the bridges), Euler (1736) could conclude that it is not possible to traverse the seven bridges over the river Preger in a single trip without doubling back, starting the trip in the same place where it should end.

Several fields still use these concepts today to quantify complex relations, ranging from social sciences to biology and especially neurosciences (Boccaletti et al., 2006, Schweitzer et al., 2009, Watts & Strogatz, 1998). Graph theory is a powerful way to describe the functional organization of the brain by treating the brain as a graph, a mathematical structure composed of a set of nodes (brain regions or cells) joined together in pairs by edges, (functional connectivity between the brain regions or cells) (Watts & Strogatz, 1998). To obtain information about functional associations between single cells or brain regions, measurements of the temporal correlation between activity traces of cells can be extracted from light-sheet neuroimaging data. With this information, graph-theoretic techniques can be applied to model brain networks and study their underlying topological properties. Graphs and their edges can be undirected or directed, depending on the flow of information, and weighted or

unweighted. The Information content of brain images acquired with light-sheet microscopy allows the construction of a weighted but undirected network, because directionality cannot be inferred from the data. Here, the weight of this network is dependent on the strength of correlation between activity traces. The brain is functionally organized as a highly complex network and its segregation and integration of information processing can be described by a variety of standard metrics, whose differences between genotypes and changes over drug treatment give insight into the topological network structure of the brain (He & Evans, 2010).

The study of network systems has recently gained attention due to many studies focusing on local properties of networks, such as clustering (Watts & Strogatz, 1998), degree distributions (Barabasi & Albert, 1999; Amaral et al., 2000) and correlations (Pastor-Satorras et al., 2001; Newman, 2002). There have also been studies that examine large-scale properties such as path lengths (Watts & Strogatz, 1998), percolation (Cohen et al., 2000; Callaway et al., 2000) or hierarchy (Ravasz & Barabasi, 2003; Clauset et al., 2008). Among these metrics, however, the ones attracting by far the most attention are the clustering coefficient, characteristic path length, modularity or community structure and small-worldness (Fig. 5) (Liao, Vasilakos & He, 2017). The clustering coefficient quantifies the extent of local cliquishness or local efficiency of information transfer in a network, the capability for parallel information propagation in terms of global efficiency can be described by the characteristic path length. There are different classes of networks, such as regular, small-world, and random networks, that can be distinguished based on clustering and characteristic path length (Liao, Vasilakos & He, 2017).

A small-world network (Fig. 5b) has a shorter characteristic path length than a regular network (high clustering and long path lengths) but a greater local interconnectivity than a random network (low clustering coefficient and short path lengths). Nature appears to have designed the functional organization of the brain with such small-world network characteristics because it allows highly efficient local information processing in specialized modules and global integration at the same time and at a relatively low wiring cost (Liao, Vasilakos & He, 2017; Watts & Strogatz, 1998). Many networks are found to possess communities or modules, groups of nodes,



which have relatively dense inter-connections but connections between the modules are sparser (Boccaletti, Latora & Moreno, 2006). Community structure together with the characteristic path length and overall clustering shape the small-world properties of a network and are of fundamental interest in these systems because of their functional implications. Modules in a neuronal network, for instance, might correspond to circuits that perform certain tasks. Small-worldness, which is shaped by the underlying clustering and characteristic path length, may indicate the balance and efficiency between local information processing and global integration (Newman, 2013; He & Evans, 2010).

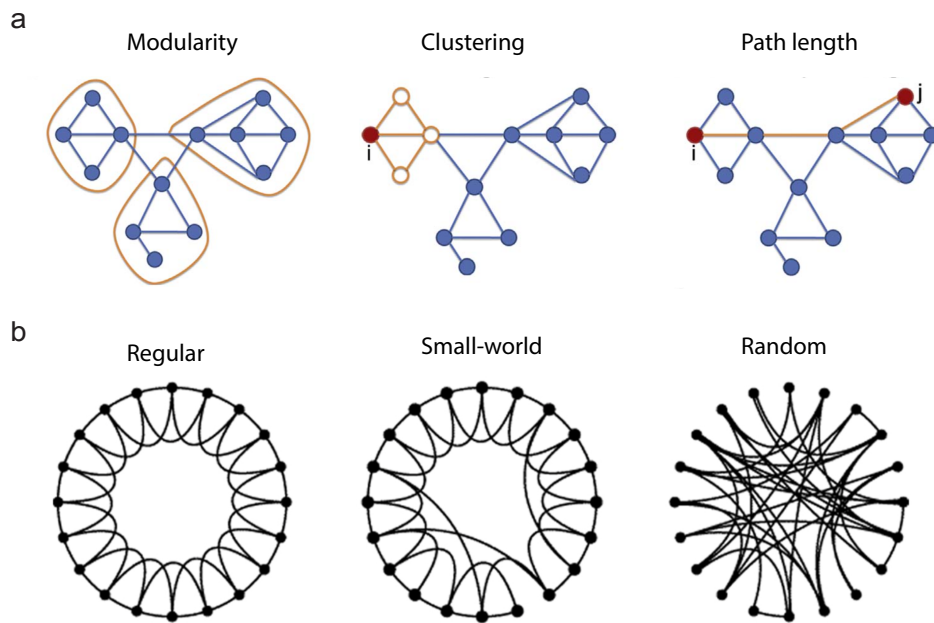


**Figure 5. Network properties.** (a) Modules in a network refer to a group of nodes with dense intra-group connections and sparse between-group connections. The optimal community structure is a subdivision of the network into non-overlapping groups of nodes in a way that maximizes the number of within-group edges and minimizes the number of between-group edges. The modularity is a measure that quantifies the degree to which the network may be subdivided into such groups. The clustering coefficient is equivalent to the fraction of node's neighbors that are neighbors of each other. It is a measure of segregation that describes clustered connectivity around individual nodes. The overall level of clustering in a network is the average of the local clustering coefficients of all the vertices. The characteristic path length is the minimum number of edges between two nodes in the network. The lengths of the paths indicate the potential for functional integration between nodes, with shorter paths implying stronger potential for integration. (b) A regular network (left) with regular connections has a

high clustering coefficient and a long characteristic path length. The random network (right) with random connections has a low clustering coefficient and a short characteristic path length. A small-world network (middle) lies between those two. It contains a large number of short connections with a few long connections and thus exhibits a high clustering coefficient with short characteristic path lengths. Figure adapted from Liao, Vasilakos, & He (2017).

By quantifying these network parameters using the graph-theoretical approach, we gain insight into genotype differences and drug effects, as well as drug x genotype interaction effects in the correlational structure of brain-wide imaging data. For this purpose, functional connectivity graphs were constructed for each recorded brain in which each node represents a cell (ROI) and each edge between two cells represents the correlation of their activity traces. By combining the graph-theoretical method with light-sheet imaging data as a scalable approach to explore various genotypes and compounds, I hope to introduce the zebrafish model system as a powerful tool to discover novel therapeutic procedures.

### 1.3 Aims of the thesis

The identification of a zebrafish experimental model with a mutation in the glucocorticoid receptor allows researchers to investigate the pathogenesis of depression. Novel tools, like photoswitchable compounds enable us to induce changes in neuronal activity remotely and with spatial and temporal precision. Light-sheet microscopy combined with a graph-theoretical analysis approach opens up the possibility to study brain-wide functional connectivity. Increased computational power allows us to handle huge datasets like whole-brain recordings with cellular resolution, and promotes the study of various disease genotypes and neuroactive compounds with the aim to implement the zebrafish model system as a vehicle for drug discovery. In the framework of this dissertation, I contributed to three publications:

In the first study, I contributed to the development of a photoswitchable agonist (LOGO) that enables the optical control of GIRK channels with temporal and spatial precision. Inhibition of GIRK channels effectively increases neuronal excitability. Thus, the channel might be an interesting new target for drug development and further increase our understanding of depression and new treatment

options. I tested the photochemical *in vivo* and designed a behavioral protocol to evaluate the compound's potential to remotely and non-invasively modify locomotor behavior in the zebrafish. This behavioral assay is designed to provide a standardized readout of neurotropic effects in zebrafish larvae. With this assay, drug treatments or genetic modifications can immediately be classified by phenotype and mechanism of action can further be investigated.

In the second study of this dissertation, I was involved in a follow up project to develop a GIRK channel photoswitch that can be controlled with visible light. For optical control of the first LOGO, potentially harmful UV irradiation was applied to inactivate the photoswitchable agonist. I contributed to discussions with valuable input about *in vivo* studies to further improve the design and application of the photoswitches. I also developed a new experimental protocol for the standardized assay to test the second version of LOGO, VLOGO (Visible Light Operated GIRK channel Opener) in our behavioral setup. VLOGO can be operated with visible light and therefore it is a valuable addition to implement these compounds for research in biological systems, e.g. drug discovery in the larval zebrafish.

In the main study of my thesis, I exploit the transparency of the body of zebrafish larvae to explore functional whole-brain connectivity with light-sheet microscopy. I combined this with a graph-theoretical analysis approach to quantify changes in brain network structure. Initially, I studied behavioural differences between wildtype fish and the  $gr^{s357}$  zebrafish mutant. This mutant harbors a missense mutation that abolishes glucocorticoid receptor transcriptional activity and results in a chronically elevated stress axis. Dysregulation of the stress axis is highly correlated with depression and behaviorally implements in the fish as increased immobility in the novel tank test as well as reduced exploration. I recorded brain activity of these fish with cellular resolution light-sheet microscopy and applied graph theory to reveal differences between genotypes. This allowed me to quantify whole-brain network parameters of functional connectivity and revealed that  $gr^{s357}$  mutant brains are organized in a greater number of functional modules with dense connections within these modules and sparse connections between the modules compared to wildtype fish. Moreover, I found that with the time spent in the experimental setup, fish might

experience stress, which I could extract and quantify as reduced clustering and small-worldness of the functional connectivity network with longer path lengths in the  $gr^{s357}$  mutant compared to wildtype fish. As a next step, I examined how known antidepressant compounds affect brain activity of larval zebrafish. For this purpose, I extracted network parameters of neuronal activity in both wildtype and  $gr^{s357}$  mutant fish, following treatment with fluoxetine, ketamine and cycloserine. Consistent with the broad expression of the glucocorticoid receptor throughout the brain, I show that antidepressants differentially affected particular metrics of the activity graphs, with some treatments restoring mutant brain activity to wildtype levels. From this, I conclude that light-sheet imaging of zebrafish brain activity is a content rich and scalable approach for studying the neural consequences of drug x genotype interactions in psychiatric disorders. Together, the results of my thesis suggest that the zebrafish model system can be advanced as a powerful discovery vehicle for drugs and innovative therapies.

The following chapter of my dissertation contains the manuscripts for these three studies. The first study, Barber et al., 2016 has been published in the peer-reviewed journal Chemical Science (Optical control of neuronal activity using a light-operated GIRK channel opener (LOGO)). The second study, Trads et al., 2017 was published in the peer-reviewed journal Organic & Biomolecular Chemistry (Optical control of GIRK channels using visible light). My main research project has recently been published in BioRxiv (Light-sheet imaging and graph analysis of antidepressant action in the larval zebrafish brain network, Burgstaller et al., 2019).

## 2 Publications

### 2.1 Optical control of neuronal activity using a light-operated GIRK channel opener (LOGO)

Barber, D. M., Schönberger, M., **Burgstaller, J.**, Levitz, J., Weaver, C. D., Isacoff, E. Y., Baier, H. & Trauner, D. (2016). Optical control of neuronal activity using a light-operated GIRK channel opener (LOGO). *Chemical Science*, 7(3), 2347-2352.

Reproduced by permission of The Royal Society of Chemistry

My involvement in this field started with the generation and *in vivo* testing of the photoswitchable GIRK channel agonist **LOGO** (the **L**ight **O**perated **G**IRK-channel **O**pener) that allows remote optical control of the channel with UV and blue light. In collaboration with the synthetic chemistry laboratory of Dirk Trauner (LMU Munich), I developed a behavioral assay (Fig. 6) to implement the zebrafish nervous system as a tool to study photoswitchable drugs and learn about GIRK channel function *in vivo*. Behavioral experiments were carried out in the DanioVision system purchased from Noldus, using the EthoVision XT Version 10.1 software. Larvae were sorted into 96-well plates using disposable pipettes, and allocated according to a randomized plate position paradigm to reduce spatial bias. To prevent the system from overheating, the chamber that comprised the plate was connected to a home-made cooling system which set the temperature constantly to 25°C. Acquisition was controlled via the EthoVision XT software with a sampling rate of 30 frames per second using an infrared-sensitive digital FireWire camera.

With these experiments, we show that this photochemical affects locomotor behavior dependent on the wavelength of the illumination. Switching the wavelength of the light from blue to UV turns the compound from an active to an inactive state and thus leads to a reversible change in locomotor behavior.

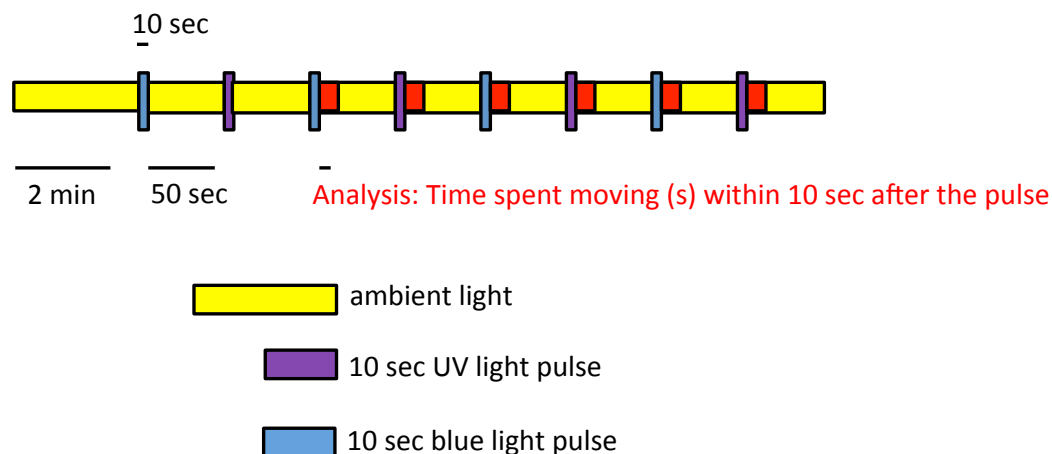


**Figure 6. Behavioral assay to test photoswitchable properties of the GIRK channel agonist LOGO.** Animals were let 2 minutes to adjust to the 96-well plate before the recording started for 8 minutes. The first 10 seconds after blue or UV light pulses of the last 3 cycles were analyzed to quantify locomotor activity of the fish.

We hope this methodological approach of testing photoswitchable compounds in a behavioral assay will chart a new route for the discovery of neuroactive pharmaceuticals. Including different disease genotypes into the assay may also support the development of therapeutic approaches to psychiatric illness in the future.



# HHS Public Access

Author manuscript

*Chem Sci.* Author manuscript; available in PMC 2017 January 13.

Published in final edited form as:

*Chem Sci.* 2016 ; 7(3): 2347–2352. doi:10.1039/C5SC04084A.

## Optical control of neuronal activity using a light-operated GIRK channel opener (LOGO)<sup>†</sup>

David M. Barber<sup>a</sup>, Matthias Schönberger<sup>a</sup>, Jessica Burgstaller<sup>b</sup>, Joshua Levitz<sup>c</sup>, C. David Weaver<sup>d</sup>, Ehud Y. Isacoff<sup>c,e</sup>, Herwig Baier<sup>b</sup>, and Dirk Trauner<sup>a</sup>

Dirk Trauner: dirk.trauner@lmu.de

<sup>a</sup>Department of Chemistry and Center for Integrated Protein Science, Ludwig Maximilians University Munich, Butenandtstraße 5-13, 81377 Munich, Germany

<sup>b</sup>Max Planck Institute of Neurobiology, Am Klopferspitz 18, 82152 Martinsried, Germany

<sup>c</sup>Department of Molecular and Cell Biology and Helen Wills Neuroscience Institute, University of California, Berkeley, California, USA

<sup>d</sup>Department of Pharmacology and Institute of Chemical Biology, Vanderbilt University School of Medicine, Nashville, Tennessee 37232, USA

<sup>e</sup>Physical Bioscience Division, Lawrence Berkeley National Laboratory, Berkeley, California, USA

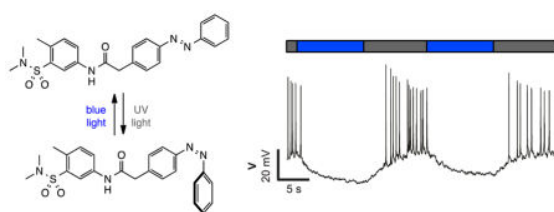
### Abstract

G-protein coupled inwardly rectifying potassium channels (GIRKs) are ubiquitously expressed throughout the human body and are an integral part of inhibitory signal transduction pathways. Upon binding of G<sub>βγ</sub> subunits released from G-protein coupled receptors (GPCRs), GIRK channels open and reduce the activity of excitable cells via hyperpolarization. As such, they play a role in cardiac output, the coordination of movement and cognition. Due to their involvement in a multitude of pathways, the precision control of GIRK channels is an important endeavour. Here, we describe the development of the photoswitchable agonist **LOGO** (the **L**ight **O**perated **G**IRK-channel **O**pener), which activates GIRK channels in the dark and is rapidly deactivated upon exposure to long wavelength UV irradiation. **LOGO** is the first K<sup>+</sup> channel opener and selectively targets channels that contain the GIRK1 subunit. It can be used to optically silence action potential firing in dissociated hippocampal neurons and **LOGO** exhibits activity *in vivo*, controlling the motility of zebrafish larvae in a light dependent fashion. We envisage that **LOGO** will be a valuable research tool to dissect the function of GIRK channels from other GPCR dependent signalling pathways.

### Graphical Abstract

<sup>†</sup>Electronic Supplementary Information (ESI) available: Experimental procedures and characterisation data. See DOI: 10.1039/x0xx00000x

Correspondence to: Dirk Trauner, dirk.trauner@lmu.de.



## Introduction

G-protein coupled inwardly rectifying potassium (GIRK) channels are an integral link between metabotropic and ionotropic pathways in neurons. They constitute a subclass of inwardly rectifying potassium channels that are natively activated by G-protein coupled receptors (GPCRs) through interactions with  $G_{\beta\gamma}$  subunits.<sup>1</sup> One of the most important effects of GIRK activation and subsequent channel opening is the hyperpolarization of cell membranes, which immediately results in a reduction of activity in excitable cells. Therefore, neurotransmitters that target both ion channels and GPCRs, including glutamate,  $\gamma$ -aminobutyric acid, acetylcholine, dopamine and serotonin, can have inhibitory effects. As a consequence, GIRK channels play crucial roles in cognition, nociception, coordination, energy homeostasis and cardiac output.<sup>2</sup> Therefore, it is unsurprising that the malfunction of GIRK channels is associated with several neurological and cardiological disorders.<sup>3</sup>

GIRK channels are comprised of homo- or heterotetramers formed by the four subunits GIRK1-4.<sup>4</sup> Although the expression patterns of GIRK subunits differs throughout the body, the prototypical GIRK channels of the central nervous system (CNS) are GIRK1/2 heteromers and the isoforms found in the cardiovascular system are GIRK1/4 channels.<sup>5</sup> Recent breakthroughs in structural biology have identified the molecular basis for GIRK channel function, such as inward rectification and polyamine block, as well as intracellular activation by sodium ions and lipids.<sup>6</sup>

It has been demonstrated that GIRK channels are inhibited by a variety of drugs, as well as polyamines and barium ions.<sup>7</sup> However, most of these compounds are not selective for GIRK channels.<sup>8,9</sup> GIRK channels can also be activated by small molecules including volatile anesthetics,<sup>10</sup> ethanol<sup>11</sup> and the natural product naringin.<sup>12</sup> Again these compounds either exhibit poor selectivity, poor potency or a combination of the two. However, the landscape of GIRK channel research was recently transformed by two small molecules, **ML297** and **VU0259369** (Fig. 1a).<sup>13</sup> These compounds were shown to be the first potent and selective activators of GIRK channels bearing the GIRK1 subunit. Subtle changes to the molecular structure of **ML297** resulted in the creation of potent GIRK1 channel inhibitors, an example of which is compound **1** (Fig. 1a).<sup>14</sup>

With the first small molecular agonists of GIRK channels at our disposal, we sought to develop photoswitchable versions that can endow light control to GIRK channels.<sup>15</sup> This approach, termed photopharmacology, is able to confer exquisite spatiotemporal control onto biological systems using the unrivalled precision of light and has previously been used to optically control ion channels,<sup>16</sup> GPCRs,<sup>17</sup> enzymes<sup>18</sup> and antibiotics.<sup>19</sup>



Herein, we present **LOGO** (the **L**ight **O**perated **G**IRK-channel **O**pener), an azobenzene photoswitch based on **VU0259369** that endows GIRK channels with remarkable photocontrol using UV and blue light. **LOGO** is the first example of a photochromic K<sup>+</sup> channel opener, as opposed to blocker,<sup>20</sup> and the first photoswitch to selectively target GIRK channels. We envisage that **LOGO** will be a valuable tool for GIRK channel research, allowing the dissection of GIRK signaling from other GPCR dependent pathways. This will further our understanding of GIRK channel function and facilitate their development as a therapeutic target.

## Results and Discussion

Using the compounds **ML297** and **VU0259369** as a basis for our photoswitch design, we employed an ‘azo-extension’ strategy to furnish our family of **LOGOs** (Fig. 1b).<sup>21</sup> In the **ML297** series, we prepared **LOGO1-4** bearing different electron-donating groups in the 4'-position of the azobenzene. In a similar fashion, **LOGO5** and **LOGO6** were derived from the compound **VU0259369**. The representative synthesis of **LOGO5** started from sulfonyl chloride **2**. Nucleophilic substitution with dimethylamine, followed by reduction of the aromatic nitro group, furnished sulfonamide **4** (Fig. 1c). An amide coupling reaction between **4** and 4-nitrophenylacetic acid (**5**) afforded nitro amide **6**, which was then reduced to the aniline **7**. Mills reaction of aniline **7** with nitrosobenzene (**8**) in the presence of acetic acid then afforded **LOGO5**. The synthesis of **LOGO1-4** and **LOGO6** proceeded in a similar fashion and is discussed in the supporting information (Fig. S1).

With our small library of **LOGOs** in hand, we set about determining their photoswitching properties using UV-Vis spectroscopy. From these experiments, we found the optimum wavelengths for the photoswitching of each of the compounds (Fig. S2). This information was then applied to our initial compound evaluation using patch clamp electrophysiology in HEK293T cells expressing GIRK1/2 channels (Fig. 2a). Beginning with **LOGO1**, we found that it could efficiently open GIRK1/2 channels as its *trans*-isomer. However, upon isomerisation to its *cis*-isomer using UV light (390 nm), only a small decrease of the current in the patch clamp experiment was observed. Based on these results, we postulated that **LOGO2-4** would endow the GIRK channels with more light dependent current because of the increased steric interactions between the ligand-binding site of the GIRK channel and the substituents in the 4'-position of the azobenzene.

Although a small increase in the photoswitching of the GIRK channel was observed, it was still minor compared to the overall activation of the channel. We therefore turned our attention to **LOGO5** and **LOGO6**, which were derived from **VU0259369** instead of **ML297**. Pleasingly, we discovered that **LOGO5** not only activates GIRK1/2 channels, but is an excellent photoswitch (Fig. 2a). We next evaluated the red-shifted photoswitch **LOGO6**, but to our surprise the photocurrent achieved was drastically reduced compared to that of **LOGO5** (Fig. 2a). Therefore, our future investigations and biological evaluation focused on **LOGO5**. Overall, analysis of **LOGO1-6** demonstrated that potent and efficacious ligands could be easily obtained by extending portions of known agonists (Fig. 1a) to include azobenzenes. By contrast, there is a narrow ‘structural window’ for photoswitchable agonists, that is compounds that dramatically change their efficacy upon light-isomerisation.

Having determined that **LOGO5** is our optimal photoswitch for the control of GIRK1/2 channels, we investigated its properties in detail using patch clamp electrophysiology and NMR spectroscopy. Firstly, we established that in the dark **LOGO5** (10  $\mu$ M) is almost as efficacious as **VU0259369** (10  $\mu$ M). The same is true under blue light illumination, where **trans-LOGO5** also predominates (Fig. 2b). Photoisomerisation using UV light (360 nm) then showed that **cis-LOGO5** is considerably less active on GIRK1/2 channels (Fig. 2b and S3). Reversible photoactivation with **LOGO5** is very robust, with no noticeable loss of photocurrent over several switching cycles in voltage-clamp mode (Fig. 2c). Highly reproducible photoswitching of **LOGO5** was also obtained when operating in current-clamp mode (Fig. S4). Next we determined the action spectrum of **LOGO5**. When the wavelength was switched between blue light (440 nm) and different wavelengths of UV light (330–380 nm), we observed large differences in current (Fig. 2d). The minimal inward current was observed at 360 nm, whereas illumination at 330, 340, 350 and 370 nm gave more inward current. This corresponds to the photostationary states (PSS) of **LOGO5** in DMSO-d<sub>6</sub> solution as determined by <sup>1</sup>H NMR spectroscopy (Fig. 2e). Here 100% **cis-LOGO5** content was observed at 360 nm, whereas 370 and 380 nm etc. gave increasing **trans-LOGO5** content. Hence the concentration of active **trans-LOGO5** can be controlled with the colour of the light (photodosing).<sup>22</sup> The kinetics of **LOGO5** activation were shown to be fast, with illumination at 440 nm for 1 second resulting in almost complete opening of the GIRK1/2 channel (Fig. S6).

Next, we monitored the action of **LOGO5** on GIRK1/2 channels expressed in HEK293T cells by elevating the holding potential in 10 mV steps from –100 mV to +50 mV. During each voltage step illumination was switched between 360/440/360 nm (Fig. 3a). Again, we found that the **cis**-isomer of **LOGO5** has very little activity at GIRK1/2 channels, whilst the **trans**-isomer of **LOGO5** shows strong GIRK1/2 activation. The amplitude of photocurrents at different holding potentials reflects the inward rectification of GIRK1/2 channels (Fig. 3b). Given the high concentration of K<sup>+</sup> ions (50 mM), the reversal potential was found to lie between –30 and –20 mV.

To evaluate the activity of **LOGO5** at different GIRK channel subtypes, we next employed the thallium flux assay technique (Fig. 4).<sup>23</sup> We found that **LOGO5** is capable of activating GIRK channels that contain the GIRK1 subunit with similar potency and efficacy (GIRK1/2: EC<sub>50</sub> = 1.2 ± 0.09  $\mu$ M, %E<sub>max</sub> = 95 ± 5.0; GIRK1/4: EC<sub>50</sub> = 1.9 ± 0.10  $\mu$ M, %E<sub>max</sub> = 101.5 ± 6.4; Table S1). However, **LOGO5** is unable to activate homodimeric GIRK2 channels, even at high concentrations.

Having demonstrated **LOGO5** on HEK293T cells, which heterologously express GIRK1/2 channels, we next wondered if this tool could be used to control excitable cells that natively express GIRK channels. To test this, we turned to dissociated rat hippocampal neurons which have been shown to express a variety of GIRK subunits.<sup>24</sup> After the application of **LOGO5** (20  $\mu$ M), pyramidal neurons exhibited large membrane hyperpolarization (15.8 ± 2.5 mV, n=7 cells) in response to illumination with blue light (450 nm), which was reversed with UV light (360 nm) (Fig. S7a). Photoswitching of **LOGO5** in both directions was stable in the dark over tens of seconds while in current-clamp mode (Fig. 5a) indicating

that constant illumination of the sample is not required. This bistability is characteristic of 'normal' azobenzenes.<sup>25</sup> In voltage-clamp mode at  $-60$  mV, blue light (450 nm) illumination induced an outward current ( $50.3 \pm 4.8$  pA,  $n=4$  cells), consistent with activation of a potassium conductance (Fig. S7b). Most importantly when at depolarised potentials, **LOGO5** was able to reversibly silence action potential firing under blue light (450 nm) illumination (Fig. 5b). Illuminating with UV light (360 nm) restored action potential firing. The photoswitching of **LOGO5** in dissociated rat hippocampal neurons was also highly reliable; photoswitching could be repeated for the entire length that a patch was maintained ( $\sim 5$ – $10$  minutes; Fig. S7c), indicating that **LOGO5** is a useful tool for experiments over extended periods of time.

With the control of native GIRK channels accomplished in rat hippocampal neurons, we investigated if **LOGO5** had any effect in living animals. We selected zebrafish larvae (*Danio rerio*) as our organism of choice as they are transparent, enabling facile light delivery and they have previously been used in conjunction with biologically active compounds containing azobenzene photoswitches.<sup>26</sup> Accordingly, zebrafish larvae 5–7 days post fertilisation were exposed to 10 second pulses of UV light (365 nm) and blue light (455 nm), in between interludes of ambient light (Fig. S8). After the first cycle of UV and blue light pulses the time that the zebrafish larvae spent swimming in the 10 seconds after the light pulse was measured to give the background swimming behaviour. The zebrafish larvae were then incubated with **LOGO5** ( $50 \mu\text{M}$ ) for 1 hour and the same protocol was used to determine the effect of the photochromic GIRK agonist by calculating the change in swimming time. Gratifyingly, the zebrafish larvae showed significantly different changes in swimming time in the presence of **LOGO5**, which could be modulated by alternating illumination with UV and blue light (Fig. 6). When illuminated with blue light, the zebrafish larvae exhibited reduced swimming times compared to the control experiments. After illuminating with UV light for 10 seconds, the zebrafish larvae dramatically increased the time they spent swimming. However, the zebrafish larvae also showed increased swimming time in the control experiment using only UV light. To dissect the effect of **LOGO5** from the native response to UV light, we performed additional experiments using the non-photoswitchable GIRK activator **ML297** (Fig. 6). These experiments demonstrated that there is almost no change in the swimming behaviour of the zebrafish larvae when illumination is switched between UV and blue light. This is in stark contrast to the results obtained using **LOGO5** and UV light.

## Conclusion

In summary, we have developed a photochromic agonist that enables the optical control of GIRK channels. Our photoswitch, **LOGO5**, is active as its trans-isomer, with UV light illumination converting it to its significantly less active *cis*-isomer. **LOGO5** has been shown to work with GIRK channels that bear the GIRK1 subunit and can be used to efficiently reduce neuronal excitability in dissociated hippocampal neurons in a light dependent manner. **LOGO5** can also be implemented *in vivo*, for instance in zebrafish larvae. Future work is focused on the advanced development of **LOGO5** as an optical tool to control GIRK channels in higher animals.

## Supplementary Material

Refer to Web version on PubMed Central for supplementary material.

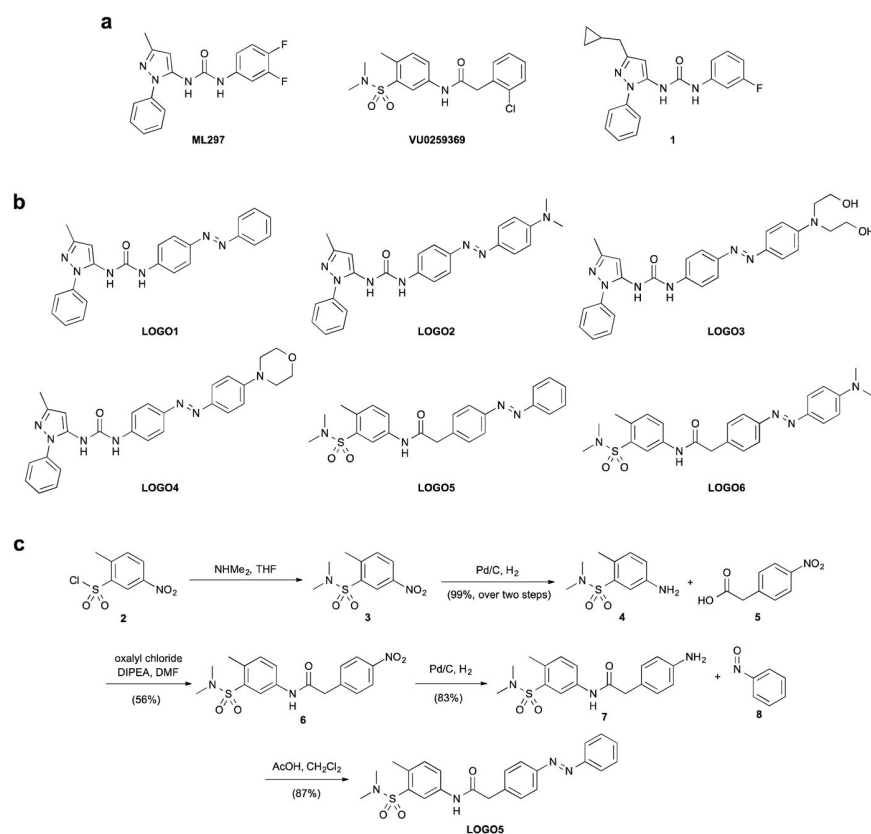
## Acknowledgments

D.M.B. gratefully acknowledges the European Commission for a Marie Skłodowska-Curie Intra-European Fellowship (PIEF-GA-2013-627990). D.T. thanks the Munich Centre for Integrated Protein Science (CIPSM) and the European Research Council (Advanced Grant 268795). D.T. and E.Y.I. thank the National Institutes of Health support of the Nanomedicine Developmental Center for the Optical Control of Biological Function (2PN2EY018241). We thank Luis de la Osa de la Rosa and Luisa Zartner for excellent technical assistance and Dr. Martin Olbrich and Cedric Hugelshofer for helpful discussions during the preparation of this manuscript.

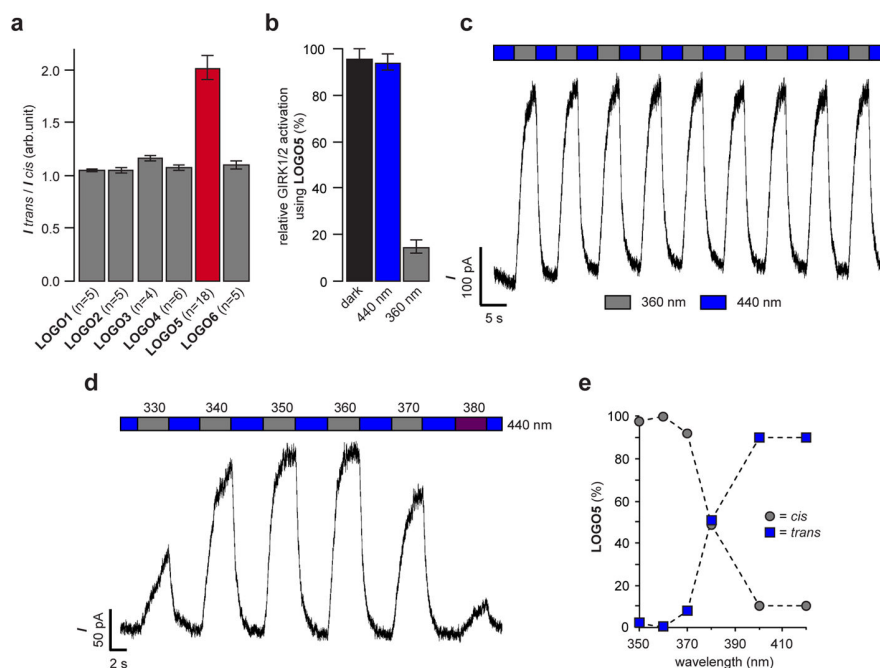
## References

1. (a) Hibino H, Inanobe A, Furutani K, Murakami S, Findlay I, Kurachi Y. *Physiol Rev*. 2010; 90:291–366. [PubMed: 20086079] (b) Lüscher C, Slesinger PA. *Nat Rev Neurosci*. 2010; 11:301–315. [PubMed: 20389305] (c) Dascal N, Kahanovitch U. *Int Rev Neurobiol*. 2015; 123:27–85. [PubMed: 26422982]
2. Luján R, Marron Fernandez de Velasco E, Aguado C, Wickman K. *Trends Neurosci*. 2014; 37:20–29. [PubMed: 24268819]
3. Walsh KB. *Front Pharmacol*. 2011; 2:64. [PubMed: 22059075]
4. (a) Lesage F, Duprat F, Fink M, Guillemare E, Coppola T, Lazdunski M, Hugnot JP. *FEBS Lett*. 1994; 353:37–42. [PubMed: 7926018] (b) Krapivinsky G, Gordon EA, Wickman K, Velimirović B, Krapivinsky L, Clapham DE. *Nature*. 1995; 374:135–141. [PubMed: 7877685]
5. Liao YJ, Jan YN, Jan LY. *J Neurosci*. 1996; 16:7137–7150. [PubMed: 8929423]
6. (a) Nishida M, MacKinnon R. *Cell*. 2002; 111:957–965. [PubMed: 12507423] (b) Whorton MR, MacKinnon R. *Cell*. 2011; 147:199–208. [PubMed: 21962516] (c) Whorton MR, MacKinnon R. *Nature*. 2013; 498:190–197. [PubMed: 23739333]
7. (a) Kobayashi T, Washiyama K, Ikeda K. *Br J Pharmacol*. 2003; 138:1119–1128. [PubMed: 12684268] (b) Kobayashi T, Washiyama K, Ikeda K. *Neuropsychopharmacol*. 2004; 29:1841–1851. (c) Hashimoto N, Yamashita T, Tsuruzoe N. *Pharmacol Res*. 2006; 54:136–141. [PubMed: 16725344]
8. Kobayashi T, Ikeda K. *Curr Pharm Des*. 2006; 12:4513–23. [PubMed: 17168757]
9. Machida T, Hashimoto N, Kuwahara I, Ogino Y, Matsuura J, Yamamoto W, Itano Y, Zamma A, Matsumoto R, Kamon J, Kobayashi T, Ishiwata N, Yamashita T, Ogura T, Nakaya H. *Circ Arrhythmia Electrophysiol*. 2011; 4:94–102.
10. Weigl LG, Schreimbayer W. *Mol Pharmacol*. 2001; 60:282–289. [PubMed: 11455015]
11. (a) Lewohl JM, Wilson WR, Mayfield RD, Brozowski SJ, Morrisett RA, Harris RA. *Nat Neurosci*. 1999; 2:1084–1090. [PubMed: 10570485] (b) Aryal P, Dvir H, Choe S, Slesinger PA. *Nat Neurosci*. 2009; 12:988–995. [PubMed: 19561601]
12. Yow TT, Pera E, Absalom N, Heblinski M, Johnston GA, Hanrahan JR, Chebib M. *Br J Pharmacol*. 2001; 163:1017–1033.
13. (a) Kaufmann K, Romaine I, Days E, Pascual C, Malik A, Yang L, Zou B, Du Y, Sliwoski G, Morrison RD, Denton J, Niswender CM, Daniels JS, Sulikowski GA, Xie X, Lindsley CW, Weaver CD. *ACS Chem Neurosci*. 2013; 4:1278–1286. [PubMed: 23730969] (b) Wydeven N, Marron Fernandez de Velasco E, Du Y, Benneyworth MA, Hearing MC, Fischer RA, Thomas MJ, Weaver CD, Wickman K. *Proc Natl Acad Sci USA*. 2014; 111:10755–10760. [PubMed: 25002517] (c) Ramos-Hunter SJ, Engers DW, Kaufmann K, Du Y, Lindsley CW, Weaver CD, Sulikowski GA. *Bioorg Med Chem Lett*. 2013; 23:5195–5198. [PubMed: 23916258]
14. (a) Wen W, Wu W, Romaine IM, Kaufmann K, Du Y, Sulikowski GA, Weaver CD, Lindsley CW. *Bioorg Med Chem Lett*. 2013; 23:4562–4566. [PubMed: 23838260] (b) Wen W, Wu W, Weaver CD, Lindsley CW. *Bioorg Med Chem Lett*. 2014; 24:5102–5106. [PubMed: 25264075]

15. (a) Fehrentz T, Schönberger M, Trauner D. *Angew Chem Int Ed*. 2011; 50:12156–12182.(b) Beharry AA, Woolley GA. *Chem Soc Rev*. 2011; 40:4422–4437. [PubMed: 21483974] (c) Briek C, Rohrbach F, Gottschalk A, Mayer G, Heckel A. *Angew Chem Int Ed*. 2012; 51:8446–8476.(d) Szymański W, Beierle JM, Kistemaker HAV, Velema WA, Feringa Ben L. *Chem Rev*. 2013; 113:6114–6178. [PubMed: 23614556] (e) Velema WA, Szymanski W, Feringa BL. *J Am Chem Soc*. 2014; 136:2178–2191. [PubMed: 24456115]
16. (a) Schönberger M, Althaus M, Fronius M, Clauss W, Trauner D. *Nat Chem*. 2014; 6:712–719. [PubMed: 25054942] (b) Damijonaitis A, Broichhagen J, Urushima T, Hüll K, Nagpal J, Laprell L, Schönberger M, Woodmansee DH, Rafiq A, Sumser MP, Kummer W, Gottschalk A, Trauner D. *ACS Chem Neurosci*. 2015; 6:701–707. [PubMed: 25741856] (c) Laprell L, Repak E, Franckevicius V, Hartrampf F, Terhag J, Hollmann M, Sumser M, Rebola N, DiGregorio DA, Trauner D. *Nat Commun*. 2015; 6:8076. [PubMed: 26311290]
17. (a) Schönberger M, Trauner D. *Angew Chem Int Ed*. 2014; 53:3264–3267.(b) Pittolo S, Gómez-Santacana X, Eckelt K, Rovira X, Dalton J, Goudet C, Pin JP, Llobet A, Giraldo J, Llebaria A, Gorostiza P. *Nat Chem Bio*. 2014; 10:813–815. [PubMed: 25173999]
18. (a) Falenczyk C, Schiedel M, Karaman B, Rumpf T, Kuzmanovic N, Grötl M, Sippl W, Jung M, König B. *Chem Sci*. 2014; 5:4794–4799.(b) Reisinger B, Kuzmanovic N, Löffler P, Merkl R, König B, Sterner R. *Angew Chem Int Ed*. 2014; 53:595–598.(c) Chen X, Wehle S, Kuzmanovic N, Merget B, Holzgrabe U, König B, Sottriffer CA, Decker M. *ACS Chem Neurosci*. 2014; 5:377–389. [PubMed: 24628027] (d) Broichhagen J, Jurastow I, Iwan K, Kummer W, Trauner D. *Angew Chem Int Ed*. 2014; 53:7657–7660.
19. (a) Velema WA, van der Berg JP, Hansen MJ, Szymanski W, Driessen AJM, Feringa BL. *Nat Chem*. 2013; 5:924–928. [PubMed: 24153369] (b) Babii O, Afonin S, Berditsch M, Reißer S, Mykhailiuk PK, Kubyshkin VS, Steinbrecher T, Ulrich AS, Komarov IV. *Angew Chem Int Ed*. 2014; 53:3392–3395.
20. (a) Banghart MR, Mourot A, Fortin DL, Yao JZ, Kramer RH, Trauner D. *Angew Chem Int Ed*. 2009; 48:9097–9101.(b) Polosukhina A, Litt J, Tochitsky I, Nemargut J, Sychev Y, De Kouchkovsky I, Huang T, Borges K, Trauner D, Van Gelder RN, Kramer RH. *Neuron*. 2012; 75:271–282. [PubMed: 22841312] (c) Mourot A, Fehrentz T, Le Feuvre Y, Smith CM, Herold C, Dalkara D, Nagy F, Trauner D, Kramer RH. *Nat Methods*. 2012; 9:396–402. [PubMed: 22343342] (d) Tochitsky I, Polosukhina A, Degtyar VE, Gallerani N, Smith CM, Friedman A, Van Gelder RN, Trauner D, Kaufer D, Kramer RH. *Neuron*. 2014; 81:800–813. [PubMed: 24559673] (e) Broichhagen J, Schönberger M, Cork SC, Frank JA, Marchetti P, Bugliani M, Shapiro AMJ, Trapp S, Rutter GA, Hodson DJ, Trauner D. *Nat Commun*. 2014; 5:5116. [PubMed: 25311795]
21. Broichhagen J, Frank JA, Trauner D. *Acc Chem Res*. 2015; 48:1947–1960. [PubMed: 26103428]
22. Bieth J, Wassermann N, Vratsanos SM, Erlanger BF. *Proc Natl Acad Sci USA*. 1970; 66:850–854. [PubMed: 5269248]
23. Weaver CD, Harden D, Dworetzky SI, Robertson B, Knox RJ. *J Biomol Screen*. 2004; 9:671–677. [PubMed: 15634793]
24. Saenz del Burgo L, Cortes R, Mengod G, Zarate J, Echevarria E, Salles J. *J Comp Neurol*. 2008; 510:581–606. [PubMed: 18698588]
25. Bandara HMD, Burdette SC. *Chem Soc Rev*. 2012; 41:1809–1825. [PubMed: 22008710]
26. (a) Szobota S, Gorostiza P, Del Bene F, Wyart C, Fortin DL, Kolstad KD, Tulyathan O, Volgraf M, Numano R, Aaron HL, Scott EK, Kramer RH, Flannery J, Baier H, Trauner D, Isacoff EHud Y. *Neuron*. 2007; 54:535–545. [PubMed: 17521567] (b) Wyart C, Del Bene F, Warp E, Scott EK, Trauner D, Baier H, Isacoff EHud Y. *Nature*. 2009; 461:407–411. [PubMed: 19759620] (c) Janovjak H, Szobota S, Wyart C, Trauner D, Isacoff EY. *Nat Neurosci*. 2010; 13:1027–1032. [PubMed: 20581843] (d) Levitz J, Pantoja C, Gaub B, Janovjak H, Reiner A, Hoagland A, Schoppik D, Kane B, Stawski P, Schier AF, Trauner D, Isacoff EY. *Nat Neurosci*. 2013; 16:507–516. [PubMed: 23455609]

**Fig. 1.**

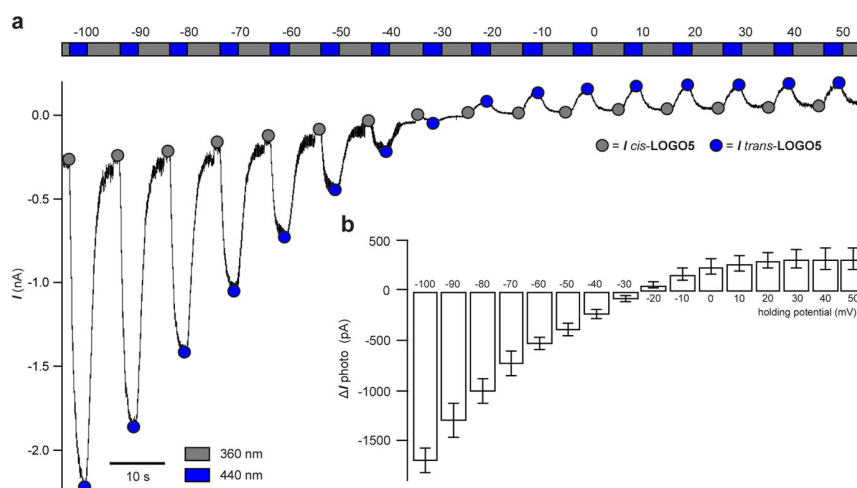
Design of the photoswitchable GIRK channel agonists **LOGO1-6** using an ‘azo-extension’ strategy. a) Chemical structures of the GIRK channel agonists **ML297** and **VU0259369**, and the GIRK channel inhibitor **1**. b) Chemical structures of the photoswitchable GIRK agonists **LOGO1-6**. c) Synthesis of **LOGO5** using a Mills reaction.

**Fig. 2.**

Whole-cell patch clamp electrophysiology of HEK293T cells expressing GIRK1/2 channels.

a) Evaluation of **LOGO1-6** (1  $\mu$ M) revealed that **LOGO5** displayed the best photoswitching behaviour. b) **LOGO5** (10  $\mu$ M) is almost as efficacious as **VU0259369** (10  $\mu$ M) in the dark and under blue light (440 nm) illumination (n=4 cells). c) The photoswitching of **LOGO5** was shown to be reversible over many switching cycles in voltage-clamp mode. d) Action spectrum of **LOGO5** (1  $\mu$ M) showing the accurate control of cellular currents by toggling the illumination wavelength between 440 nm and 330–380 nm. e) Photoswitching of **LOGO5** in DMSO- $d_6$  solution using  $^1\text{H}$  NMR spectroscopy (see ESI for details). Values represent mean  $\pm$  SEM.



**Fig. 3.**

Inward rectification of GIRK1/2 channels in the presence of **LOGO5** (10  $\mu$ M) in voltage-clamp mode. a) The holding potential was elevated in 10 mV steps from -100 mV to +50 mV illuminating with 360/440/360 nm at each step to give the *cis*-isomer of **LOGO5** (360 nm) and the *trans*-isomer of **LOGO5** (440 nm). Respective peak currents are indicated as grey and blue circles. b) Averaged photocurrent amplitudes ( $\Delta I = I_{trans-LOGO5} - I_{cis-LOGO5}$ ). Inward rectification is also translated into the photocurrents  $\Delta I$  (n=3 cells). Values represent mean  $\pm$  SEM.



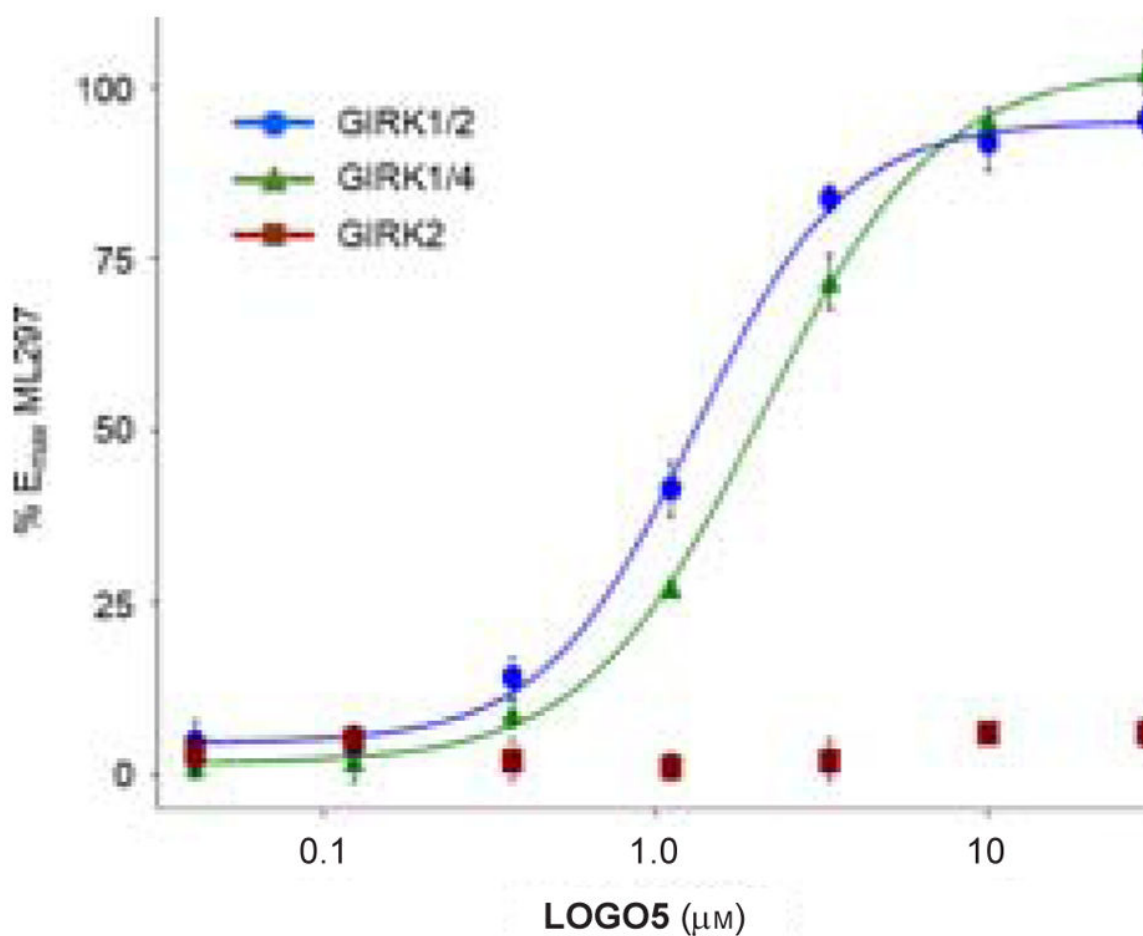


**Fig. 4.**

Potency, efficacy and selectivity of **LOGO5**. Shown are fits to representative data obtained from testing multiple concentrations of **LOGO5** on cell lines stably expressing GIRK1/2 (blue circles), GIRK1/4 (green triangles) and GIRK2 (red squares). The measured potencies for GIRK1/2 and GIRK1/4 were  $1.2 \pm 0.09 \mu\text{M}$  and  $1.9 \pm 0.1 \mu\text{M}$ , respectively. **LOGO5** was inactive on cells that only express GIRK2. Efficacy values were normalised to the maximum activity observed using **ML297** ( $10 \mu\text{M}$ ) on GIRK1/2-expressing cells. Error bars represent  $\pm$  SEM obtained from triplicate wells. Reported potency values represent the SEM obtained from three independent experiments.

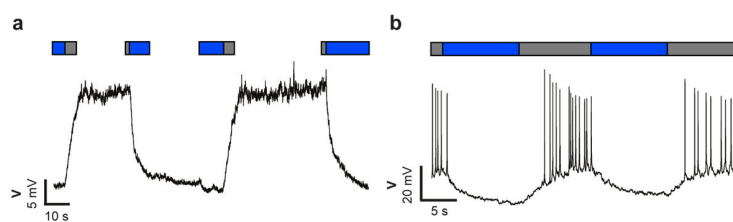


**Fig. 5.**

Optical control of excitability via endogenous GIRK channels using **LOGO5** in rat hippocampal neurons. a) Photoswitching of **LOGO5** reversibly and repeatedly manipulated membrane potentials by 10–20 mV. Light responses were stable in the dark for tens of seconds due to the slow relaxation of the *cis*- and *trans*-isomers of **LOGO5**. b) Photoswitching of **LOGO5** results in the control of spontaneous action potential firing. (grey = 360 nm; blue = 450 nm).

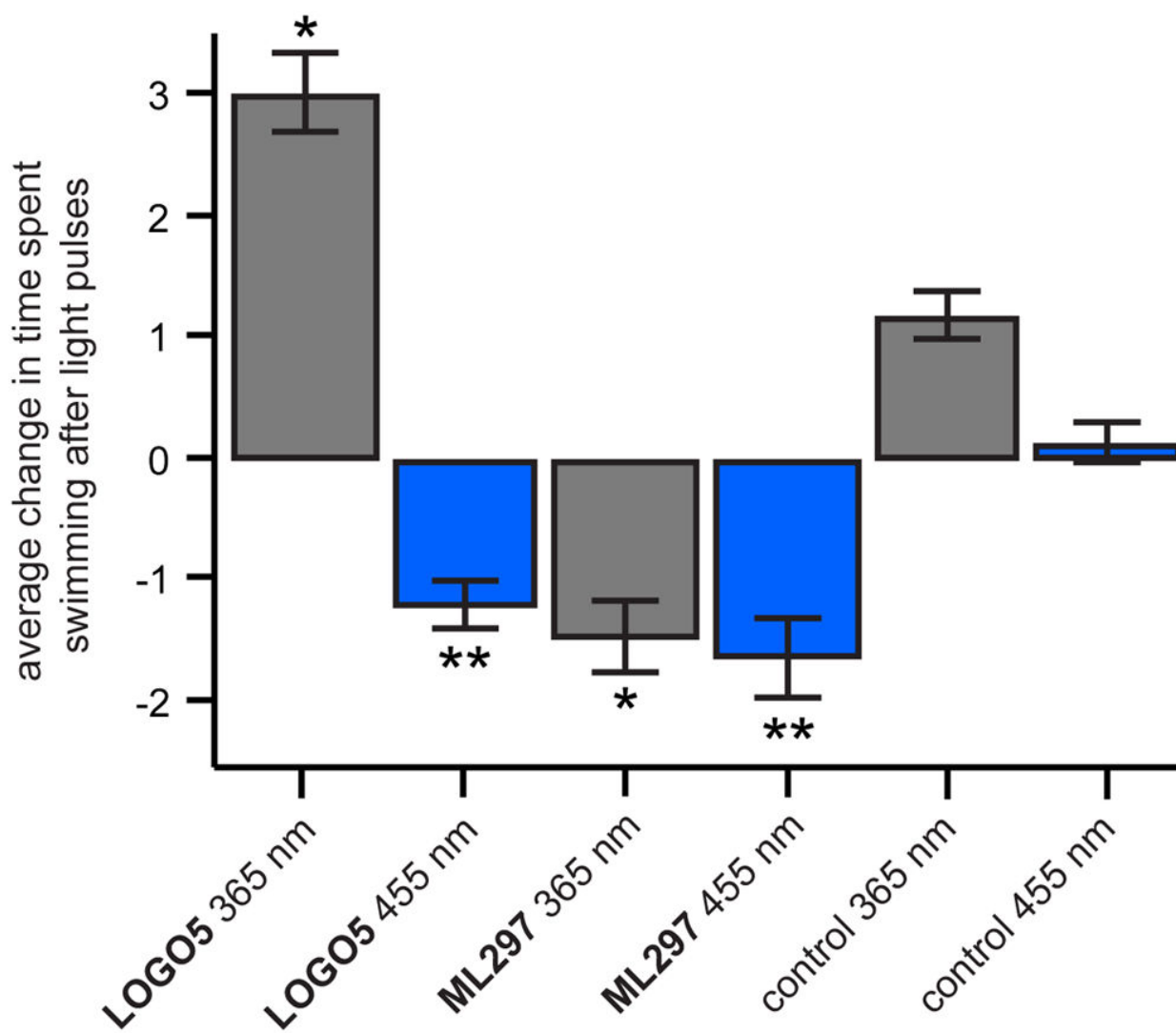


**Fig. 6.**

Optical control of zebrafish motility in the presence of **LOGO5**. After the application of **LOGO5** (50  $\mu$ M), the swimming behaviour of the zebrafish larvae was reduced under blue light illumination and increased under UV light illumination when compared to the control (1% DMSO) zebrafish. Experiments using the non-photoswitchable GIRK opener **ML297** (50  $\mu$ M) showed reduction of the zebrafish motility independent of UV and blue light illumination. (**LOGO5** n=36 zebrafish; **ML297** n=36 zebrafish; control (1% DMSO) n=72 zebrafish) (\*P < 0.01 versus control 365 nm; \*\*P < 0.001 versus control 455 nm). Values represent mean  $\pm$  SEM.

## 2.2 Optical control of GIRK channels using visible light

Trads, J. B., **Burgstaller, J.**, Laprell, L., Konrad, D. B., Weaver, C. D., Baier, H., ... & Barber, D. M. (2017). Optical control of GIRK channels using visible light. *Organic & Biomolecular Chemistry*, 15(1), 76-81.

Reproduced by permission of The Royal Society of Chemistry



Cite this: *Org. Biomol. Chem.*, 2017, **15**, 76

Received 4th October 2016,  
Accepted 7th November 2016

DOI: 10.1039/c6ob02153k

www.rsc.org/obc

## Optical control of GIRK channels using visible light†

Julie B. Trads,<sup>a,b</sup> Jessica Burgstaller,<sup>c</sup> Laura Laprell,<sup>a</sup> David B. Konrad,<sup>a</sup> Luis de la Osa de la Rosa,<sup>a</sup> C. David Weaver,<sup>d</sup> Herwig Baier,<sup>c</sup> Dirk Trauner<sup>\*a</sup> and David M. Barber<sup>\*a</sup>

G-protein coupled inwardly rectifying potassium (GIRK) channels are an integral part of inhibitory signal transduction pathways, reducing the activity of excitable cells *via* hyperpolarization. They play crucial roles in processes such as cardiac output, cognition and the coordination of movement. Therefore, the precision control of GIRK channels is of critical importance. Here, we describe the development of the azobenzene containing molecule VLOGO (Visible Light Operated GIRK channel Opener), which activates GIRK channels in the dark and is promptly deactivated when illuminated with green light. VLOGO is a valuable addition to the existing tools for the optical control of GIRK channels as it circumvents the need to use potentially harmful UV irradiation. We therefore believe that VLOGO will be a useful research tool for studying GIRK channels in biological systems.

## Introduction

G-protein coupled inwardly rectifying potassium (GIRK) channels are a family of potassium channels that are opened *via* interactions with G $\beta\gamma$  protein complexes.<sup>1</sup> Upon channel opening, GIRK channels hyperpolarize cell membranes causing a reduction in the activity of excitable cells. Therefore, GIRK channels are involved in processes such as nociception, cognition and cardiac output<sup>2</sup> and are associated with numerous neurological and cardiovascular conditions.<sup>3</sup>

GIRK channels exist as either homo- or heterotetramers comprised of the four subunits GIRK1-4, which exhibit distinct

expression patterns throughout the body.<sup>4</sup> For example, GIRK1/2 channels are typically found in the central nervous system (CNS) and GIRK1/4 channels are characteristic of the cardiovascular system.<sup>5</sup> It has been shown that GIRK channels are activated by a variety of small molecules, albeit with varying degrees of selectivity.<sup>6</sup> The compounds **ML297** and **VU0259369** are exceptions as they are potent and selective activators of GIRK channels bearing the GIRK1 subunit (Fig. 1a).<sup>7</sup>

We recently demonstrated that GIRK channels can be endowed with light control using photopharmacology.<sup>8</sup> Our freely diffusible photoswitch **LOGO**, is a derivative of **VU0259369** that contains an azobenzene moiety as the photo-responsive element (Fig. 1a).<sup>9</sup> It harnesses the precision of light to accurately control the spontaneous action potential firing of dissociated hippocampal neurons and the swimming behaviour of zebrafish larvae. However, a significant drawback of **LOGO** is that UV and blue light are required for its *cis/trans* photoisomerisation. This results in increased levels of photo-toxicity<sup>10</sup> and limits the amount of tissue penetration.<sup>11</sup> By employing photoswitches that respond to red-shifted wavelengths of light we would be able to improve these properties.<sup>12</sup>

Herein, we present **VLOGO** (Visible Light Operated GIRK channel Opener), which is an *ortho*-fluorinated azobenzene photoswitch that enables the optical control of GIRK channels using violet and green light. The red-shifted properties of **VLOGO** improve its suitability for experiments *in vivo* and we therefore envisage that **VLOGO** will be a valuable tool for GIRK channel research.

## Results and discussion

Many methods can be employed to create azobenzene photoswitches that isomerise using visible light.<sup>13</sup> One of the simplest methods is to increase the electron density of the azobenzene moiety by incorporating electron-donating groups in its *para*-position.<sup>14</sup> We initially investigated this avenue by preparing a series of photoswitchable GIRK channel openers (**1–4**)

<sup>a</sup>Department of Chemistry and Center for Integrated Protein Science, Ludwig Maximilians University Munich, Butenandtstraße 5-13, 81377 Munich, Germany. E-mail: dirk.trauner@lmu.de, david.barber@cup.uni-muenchen.de

<sup>b</sup>Center for DNA Nanotechnology, Department of Chemistry and iNANO, Aarhus University, Gustav Wieds Vej 14, 8000 Aarhus C, Denmark  
<sup>c</sup>Max Planck Institute of Neurobiology, Am Klopferspitz 18, 82152 Martinsried, Germany

<sup>d</sup>Department of Pharmacology and Institute of Chemical Biology, Vanderbilt University School of Medicine, Nashville, Tennessee 37232, USA

† Electronic supplementary information (ESI) available: Experimental procedures and characterisation data. See DOI: 10.1039/c6ob02153k

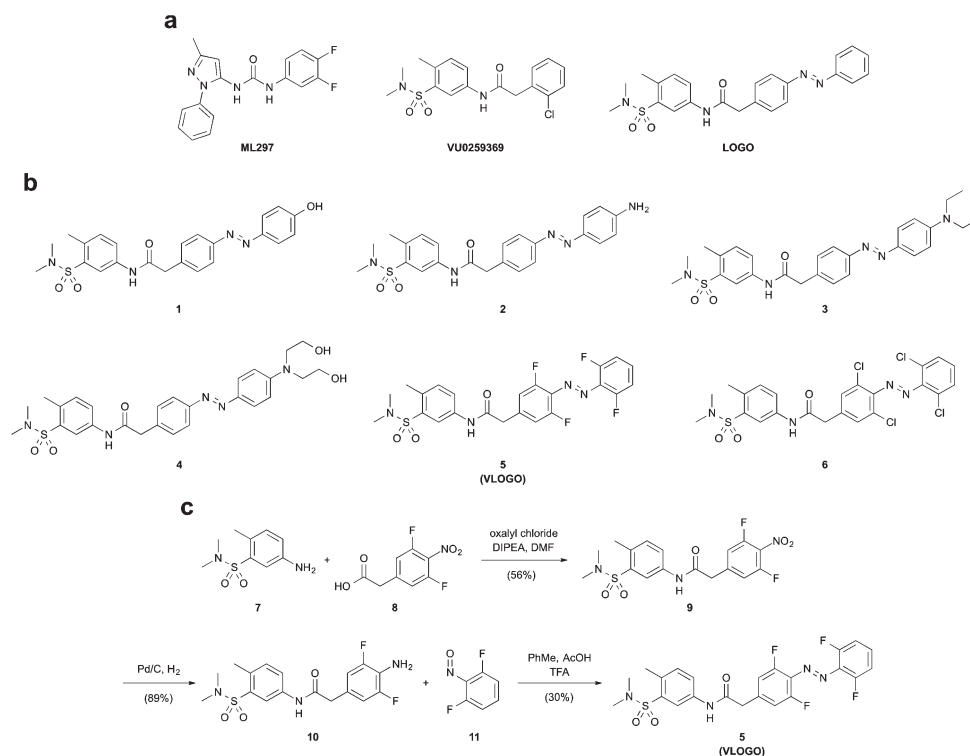


**Fig. 1** Design of the red-shifted photoswitchable GIRK channel agonists **1–6**. (a) Chemical structures of the GIRK channel agonists **ML297** and **VU0259369**, and the photoswitchable GIRK channel agonist **LOGO**. (b) Chemical structures of the red-shifted GIRK channel agonists **1–6**. (c) Synthesis of **VLOGO** using a Mills reaction.

that had electron-donating groups in the 4'-position of the azobenzene (Fig. 1b). This was achieved by forming the diazonium salt of an intermediate aniline and trapping it with a range of electron rich aromatic compounds (Fig. S1†). More recently, several research groups have shown that exchanging the *ortho*-positions of the azobenzene with halogen substituents can create photoswitches that undergo *cis/trans* isomerisation when exposed to long wavelength visible light.<sup>15</sup> We therefore became interested in preparing GIRK channel openers bearing *ortho*-fluoro and *ortho*-chloro substituted azobenzenes. An amide coupling between aniline **7** and acid **8** furnished amide **9**, which was subsequently reduced in the presence of palladium on carbon to afford difluoro aniline **10**. A Mills reaction between difluoro aniline **10** and difluoro nitrosobenzene **11** furnished **VLOGO** in a moderate 30% yield (Fig. 1c). In contrast, the *ortho*-chloro azobenzene **6** was synthesised using a recently reported C–H activation strategy (Fig. S1†).<sup>16</sup>

With our small library of compounds in hand, we determined their optimum photoswitching properties using UV-Vis spectroscopy (Fig. S2†). We then applied this information to our initial compound analysis using patch clamp electrophysiology of GIRK1/2 channels expressed in HEK293T cells (Fig. 2a). Starting with the 4'-substituted azobenzenes **1–4** (Fig. 2a), we observed small amounts of GIRK1/2 channel opening and moderate levels of current modulation upon photoswitching with the 4'-amino azobenzene **2** and the 4'-*N*,

*N*-diethyl azobenzene **3**. In contrast, almost no change in current was observed upon photoswitching using azobenzenes **1** and **4**. We next evaluated **VLOGO** and found it to be an excellent photoswitchable opener of GIRK1/2 channels using 400 and 500 nm light (Fig. 2a). Spurred on by this result we assessed *ortho*-chloro azobenzene **6**. However, we discovered that this photoswitch could not endow GIRK1/2 with significant amounts of light control. This was an unfortunate result, as azobenzene **6** would have allowed longer wavelengths of light to be used for the optical control of GIRK channels. When examining all of the results, it becomes clear that only small modifications to the azobenzene photoswitch are tolerated in order to retain both potent agonism and good photo-switching behaviour at GIRK1/2 channels.

With *ortho*-fluoro azobenzene **VLOGO** identified as our optimal red-shifted photoswitch for GIRK1/2 channels, we further investigated its properties using patch clamp electrophysiology. Firstly, we investigated the action spectrum of **VLOGO** by switching the wavelength between violet light (400 nm) and different wavelengths of blue/green light (440–540 nm), we observed large differences in current (Fig. 2b). The minimal inward current was exhibited when illuminating at 500 nm. In contrast, 440, 460, 480, 520 and 540 nm resulted in more inward current (Fig. S3†). We then established that reversible photoactivation of **VLOGO** (10 μM) is very robust, with almost no loss of photocurrent over many switching cycles (Fig. 2c). The *trans*-isomer of **VLOGO**, which

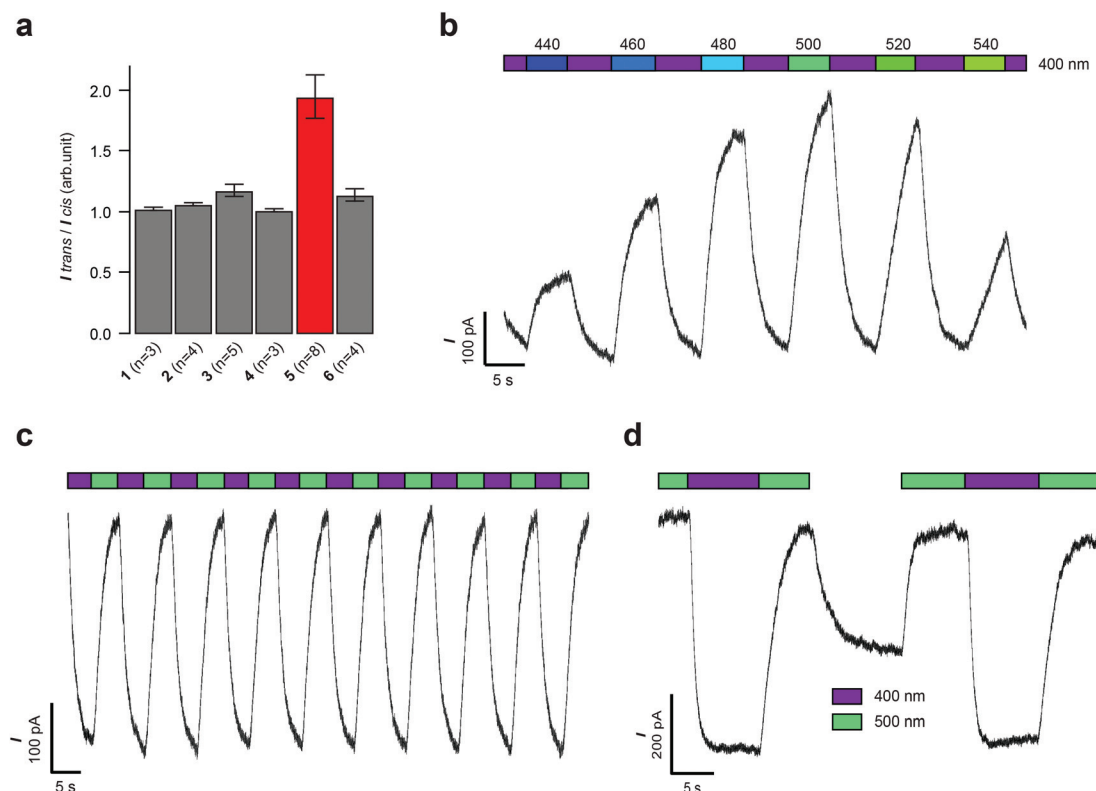


**Fig. 2** Whole-cell patch clamp electrophysiology of HEK293T cells expressing GIRK1/2 channels. (a) Evaluation of compounds 1–6 ( $10\ \mu\text{M}$ ) revealed that **VLOGO** displayed the best photoswitching behaviour ( $n$  = number of experiments). (b) Action spectrum of **VLOGO** ( $10\ \mu\text{M}$ ) showing the precise control of HEK293T cell currents by toggling the illumination wavelength between 400 nm and 440–540 nm. (c) Reversible photoswitching of **VLOGO** ( $10\ \mu\text{M}$ ) recorded in voltage-clamp mode. (d) Observed current increase when no light stimulus is applied to the *cis*-isomer of **VLOGO**. Error bars represent mean  $\pm$  SEM.

predominates in the dark and under violet light (400 nm) illumination, is the most active form of **VLOGO**. Upon photoisomerisation using green light (500 nm), the considerably less active *cis*-isomer of **VLOGO** is formed, causing a reduction in the observed current. When operating in current clamp mode the photoswitching of **VLOGO** was also found to be highly reproducible (Fig. S4†). Lastly, we examined the stability of *cis*-**VLOGO** in the dark (Fig. 2d). After the full *cis*-isomer content had been reached under 500 nm light illumination, **VLOGO** was exposed to dark conditions, quickly resulting in increased inward current. The minimal inward current was achieved again using 500 nm light. This result demonstrates that constant illumination of **VLOGO** is required to maintain the maximum *cis*-isomer content.

Having characterised **VLOGO** using patch-clamp electrophysiology in HEK293T cells, we subsequently evaluated the activity of **VLOGO** towards different GIRK channel subtypes using the thallium flux assay technique (Fig. 3).<sup>17</sup> We found that **VLOGO** activates GIRK channels containing the GIRK1 subunit, whilst not affecting homodimeric GIRK2 channels. **VLOGO** exhibits similar potency at GIRK channels (GIRK1/2:  $\text{EC}_{50} = 2.0 \pm 0.11\ \mu\text{M}$ ; GIRK1/4:  $\text{EC}_{50} = 1.9 \pm 0.06\ \mu\text{M}$ ) as the non-substituted photoswitchable GIRK channel agonist **LOGO**.<sup>9</sup> However, the efficacy of **VLOGO** is significantly reduced (GIRK1/2:  $\%E_{\text{max}} = 49.4 \pm 4.7$ ; GIRK1/4:  $\%E_{\text{max}} = 30.9 \pm 5.2$ ).

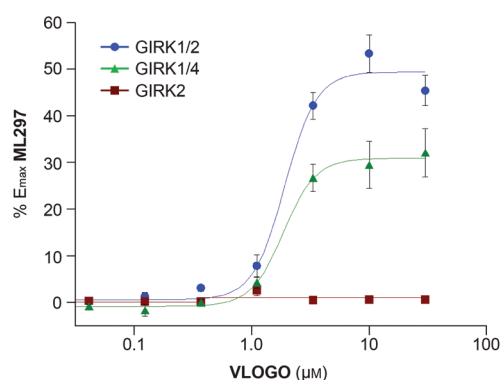


**Fig. 3** Potency, efficacy and selectivity profile of **VLOGO**. Shown are fits to representative data obtained from testing multiple concentrations of **VLOGO** on cell lines stably expressing GIRK1/2 (blue circles), GIRK1/4 (green triangles) and GIRK2 (red squares). The measured potencies for GIRK1/2 and GIRK1/4 were  $2.0 \pm 0.11\ \mu\text{M}$  and  $1.9 \pm 0.06\ \mu\text{M}$ , respectively. Efficacy values were normalised to the maximum activity observed using **ML297** ( $10\ \mu\text{M}$ ) on GIRK1/2-expressing cells. Error bars represent mean  $\pm$  SEM obtained from triplicate wells. Reported potency values represent the mean  $\pm$  SEM obtained from three independent experiments.<sup>18</sup>

After demonstrating that **VLOGO** can optically control cellular currents in HEK293T cells heterologously expressing GIRK1/2 channels, we next investigated if it could be used to



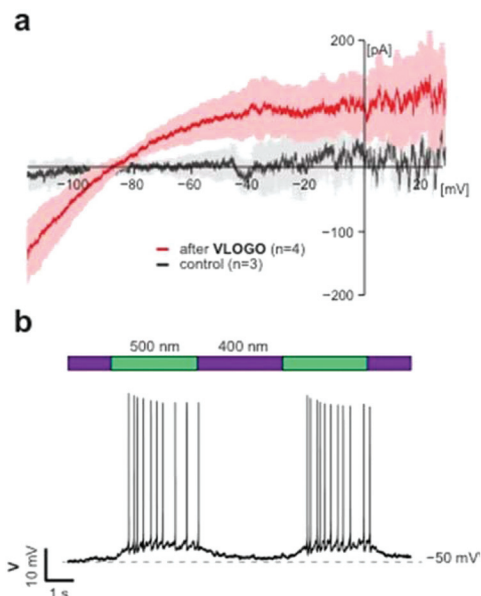


**Fig. 4** Optical control of cell excitability in mouse hippocampal neurons. (a) Current–voltage ( $I$ – $V$ ) relationships indicative of GIRK channels. Black; current–voltage relationship of control neuron ( $n = 3$  cells). Red; current–voltage relationship of **VLOGO** mediated currents under ambient light conditions ( $n = 4$  cells). All recordings were conducted in the presence of tetrodotoxin (TTX) ( $1 \mu\text{M}$ ) using  $-120 \text{ mV}$  to  $+30 \text{ mV}$  voltage ramp over 3 seconds and residual potassium currents were subtracted from the ramp recording. (b) Photoswitching of **VLOGO** in current clamp mode enables the optical control of spontaneous action potential firing. Error bars represent mean  $\pm$  SEM.

control GIRK channels in excitable cells.<sup>19</sup> For this endeavour we conducted electrophysiological experiments on CA1 hippocampal neurons found in acute brain slice preparations from wild type mice. Firstly, we recorded current–voltage ( $I$ – $V$ ) relationships comparing the control traces with those obtained in the presence of **VLOGO** (Fig. 4a). Due to the inwardly rectifying nature of GIRK channels, we would expect to see increasing amounts of inward current as the voltage becomes more negative. After the application of **VLOGO** ( $100 \mu\text{M}$ ) and subsequent wash out, the hippocampal neuron exhibited increasing inward current at voltages lower than  $-90 \text{ mV}$  during a  $-120 \text{ mV}$  to  $+30 \text{ mV}$  voltage ramp. This is indicative of GIRK channel opening.<sup>7</sup> Most importantly **VLOGO** was able to reversibly silence spontaneous action potential firing under violet light ( $400 \text{ nm}$ ) illumination when the hippocampal neurons were held at depolarised potentials (Fig. 4b). Changing the illumination wavelength to  $500 \text{ nm}$  then efficiently restored the action potential firing.

After accomplishing the control of native GIRK channels in mouse hippocampal neurons using **VLOGO**, we investigated if it could be used to optically control the movement of living animals. For these experiments we selected zebrafish larvae (*Danio rerio*) as light can easily be delivered to them due to their transparency.<sup>20</sup> Accordingly, zebrafish larvae 5–7 days post fertilisation were exposed to 2 minute intervals of alternating violet light ( $420 \text{ nm}$ ) and green light ( $520 \text{ nm}$ )

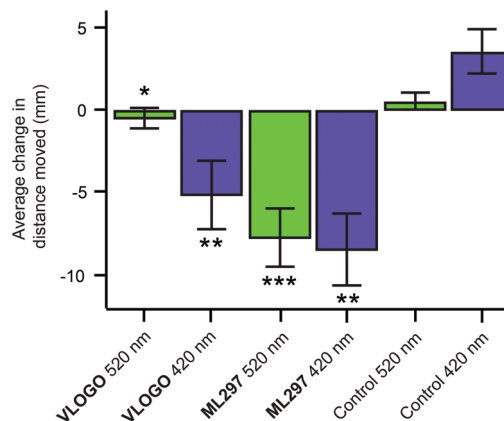


**Fig. 5** Optical control of zebrafish motility in the presence of **VLOGO**. After the application of **VLOGO** ( $100 \mu\text{M}$ ), the swimming activity of the zebrafish larvae was reduced under violet light ( $420 \text{ nm}$ ) illumination and back to baseline under green light ( $520 \text{ nm}$ ) illumination when compared to the control (1% DMSO) zebrafish. Experiments using the non-photoswitchable GIRK opener **ML297** ( $100 \mu\text{M}$ ) showed reduction of the zebrafish motility independent of violet and green light illumination. (**VLOGO**  $n = 18$  zebrafish; **ML297**  $n = 15$  zebrafish; control (1% DMSO)  $n = 15$  zebrafish) (\* n.s. versus control 520 nm; \*\* $P < 0.001$  versus control 420 nm; \*\*\* $P < 0.001$  versus control 520 nm). Error bars represent mean  $\pm$  SEM.

(Fig. S5†). After the first cycle of violet and green light, the distance (mm) that the zebrafish larvae moved in a 10 second time period within a representative section of each 2 minute interval was measured to give the background swimming behaviour for each condition. The zebrafish larvae were then incubated with **VLOGO** ( $100 \mu\text{M}$ ) for 1 hour and the same protocol was used to determine its effect by calculating the change in swimming distance. Pleasingly, the zebrafish larvae showed significantly different swimming distances in the presence of **VLOGO**, which could be modulated by changing the illumination from violet to green light (Fig. 5). The zebrafish larvae exhibited reduced swimming distances when illuminated with violet light compared to the control zebrafish. After illuminating with green light for a total of 2 minutes, the swimming distance of the zebrafish was not significantly different from the control experiment. We then performed additional experiments using the non-photoswitchable GIRK activator **ML297** in an effort to dissect the effect of **VLOGO** from the native responses to violet and green light. These experiments confirmed that there is almost no change in the swimming distances of zebrafish larvae when illumination is changed between violet and green light. This is significantly different from the results obtained using **VLOGO** in conjunction with violet and green light.

## Conclusion

In summary, we have developed a photochromic compound that enables the optical control of GIRK channels using visible light. The photoswitch, **VLOGO**, is transiently active in the



dark and when illuminated with violet light. Green light illumination then rapidly converts it to its significantly less active *cis*-isomer. We have demonstrated that **VLOGO** opens GIRK channels bearing the GIRK1 subunit and that it can be used to optically reduce neuronal excitability in dissociated hippocampal neurons. **VLOGO** also exhibits *in vivo* activity, controlling the motility of zebrafish larvae in a light dependent manner. Future work is concentrated on the development of **VLOGO** as a tool for the optical control of GIRK channels in higher animals.

## Conflict of interest statement

C. D. W. receives royalties from the sale of the thallium-sensitive dye, Thallol, through a licensing agreement between Vanderbilt University and TEFlabs. C. D. W. is an owner of WaveFront Biosciences, the maker of the Panoptic instrument used to perform the thallium flux assays.

## Live subject statement

Animal procedures were in accord with EU and national law and were licensed by the Regierung Oberbayern.

## Acknowledgements

J. B. T. thanks the Danish National Research Foundation Center for DNA Nanotechnology (DNRF81) and Aarhus University, Faculty of Science and Technology for financial support. D. B. K. thanks the Friedrich-Ebert-Stiftung for a PhD scholarship. D. T. was supported by the European Research Council (Advanced Grant 268795). D. T. and H. B. thank the Centre for Integrated Protein Science Munich (CIPSM). D. M. B. thanks the European Commission for a Marie Skłodowska-Curie Intra-European Fellowship (PIEF-GA-2013-627990). We thank Achim Keidel for assistance with the chemical synthesis and Dr. Martin Sumser for helpful discussions during the preparation of this manuscript.

## References

- (a) H. Hibino, A. Inanobe, K. Furutani, S. Murakami, I. Findlay and Y. Kurachi, *Physiol. Rev.*, 2010, **90**, 291–366; (b) C. Lüscher and P. A. Slesinger, *Nat. Rev. Neurosci.*, 2010, **11**, 301–315; (c) N. Dascal and U. Kahanovitch, *Int. Rev. Neurobiol.*, 2015, **123**, 27–85.
- R. Luján, E. Marron Fernandez de Velasco, C. Aguado and K. Wickman, *Trends Neurosci.*, 2014, **37**, 20–29.
- K. B. Walsh, *Front. Pharmacol.*, 2011, **2**, 64.
- (a) F. Lesage, F. Duprat, M. Fink, E. Guillemare, T. Coppola, M. Lazdunski and J. P. Hugnot, *FEBS Lett.*, 1994, **353**, 37–42; (b) G. Krapivinsky, E. A. Gordon, K. Wickman, B. Velimirović, L. Krapivinsky and D. E. Clapham, *Nature*, 1995, **374**, 135–141.
- Y. J. Liao, Y. N. Jan and L. Y. Jan, *J. Neurosci.*, 1996, **16**, 7137–7150.
- (a) J. M. Lewohl, W. R. Wilson, R. D. Mayfield, S. J. Brozowski, R. A. Morrisett and R. A. Harris, *Nat. Neurosci.*, 1999, **2**, 1084–1090; (b) G. Weigl and W. Schreibmayer, *Mol. Pharmacol.*, 2001, **60**, 282–289; (c) T. T. Yow, E. Pera, N. Absalom, M. Heblinski, G. A. Johnston, J. R. Hanrahan and M. Chebib, *Br. J. Pharmacol.*, 2001, **163**, 1017–1033; (d) P. Aryal, H. Dvir, S. Choe and P. A. Slesinger, *Nat. Neurosci.*, 2009, **12**, 988–995.
- (a) K. Kaufmann, I. Romaine, E. Days, C. Pascual, A. Malik, L. Yang, B. Zou, Y. Du, G. Sliwoski, R. D. Morrison, J. Denton, C. M. Niswender, J. S. Daniels, G. A. Sulikowski, X. Xie, C. W. Lindsley and C. D. Weaver, *ACS Chem. Neurosci.*, 2013, **4**, 1278–1286; (b) N. Wydeven, E. Marron Fernandez de Velasco, Y. Du, M. A. Benneyworth, M. C. Hearing, R. A. Fischer, M. J. Thomas, C. D. Weaver and K. Wickman, *Proc. Natl. Acad. Sci. U. S. A.*, 2014, **111**, 10755–10760; (c) S. J. Ramos-Hunter, D. W. Engers, K. Kaufmann, Y. Du, C. W. Lindsley, C. D. Weaver and G. A. Sulikowski, *Bioorg. Med. Chem. Lett.*, 2013, **23**, 5195–5198.
- (a) T. Fehrentz, M. Schönberger and D. Trauner, *Angew. Chem., Int. Ed.*, 2011, **50**, 12156–12182; (b) A. A. Beharry and G. A. Woolley, *Chem. Soc. Rev.*, 2011, **40**, 4422–4437; (c) C. Brieke, F. Rohrbach, A. Gottschalk, G. Mayer and A. Heckel, *Angew. Chem., Int. Ed.*, 2012, **51**, 8446–8476; (d) W. Szymański, J. M. Beierle, H. A. V. Kistemaker, W. A. Velema and B. L. Feringa, *Chem. Rev.*, 2013, **113**, 6114–6178; (e) W. A. Velema, W. Szymanski and B. L. Feringa, *J. Am. Chem. Soc.*, 2014, **136**, 2178–2191; (f) J. Broichhagen, J. A. Frank and D. Trauner, *Acc. Chem. Res.*, 2015, **48**, 1947–1960; (g) A. Damijonaitis, D. M. Barber and D. Trauner, *Neurotransmitter*, 2016, **3**, e1292; (h) M. M. Lerch, M. J. Hansen, G. M. van Dam, W. Szymanski and B. L. Feringa, *Angew. Chem., Int. Ed.*, 2016, **55**, 10978–10999.
- D. M. Barber, M. Schönberger, J. Burgstaller, J. Levitz, C. D. Weaver, E. Y. Isacoff, H. Baier and D. Trauner, *Chem. Sci.*, 2016, **7**, 2347–2352.
- (a) M. Protic-Sabljic, N. Tuteja, P. Munson, J. Hauser, K. Kraemer and K. Dixon, *Mol. Cell. Biol.*, 1986, **6**, 3349–3356; (b) D. Brash, J. Rudolph, J. Simon, A. Lin, G. McKenna, H. Baden, A. Halperin and J. Ponten, *Proc. Natl. Acad. Sci. U. S. A.*, 1991, **88**, 10124–10128; (c) G. Banerjee, N. Gupta, A. Kapoor and G. Raman, *Cancer Lett.*, 2005, **223**, 275–284.
- K. Kalka, H. Merk and H. Mukhtar, *J. Am. Acad. Dermatol.*, 2000, **42**, 389–413.
- C. C. Frazier, *Int. J. Dermatol.*, 1996, **35**, 312–316.
- (a) J. García-Amorós and D. Velasco, *Beilstein J. Org. Chem.*, 2012, **8**, 1003–1017; (b) H. M. Dhammika Bandarab and S. C. Burdette, *Chem. Soc. Rev.*, 2012, **41**, 1809–1825;

- (c) Y. Yang, R. P. Hughes and I. Aprahamian, *J. Am. Chem. Soc.*, 2012, **134**, 15221–15224; (d) Y. Yang, R. P. Hughes and I. Aprahamian, *J. Am. Chem. Soc.*, 2014, **136**, 13190–13193; (e) M. Dong, A. Babalhavaeji, S. Samanta, A. A. Beharry and G. A. Woolley, *Acc. Chem. Res.*, 2015, **48**, 2662–2670; (f) D. Bléger and S. Hecht, *Angew. Chem., Int. Ed.*, 2015, **54**, 11338–11349.
- 14 (a) J. Broichhagen, M. Schönberger, S. C. Cork, J. A. Frank, P. Marchetti, M. Bugliani, A. M. J. Shapiro, S. Trapp, G. A. Rutter, D. J. Hodson and D. Trauner, *Nat. Commun.*, 2014, **5**, 5116; (b) J. Broichhagen, J. A. Frank, N. R. Johnston, R. K. Mitchell, K. Šmid, P. Marchetti, M. Bugliani, G. A. Rutter, D. Trauner and D. J. Hodson, *Chem. Commun.*, 2015, **51**, 6018–6021.
- 15 (a) D. Bléger, J. Schwarz, A. M. Brouwer and S. Hecht, *J. Am. Chem. Soc.*, 2012, **134**, 20597–20600; (b) S. Samanta, A. A. Beharry, O. Sadowski, T. M. McCormick, A. Babalhavaeji, V. Tropepe and G. A. Woolley, *J. Am. Chem. Soc.*, 2013, **135**, 9777–9784; (c) C. Knie, M. Utecht, F. Zhao, H. Kulla, S. Kovalenko, A. M. Brouwer, P. Saalfrank, S. Hecht and D. Bléger, *Chem. – Eur. J.*, 2014, **20**, 16492–16501.
- 16 D. B. Konrad, J. A. Frank and D. Trauner, *Chem. – Eur. J.*, 2016, **22**, 4364–4368.
- 17 C. D. Weaver, D. Harden, S. I. Dworetzky, B. Robertson and R. J. Knox, *J. Biomol. Screening*, 2004, **9**, 671–677.
- 18 The data were acquired using  $494 \pm 10$  nm excitation (20 ms). The excitation wavelength of 494 nm could result in *trans/cis* isomerisation of **VLOGO** compromising the measured values. Therefore, we added a second light pulse at  $405 \pm 10$  nm to ensure that **VLOGO** remained as its *trans*-isomer [ $494 \pm 10$  nm excitation (20 ms) then  $405 \pm 10$  nm (200 ms)].
- 19 H. M. D. Bandara and S. C. Burdette, *Chem. Soc. Rev.*, 2012, **41**, 1809–1825.
- 20 (a) S. Szobota, P. Gorostiza, F. Del Bene, C. Wyart, D. L. Fortin, K. D. Kolstad, O. Tulyathan, M. Volgraf, R. Numano, H. L. Aaron, E. K. Scott, R. H. Kramer, J. Flannery, H. Baier, D. Trauner and E. Y. Isacoff, *Neuron*, 2007, **54**, 535–545; (b) C. Wyart, F. Del Bene, E. Warp, E. K. Scott, D. Trauner, H. Baier and E. Y. Isacoff, *Nature*, 2009, **461**, 407–411; (c) H. Janovjak, S. Szobota, C. Wyart, D. Trauner and E. Y. Isacoff, *Nat. Neurosci.*, 2010, **13**, 1027–1032; (d) J. Levitz, C. Pantoja, B. Gaub, H. Janovjak, A. Reiner, A. Hoagland, D. Schoppik, B. Kane, P. Stawski, A. F. Schier, D. Trauner and E. Y. Isacoff, *Nat. Neurosci.*, 2013, **16**, 507–516.

### 2.3 Light-sheet imaging and graph analysis of antidepressant action in the larval zebrafish brain network

**Burgstaller, J.**, Hindinger, E., Donovan, J., Dal Maschio, M., Kist, A. M., Gesierich, B., Nelson, C., Portugues, R. & Baier, H. (2019). Light-sheet imaging and graph analysis of antidepressant action in the larval zebrafish brain network. *BioRxiv*.

# **Light-sheet imaging and graph analysis of antidepressant action in the larval zebrafish brain network**

Jessica Burgstaller<sup>1</sup>, Elena Hindinger<sup>1</sup>, Joseph Donovan<sup>1</sup>, Marco Dal Maschio<sup>1,3</sup>, Andreas M. Kist<sup>1,4</sup>, Benno Gesierich<sup>2</sup>, Chas Nelson<sup>5</sup>, Ruben Portugues<sup>1</sup>, Herwig Baier<sup>1</sup>

<sup>1</sup>Max Planck Institute of Neurobiology, Am Klopferspitz 18, 82152 Martinsried, Germany

<sup>2</sup>Institute for Stroke and Dementia Research (ISD), University Hospital, LMU Munich, Germany

<sup>3</sup>Current address: Department of Biomedical Sciences, University of Padua, Padua Neuroscience Center, University of Padua via Ugo Bassi 58B, 35131 Padova, Italy

<sup>4</sup>Current address: Department of Phoniatics and Pediatric Audiology, University Hospital Erlangen, Medical School, Friedrich-Alexander-University Erlangen-Nürnberg, Germany

<sup>5</sup>School of Physics and Astronomy, University of Glasgow, United Kingdom

## *Author Note*

Correspondence concerning this article should be addressed to H. B.

(hbaier@neuro.mpg.de).

The authors declare that there are no potential conflicts of interest with respect to the research, authorship, and/or publication of this article.

Article body: 4100 words

Abstract: 247 words

Figures: 6

Box: 1

Table: 1

Supplemental information: 2 Videos

## Abstract

The zebrafish is increasingly being employed as an experimental platform to model neuropsychiatric diseases and to screen for novel neuro-active compounds. While the superb genetic and optical access that this system offers has long been recognized, these features have not been fully exploited to investigate disease mechanisms and possible therapeutic interventions. Here we introduce a light-sheet imaging and graph-theoretical analysis pipeline to determine the effects of the known or suspected antidepressant compounds fluoxetine, ketamine and cycloserine on brain-wide neural activity patterns. We imaged the brains of both wildtype fish and  $gr^{s357}$  mutants, which harbor a missense mutation that abolishes glucocorticoid receptor (GR) transcriptional activity. The  $gr^{s357}$  mutation results in a chronically elevated stress axis together with behavioral endophenotypes of depression. Consistent with broad expression of the glucocorticoid receptor throughout the brain, we show that the mutant fish exhibit an altered correlational structure of resting-state brain activity. Intriguingly, in  $gr^{s357}$  mutant fish, an increased ‘modularity’, which represents the degree of segregation of the network into highly clustered modules, was restored by acute fluoxetine administration to wildtype levels. Ketamine and cycloserine also normalized specific parameters of the graph. Fluoxetine altered network function in the same direction in mutant and wildtype, while ketamine and cycloserine had effects that were opposite for the two genotypes. We propose that light-sheet imaging, followed by graph analysis, is a content-rich and scalable first-pass approach for studying the neural consequences of drug effects and drug x genotype interactions in zebrafish models of psychiatric disorders.

## Introduction

Recent work has highlighted the promise of the zebrafish model to understand mutations in psychiatric disease genes and drug actions (for a review, see Haesemeyer & Schier, 2015). Zebrafish larvae carrying a mutation of the GR ( $gr^{s357}$ ) have a chronically elevated hypothalamic-pituitary-adrenal (HPA) axis due to disruption of negative feedback via cortisol (Fig. 1a). The  $gr^{s357}$  mutants swim less and startle more than wildtype siblings at larval stages. When repeatedly placed into a novel tank, adult mutants fail to habituate and rather exaggerate their behavioral response ('freezing') to this mild stressor. Importantly, their HPA activation and behavior can be normalized by acute or chronic treatment with the selective serotonin reuptake inhibitor (SSRI) fluoxetine (Griffith et al., 2012; Ziv et al., 2013). Moreover, it has been shown that reducing HPA axis activity and enhancing serotonergic transmission via treatment with fluoxetine shifts neuronal responses and processing of food stimuli in the fish (Filosa et al., 2016). One of our goals therefore was to evaluate the potential of fluoxetine to restore altered brain function.

In addition to fluoxetine, we investigated ketamine and cycloserine, two potential antidepressant compounds with different mechanisms of action. Ketamine is a rapid-acting *N*-methyl-D-aspartate (NMDA) receptor antagonist and has recently been approved by the US Food and Drug Administration (FDA) as a nasal spray for the treatment of SSRI-resistant depression. Ketamine has also been shown to modulate zebrafish behavior (Michelotti et al., 2018), although its range of actions in this model system is poorly understood. Cycloserine is a natural antibiotic product of *Streptomyces orchidaceus* and *Streptomyces garyphalus* and has been employed in tuberculosis therapy since the late 1950s (Offe, 1988). Years later it was postulated, and later proven in slice preparations, that the compound influences long-term potentiation, a neuronal mechanism thought to be relevant for learning (Watanabe et al., 1992). Cycloserine is a partial NMDA agonist (Watson et al., 1990); in vivo, it acts like an agonist at low doses, but has antagonistic features at high doses. Its potential for the treatment of neurological and psychiatric conditions, such as major depression, is currently being investigated.

Here we used light-sheet calcium imaging for recording of spontaneous brain-wide activity in zebrafish (Ahrens et al., 2013) and analyzed the correlational

structure of the data with a computational platform based on graph theory. This approach was inspired by work in human functional magnetic resonance imaging (fMRI; Ye et al., 2015), which employs voxel-based graphs to reveal global patterns of brain activity. Recording of tens of thousands of single-cell activity traces generates a deluge of data, and we reasoned that graph analysis offers a relatively straightforward method to extract informative statistical parameters from the resulting adjacency matrix. Using a similar graph-based approach, albeit with far fewer nodes, Avitan et al. (2017) studied the developmental reorganization of spontaneous activity in the tectum. We compared whole-brain functional connectivity in wildtype and *gr<sup>s357</sup>* mutants and detected genotype-linked differences. Finally, we showed that, in line with normalizing *gr<sup>s357</sup>* behavior (Griffith et al., 2012; Ziv et al., 2013), acute fluoxetine administration restored disrupted network parameters in the mutant fish. Ketamine and cycloserine also differentially affected specific parameters of whole-brain functional connectivity. Our experimental workflow, light-sheet imaging followed by first-pass graph analysis, represents a content-rich, sensitive and scalable method to explore genetic and pharmacological alterations of brain-wide network activity in larval zebrafish.

## Results and Discussion

### Light-sheet imaging of resting-state brain activity in larval zebrafish

To record spontaneous (resting state) whole-brain activity, we embedded mutant and wildtype zebrafish larvae, at 6 days post fertilization (dpf), in low-melting agarose gel. The animals carried the transgene *Tg(elavl3:H2B-GCaMP6s)*, encoding a nuclear-localized GCaMP6s under the control of a pan-neuronal promoter (Fig. 1d, e). For each condition, eight *gr<sup>s357</sup>* mutants and eight wildtype fish were imaged at cellular-resolution with a custom-built light-sheet microscope, as described in Methods. Data were acquired in 5 min whole-brain recordings at 2 Hz, resulting in 600 scanned volumes at baseline and after incubation with fluoxetine (20 $\mu$ M), ketamine (20 $\mu$ M) and cycloserine (20 $\mu$ M) for 1.5h and 3h in each fish (Fig. 1b). The concentration of 20 $\mu$ M was chosen to approximate the conditions of small-molecule compound screens in zebrafish larvae (Rihel et al., 2010; Kokel & Peterson, 2011). A

recording time of 5 min was chosen to simulate measurements of resting-state brain activity by fMRI for functional connectivity analysis in human subjects with major depression (Greicius et al., 2007). We reasoned that this time window should be long enough to capture the normally occurring cycles of spontaneous brain activity in zebrafish. Although not tested systematically, drug incubation longer than 3h, or more frequent recordings within the 3 hour time window, appeared to result in inconsistent results, probably caused by stress, drug toxicity, photo-damage in the light-sheet microscope, or combinations thereof. Examples of motion-corrected, but otherwise raw fluorescence signals from single imaging planes are provided in two supplementary movies (Suppl. Movies M1 and M2: mutant and wildtype).

#### Segmentation of brain-wide functional imaging data at single-cell resolution

To examine functional connectivity, four-dimensional imaging stacks (time, x, y, z) were split into time series of single planes and corrected for motion artefacts using a customized version of the CaImAn package (Pnevmatikakis et al., 2017; Giovannucci et al., 2019) (see Methods). Regions of interest (ROIs) were spatial clusters of co-active pixels, likely corresponding to single neurons (Fig. 1f, g) (Portugues et al., 2014). The CaImAn algorithm picked up between 20,000 and 40,000 cells for each fish brain, i. e., ca 25% of all neurons. A subset of them, 10,000 ROIs were selected randomly for further analysis of network properties (Fig. 1g). Subsampling and this reduction in the number of cells analyzed reduced the computational load, and thus CPU time, generated by the high-dimensional connectivity matrix by two orders of magnitude (100 Million vs. 1600 Million matrix components) without noticeably affecting the statistics of the overall network structure, e.g. the degree distribution for different numbers of subsampled neurons (Fig. 2). Functional connectivity was computed as Pearson's correlation coefficients between  $\Delta F/F$  signal time series of these ROIs (Fig. 1h).

#### Analysis of functional imaging data by graph analysis

A powerful way to describe the functional organization of the whole brain is to treat the brain network as a graph. A graph is defined as a mathematical object consisting of a set of items, called nodes, and pairwise relationships between them, called edges (Bollobas, 1998). In our datasets, nodes were defined as the  $10^4$



randomly selected cells (ROIs), and edges were defined by calculating Pearson correlation coefficients between ROI signal time courses. Hence, the entirety of all edges was represented by a  $10^4 \times 10^4$  correlation matrix (Fig. 1h). Because edges from a node to itself are not allowed in simple graphs, the diagonal of each matrix was set to zero and the matrix was thresholded at 0.25, in order to ignore negative edges and remove spurious connections. The threshold of 0.25 was not tested systematically but is commonly used for such analysis because results are not particularly sensitive to the precise value of the threshold chosen. Interactions between network nodes are best described by weighted connections, where the weight indicates the score of correlation and strength of interaction between nodes. Thus, a weighted connectivity matrix was derived to extract neural assemblies from the recordings (see Methods).

Many studies have focused on local properties of networks, such as clustering (Watts & Strogatz, 1998), degree distributions (Barabasi & Albert, 1999; Amaral et al., 2000) and correlations (Pastor-Satorras et al., 2001; Newman, 2002). There have also been studies that examine large-scale properties such as path lengths (Watts & Strogatz, 1998), percolation (Cohen et al., 2000; Callaway et al., 2000) or hierarchy (Ravasz & Barabasi, 2003; Clauset et al., 2008). For our study, we chose the following standard metrics (Box 1): 1) clustering coefficient, 2) characteristic path length, 3) modularity and 4) small-worldness.

#### Differences in functional connectivity between $gr^{s357}$ mutants and wildtype

We explored genotype differences in the dataset after incubation with DMSO in the control condition (Fig. 3). Due to deviations of the data from a normal distribution according to Shapiro Wilk test statistics, non-parametric testing with the Mann-Whitney U test was performed and the  $\alpha$ -level was Bonferroni corrected according to multiple comparisons. The clustering coefficient (Fig. 3a), characteristic path length (Fig. 3c) and small-worldness (Fig. 3d) were not significantly different between  $gr^{s357}$  mutant and wildtype fish at baseline ( $p > 0.05$ ). However, modularity (Fig. 3b) was significantly higher in the  $gr^{s357}$  mutant fish ( $p = 0.007$ ). In an intermediate step of calculating modularity, ROIs were assigned to distinct modules. ROIs that were grouped together within one module based on the calculation were extracted and color-coded to visualize their anatomical location.

Mapping back the ROIs of detected modules to individual fish brains revealed that the number of modules in  $gr^{s357}$  mutant fish was significantly greater compared to wildtype fish at baseline (Fig. 4a, b) ( $p = 0.034$ ). These results suggest that the functional organization of the mutant brain comprises a greater number of relatively more isolated communities of neurons that seem to be diversely distributed across the brain (Fig. 4b). In wildtype fish the modules seem to be rather separated and located in distinct regions, with the forebrain comprising one module and a second module being located in the hindbrain (Fig. 4a). After 1.5h in the setup and incubation with DMSO, the clustering coefficient was significantly lower in the  $gr^{s357}$  mutant compared to the wildtype fish ( $p = 0.005$ ). The same holds true for small-worldness in the brain network ( $p = 0.001$ ). The characteristic path length was significantly higher in the  $gr^{s357}$  mutant fish compared to wildtype ( $p = 0.029$ ). After incubation for 3h, genotype differences were present in all variables. Clustering and small-worldness were significantly lower in the  $gr^{s357}$  mutant fish compared to wildtype ( $p = 0.001$ ;  $p < 10^{-5}$ ), while characteristic path length and modularity were significantly ( $p = 0.011$ ;  $p = 0.008$ ) increased. These results suggest that time spent in the setup seems to differentially affect mutant and wildtype fish. Whilst the mutant fish have a chronically elevated stress level, wildtype fish might naturally respond to the stress experienced during the experimental procedure, which in turn affect network properties. A change in network parameters observed in wildtype, while absent in mutants, may imply a ceiling effect of the stress axis on functional connectivity in the  $gr^{s357}$  brain.

#### Normalization of brain-wide connectivity in the $gr^{s357}$ mutant by fluoxetine

We hypothesized that acute fluoxetine administration might restore network connectivity in  $gr^{s357}$  fish. Indeed, we observed that clustering ( $p = 0.125$ ), characteristic path length ( $p = 0.171$ ), modularity ( $p = 0.476$ ) and small-worldness ( $p = 0.076$ ) were no longer significantly different between fluoxetine-treated mutant and (DMSO-treated) wildtype brains. The same holds true for incubation over 3h, where there is no difference in clustering ( $p = 0.492$ ), characteristic path length ( $p = 0.303$ ), modularity ( $p = 0.090$ ), number of modules ( $p = 0.473$ ) (Fig. 3c) and small-worldness ( $p = 0.235$ ). We propose that acute fluoxetine treatment has the potential to restore whole-brain functional organization of the mutant fish brain, an effect that may

explain the normalizing effect on behavior observed in our earlier study (Griffiths et al., 2012).

When comparing drug effects, we observed that fluoxetine affects all network parameters, albeit not all of them with statistical significance, in the same direction for both genotypes. Incubation with fluoxetine for 3h increased clustering in mutants and wildtype (Fig. 3a; GR DMSO vs. GR fluoxetine:  $p < 10^{-5}$ ; WT DMSO vs. WT fluoxetine:  $p = 0.085$ ), decreased characteristic path length (Fig. 3c; GR DMSO vs. GR fluoxetine:  $p = 0.016$ ; WT DMSO vs. WT fluoxetine:  $p = 0.091$ ), and increased small-worldness (Fig. 3d; GR DMSO vs. GR fluoxetine:  $p = 0.001$ ; WT DMSO vs. WT fluoxetine:  $p = 0.165$ ). Modularity was not significantly different between genotypes after 3h incubation (Fig. 3b; GR DMSO vs. GR fluoxetine:  $p = 0.197$ ; WT DMSO vs. WT fluoxetine:  $p = 0.165$ ). We conclude that there is little, if any, drug x genotype interaction (Table 1), and the direction of fluoxetine's effect on whole-brain functional connectivity is independent of the animal's chronic stress level.

#### Restoration of clustering in $gr^{s357}$ mutants by ketamine

After 1.5h of incubation with ketamine (20 $\mu$ M), clustering (Fig. 5a) was significantly reduced in  $gr^{s357}$  mutants compared to wildtype control ( $p = 0.002$ ). The characteristic path length (Fig. 5c) was increased ( $p = 0.005$ ), modularity (Fig. 5b) was not significantly different ( $p = 0.109$ ), and small-worldness (Fig. 5d) was reduced ( $p = 0.002$ ). After incubation for 3h, there was no difference in clustering ( $p = 0.166$ ), but modularity and characteristic path length were significantly higher in the ketamine treated  $gr^{s357}$  fish compared to wildtype control ( $p = 0.038$ ;  $p = 0.047$ ). Small-worldness was significantly reduced in the mutant brain network ( $p = 0.033$ ). These results suggest that clustering is the network parameter most affected by treatment with ketamine. Since brain networks of ketamine-treated  $gr^{s357}$  mutants show similar clustering as wildtype, we conclude that ketamine reduces segregation and thus enhances the efficiency of local information transfer in the mutant brain. This may be the functional correlate of reduced inhibition in the brain by ketamine acting as an NMDA receptor antagonist.

Interestingly, ketamine differentially affected the two genotypes (Fig. 5). The Kruskal-Wallis test showed that there was a statistically significant difference in

network parameters between genotypes and drug treatments. Significant effects, e.g. for clustering (Chi square = 50.32,  $p < 10^{-5}$ , df = 9) were further explored using post-hoc testing. After incubation for 1.5h with ketamine, clustering (Fig. 5a; GR DMSO vs. GR ketamine:  $p = 0.019$ ) was significantly reduced in  $gr^{s357}$  mutants, while characteristic path length (Fig. 5c; GR DMSO vs. GR ketamine:  $p = 0.049$ ) was increased. In wildtype, clustering (Fig. 5a; WT DMSO vs. WT ketamine:  $p = 0.006$ ) and small-worldness (Fig. 5d; WT DMSO vs. WT ketamine:  $p = 0.003$ ) were significantly reduced after incubation with ketamine compared to the wildtype DMSO control, while characteristic path length (Fig. 5c; WT DMSO vs. WT ketamine:  $p = 0.023$ ) was increased. After 3h incubation with ketamine, we observed higher clustering (Fig. 5a; GR DMSO vs. GR ketamine:  $p = 0.026$ ) and increased small-worldness (Fig. 5d; GR DMSO vs. GR ketamine:  $p = 0.043$ ) in ketamine-treated  $gr^{s357}$  mutant fish compared to the  $gr^{s357}$  mutant DMSO control. In wildtype fish, differences appeared in all network parameters after 3h incubation with ketamine compared to wildtype DMSO control: Clustering (Fig. 5a; WT DMSO vs. WT ketamine:  $p = 0.001$ ) and small-worldness (Fig. 5d; WT DMSO vs. WT ketamine:  $p = 0.000$ ) were significantly reduced, whereas characteristic path length (Fig. 5c; WT DMSO vs. WT ketamine:  $p = 0.002$ ) and modularity (Fig. 5b; WT DMSO vs. WT ketamine:  $p = 0.001$ ) were increased. Thus, we observed a drug x genotype interaction effect (Table 1): Ketamine seems to increase functional connections and efficiency of global and local integration in the mutant. The opposite effect was observed in wildtype fish, where ketamine reduced both clustering and small-world properties of the neuronal network.

#### Restoration of brain network function in $gr^{s357}$ mutants by cycloserine

Cycloserine is an NMDA receptor agonist at low and an NMDA antagonist at high dosages. After 1.5h incubation with cycloserine, statistical tests revealed that there was no significant difference in clustering ( $p = 0.160$ ) (Fig. 6a), characteristic path length ( $p = 0.158$ ) (Fig. 6c), modularity ( $p = 0.428$ ) (Fig. 6b) or small-worldness ( $p = 0.087$ ) (Fig. 6d) between cycloserine treated  $gr^{s357}$  mutants and wildtype controls. After incubation for 3h, clustering was significantly lower in cycloserine treated  $gr^{s357}$  fish compared to the wildtype DMSO control ( $p = 0.004$ ); characteristic path length ( $p = 0.015$ ) and modularity ( $p = 0.01$ ) were increased, whereas small-worldness was

reduced. These results suggest that cycloserine shows similar effects on network parameters as fluoxetine. Network parameters were not significantly different from wildtype control fish after application of the drug. However, this effect was not stable: after 3h of incubation, the normalizing effect of cycloserine disappears. Cycloserine dosage may be decreasing after 1.5h or may reach a concentration at which it acts as an NMDA receptor agonist; therefore, its antidepressant potential may be short-lived.

Kruskal-Wallis test statistics revealed that cycloserine differentially affected *gr<sup>s357</sup>* mutants and wildtype in several network parameters including clustering and small-worldness (Chi square = 47.15,  $p < 10^{-5}$ , df = 9). Incubation for 1.5h with cycloserine, increased clustering (Fig. 6a; GR DMSO vs. GR cycloserine:  $p = 0.028$ ) and small-worldness (Fig. 6d; GR DMSO vs. GR cycloserine:  $p = 0.013$ ) in mutants, but not in wildtype. This effect of cycloserine in mutants disappeared again after 3 hours, while clustering (Fig. 6a; WT DMSO vs. WT cycloserine:  $p = 0.020$ ) and small-worldness (Fig. 6d; WT DMSO vs. WT cycloserine:  $p = 0.002$ ) were reduced, and modularity (Fig. 6b; WT DMSO vs. WT cycloserine:  $p = 0.003$ ) as well as characteristic path length (Fig. 6c; WT DMSO vs. WT cycloserine:  $p = 0.013$ ) were increased in wildtype. These results suggest that, for cycloserine, there is a drug x genotype interaction over the course of the 3h experiment (Table 1). We assume that, after incubation for 1.5h, cycloserine's antagonistic effect is at its peak and decreasing inhibition in the mutant fish brain leads to a highly clustered functional network with augmented local and global efficiency in information processing and integration. In wildtype brains, we could not observe this effect. After 3h incubation, this effect disappeared in the mutant. For wildtype fish, functional connectivity was affected after 3h and network parameters are shifted, but interestingly in the opposite direction as in mutants. At this point, cycloserine may have increased inhibition in the wildtype brain. Due to a potentially higher baseline level of inhibition, this effect was not present in the *gr<sup>s357</sup>* mutant fish.

### Conclusions and outlook

Taken together, our results demonstrate that graph analysis of light-sheet calcium imaging data is suited to reveal the global correlational structure of zebrafish whole-brain activity and has the sensitivity and resolution to detect changes caused by genetic or pharmacological perturbations. The construction of graphs from

automatically segmented neurons allowed us to extract brain-wide network parameters. We propose that exploring drug effects and genotype x drug interactions in a computational pipeline that employs rapid light-sheet imaging followed by a first-pass graph analysis opens up new possibilities for understanding altered brain states in zebrafish larvae. Streamlining and further automating this pipeline may enable a small-molecule compound screen for the identification of novel antidepressants. In the future, this scalable approach can be applied to a variety of zebrafish disease models and tailored interventions in order to accelerate our understanding of disease conditions and their therapies.

## Methods

### Animal care and transgenic lines

All animal procedures conformed to the institutional guidelines of the Max Planck Society and the local government (Regierung von Oberbayern). Experimental protocols were approved by Regierung von Oberbayern (55.2-1-54-2532-41-2016 and 55.2-1-54-2532-31-2016). Fish were raised on a 14h light/10h dark cycle at 28°C according to standard procedures. Transgenic lines carrying the  $gr^{s357}$  mutation were generated as described previously (Ziv et al., 2013), and for imaging purposes crossed to *Tg(elavl3:H2B-GCaMP6s)* obtained from Misha Ahrens (Janelia Research Campus).

### Light-sheet imaging

Larvae ( $gr^{s357/s357}$  or  $gr^{s357/+}$ ; *Tg(elavl3:H2B-GCaMP6s)*) were pre-screened for expression of the genetically encoded calcium sensor GCaMP6s under the fluorescent microscope at 5 dpf. On the following day, fish were embedded in 1.5% low-melting-point agarose (Invitrogen) in a custom-designed, 3D-printed chamber and aligned to a template (see Fig. 1c, d, e). Once hardened, the block of agarose was cut to reduce scattering of the beam and immersed in Danieau's solution to fill a total volume of 3 ml. Embedded larvae were allowed to accommodate in the setup for at least 30 minutes before the start of imaging.

The light-sheet microscope consists of two orthogonal excitation arms for frontal and lateral scanning, and a detection arm for imaging from above. A laser beam (473 nm wavelength, 3-5 mW power) is split by a dichroic mirror and guided to the excitation arms by six dielectric mirrors. Two pairs of mirror galvanometers oscillate horizontally and vertically to create a sheet of light (Fig. 1c) and scan the sample in z, respectively. Two serial lenses act as a pinhole and focus the sheet into the back aperture of a 4x objective. The detection arm consists of a 20x detection objective, a piezoelectric component to adjust the focus (10 V displacement, corresponds to a 400 µm range in z), a tube lens, fluorescence filter and an Orcaflash 4.0 sCMOS camera. The chamber containing the sample sits on a lab jack stage, which is brought into the field of view of the camera by x, y and z actuators.

Spontaneous brain activity of the larvae was imaged with a light sheet microscope at 6 ms exposure time and 30 planes in z, resulting a frequency of 2 Hz per brain volume for a duration of 5 min in each condition. The ventral-dorsal range was specific to every larva, but usually ranged 200 – 224  $\mu\text{m}$ , respectively, resulting in a gap of approximately 7  $\mu\text{m}$  between planes. To minimize file size, a binning of 4x4 pixels was applied, where one pixel width corresponds to 330 nm (before binning) and 1.32  $\mu\text{m}$  (after binning), respectively.

### Drug treatment

In three treatment conditions, the drug compounds (fluoxetine: Sigma-Aldrich, CAS No. 56296-78-7; ketamine: Sigma-Aldrich, CAS No. 1867-66-9; cycloserine: Sigma-Aldrich, CAS No. 68-41-7) were diluted in DMSO and applied in the setup to reach a final concentration of 20 $\mu\text{M}$  for each compound. In the control condition, fish larvae were incubated with DMSO only. Three light sheet recordings were acquired per fish, each lasting 5 min. The first recording was taken right before drug incubation started (baseline condition), and the other two were taken after 1.5 and 3 hours of incubation with the drug or control medium (see Fig. 1b). For image acquisition, genotypes and drug treatments were randomized. We recorded up to three fish per day. Overall data from 64 fish were recorded, 8 for each combination of genotype (8 *gr<sup>s357</sup>* mutants, 8 wildtype) and 4 treatments (3 drugs, control).

### Analysis of functional imaging data

Four-dimensional imaging stacks (time, z, y, x) were split into time series of single planes and corrected for motion artifacts using an adapted version of the CalmAn package (Pnevmatikakis et al., 2017; Giovannucci et al., 2019). In brief, this consists of a rigid transformation, which grossly rotates the images in x and y, followed by an optic flow transformation for finer features. Individual neurons were detected using a procedure described previously (Portugues et al., 2014). In short, regions of interest (ROIs), predominantly corresponding to individual cells, were defined as clusters of co-active pixels, using time series correlations of each pixel with its neighboring pixels (see Fig. 1f, g). The algorithm picked up between 20,000 and 40,000 ROIs for each fish brain, of which 10,000 cells were selected randomly to construct the functional connectivity matrix used for graph analysis. Activity traces of



detected ROIs were only included in the analysis if fluorescence signals varied over the time course of the recording. Thereby, stable auto-fluorescence signals of blood, eye, skin or pigment cells could be eliminated. Functional connectivity was computed as Pearson's correlation coefficients between signal time series of these ROIs (see Fig. 1h). Using MATLAB (R2016b, The MathWorks, Natick, MA) and the Brain Connectivity Toolbox (Rubinov & Sporns, 2010), we then calculated the following graph-theoretic metrics: the clustering coefficient (reflecting functional segregation in the network), the characteristic path length (reflecting functional integration), modularity (reflecting the degree of segregation of the network into highly clustered modules), and small-worldness (reflecting an optimal balance of functional integration and segregation).

#### Statistical analysis of network parameters

The Shapiro-Wilk test was used to test the null hypothesis that data for all variables originate from a normally distributed population. For further analysis non-parametric tests were used, because the test revealed that our data are not normally distributed. Network parameters including the clustering coefficient, modularity, characteristic path length and small-worldness were analyzed for differences between groups of genotypes and drug treatments at baseline and after 1.5h and 3h incubation with the Kruskal-Wallis test using the Python module SciPy. Post-hoc testing with the Mann-Whitney U test was applied to further explore group differences. To correct for multiple comparisons, we used Bonferroni correction. The corrected  $p$  value was obtained by dividing the original  $\alpha$ -value by the number of analyses on the dependent variable. In our dataset we performed two comparisons for each variable, the first between drug treated mutant and DMSO treated wildtype and the second between drug treated and DMSO treated fish within each genotype group. The  $p$  values quoted in the text are already adjusted, where appropriate, according to these corrections.

## Acknowledgments

We thank all members of our laboratory for discussions and support, especially Krasimir Slanchev. Misha Ahrens (Janelia Research Institute) provided the *elavl3:H2B-GCaMP6s* fish. The light-sheet microscope was built with advice from Michael Orger (Champalimaud Institute, Lisbon).

## Author Contributions

J.B. and H.B. conceived and designed the project. J.D., M.D.M., A.M.K. and R.P. set up the light-sheet microscope. J.B. and E.H. performed imaging experiments. J.B. performed graph analysis. B.G. provided MATLAB scripts. J.B. and C.N. performed data analysis. J.B., E.H. and H.B. wrote the manuscript.

## References

- Ahrens, M. B., Orger, M. B., Robson, D. N., Li, J. M., & Keller, P. J. (2013). Whole-brain functional imaging at cellular resolution using light-sheet microscopy. *Nature Methods*, 10(5), 413.
- Amaral, L. A. N., Scala, A., Barthélemy, M., & Stanley, H. E. (2000). Classes of small-world networks. *Proceedings of the National Academy of Sciences*, 97(21), 11149-11152.
- Avitan, L., Pujic, Z., Mölter, J., Van De Poll, M., Sun, B., Teng, H., ... & Goodhill, G. J. (2017). Spontaneous activity in the zebrafish tectum reorganizes over development and is influenced by visual experience. *Current Biology*, 27(16), 2407-2419.
- Barabási, A. L., & Albert, R. (1999). Emergence of scaling in random networks. *Science*, 286(5439), 509-512.
- Bollobas, B. *Modern Graph Theory*. Springer (1998).
- Callaway, D. S., Newman, M. E., Strogatz, S. H., & Watts, D. J. (2000). Network robustness and fragility: Percolation on random graphs. *Physical Review Letters*, 85(25), 5468.

- Clauset, A., Moore, C., & Newman, M. E. (2008). Hierarchical structure and the prediction of missing links in networks. *Nature*, 453(7191), 98.
- Cohen, R., Erez, K., Ben-Avraham, D., & Havlin, S. (2000). Resilience of the internet to random breakdowns. *Physical Review Letters*, 85(21), 4626.
- Filosa, A., Barker, A. J., Dal Maschio, M., & Baier, H. (2016). Feeding state modulates behavioral choice and processing of prey stimuli in the zebrafish tectum. *Neuron*, 90(3), 596-608.
- Giovannucci, A., Friedrich, J., Gunn, P., Kalfon, J., Koay, S. A., Taxidis, J., ... & Chklovskii, D. B. (2018). CaImAn: An open source tool for scalable Calcium Imaging data Analysis. *BioRxiv*.
- Greicius, M. D., Flores, B. H., Menon, V., Glover, G. H., Solvason, H. B., Kenna, H., ... & Schatzberg, A. F. (2007). Resting-state functional connectivity in major depression: abnormally increased contributions from subgenual cingulate cortex and thalamus. *Biological Psychiatry*, 62(5), 429-437.
- Griffiths, B., Schoonheim, P. J., Ziv, L., Voelker, L., Baier, H., & Gahtan, E. (2012). A zebrafish model of glucocorticoid resistance shows serotonergic modulation of the stress response. *Frontiers in Behavioral Neuroscience*, 6, 68.
- Haesemeyer, M., & Schier, A. F. (2015). The study of psychiatric disease genes and drugs in zebrafish. *Current Opinion in Neurobiology*, 30, 122-130.
- Kokel, D., & Peterson, R. T. (2011). Using the zebrafish photomotor response for psychotropic drug screening. In *Methods in Cell Biology* (Vol. 105, pp. 517-524). Academic Press.
- Michelotti, P., Quadros, V. A., Pereira, M. E., & Rosemberg, D. B. (2018). Ketamine modulates aggressive behavior in adult zebrafish. *Neuroscience Letters*, 684, 164-168.

- Newman, M. E. (2002). Assortative mixing in networks. *Physical Review Letters*, 89(20), 208701.
- Offe, H. A. (1988). Historical introduction and chemical characteristics of antituberculosis drugs. In *Antituberculosis Drugs* (pp. 1-30). Springer, Berlin, Heidelberg.
- Pastor-Satorras, R., Vázquez, A., & Vespignani, A. (2001). Dynamical and correlation properties of the Internet. *Physical Review Letters*, 87(25), 258701.
- Pnevmatikakis, E., & Giovannucci, A. (2017). Normcorre: An online algorithm for piecewise rigid motion correction of calcium imaging data. *BioRxiv*.
- Portugues, R., Feierstein, C. E., Engert, F., & Orger, M. B. (2014). Whole-brain activity maps reveal stereotyped, distributed networks for visuomotor behavior. *Neuron*, 81(6), 1328-1343.
- Ravasz, E., & Barabási, A. L. (2003). Hierarchical organization in complex networks. *Physical Review E*, 67(2), 026112.
- Rihel, J., Prober, D. A., Arvanites, A., Lam, K., Zimmerman, S., Jang, S., ... & Schier, A. F. (2010). Zebrafish behavioral profiling links drugs to biological targets and rest/wake regulation. *Science*, 327(5963), 348-351.
- Rubinov, M., & Sporns, O. (2010). Complex network measures of brain connectivity: uses and interpretations. *Neuroimage*, 52(3), 1059-1069.
- Watanabe, Y., Saito, H., & Abe, K. (1992). Effects of glycine and structurally related amino acids on generation of long-term potentiation in rat hippocampal slices. *European Journal of Pharmacology*, 223(2-3), 179-184.
- Watson, G. B., Bolanowski, M. A., Baganoff, M. P., Deppeler, C. L., & Lanthorn, T. H. (1990). D-Cycloserine acts as a partial agonist at the glycine modulatory site of the NMDA receptor expressed in *Xenopus* oocytes. *Brain Research*, 510(1), 158-160.

Watts, D. J., & Strogatz, S. H. (1998). Collective dynamics of ‘small-world’ networks. *Nature*, 393(6684), 440.

Ye, M., Yang, T., Qing, P., Lei, X., Qiu, J., & Liu, G. (2015). Changes of functional brain networks in major depressive disorder: a graph theoretical analysis of resting-state fMRI. *PloS One*, 10(9), e0133775.

Ziv, L., Muto, A., Schoonheim, P. J., Meijsing, S. H., Strasser, D., Ingraham, H. A., ... & Baier, H. (2013). An affective disorder in zebrafish with mutation of the glucocorticoid receptor. *Molecular Psychiatry*, 18(6), 681.

## Figures

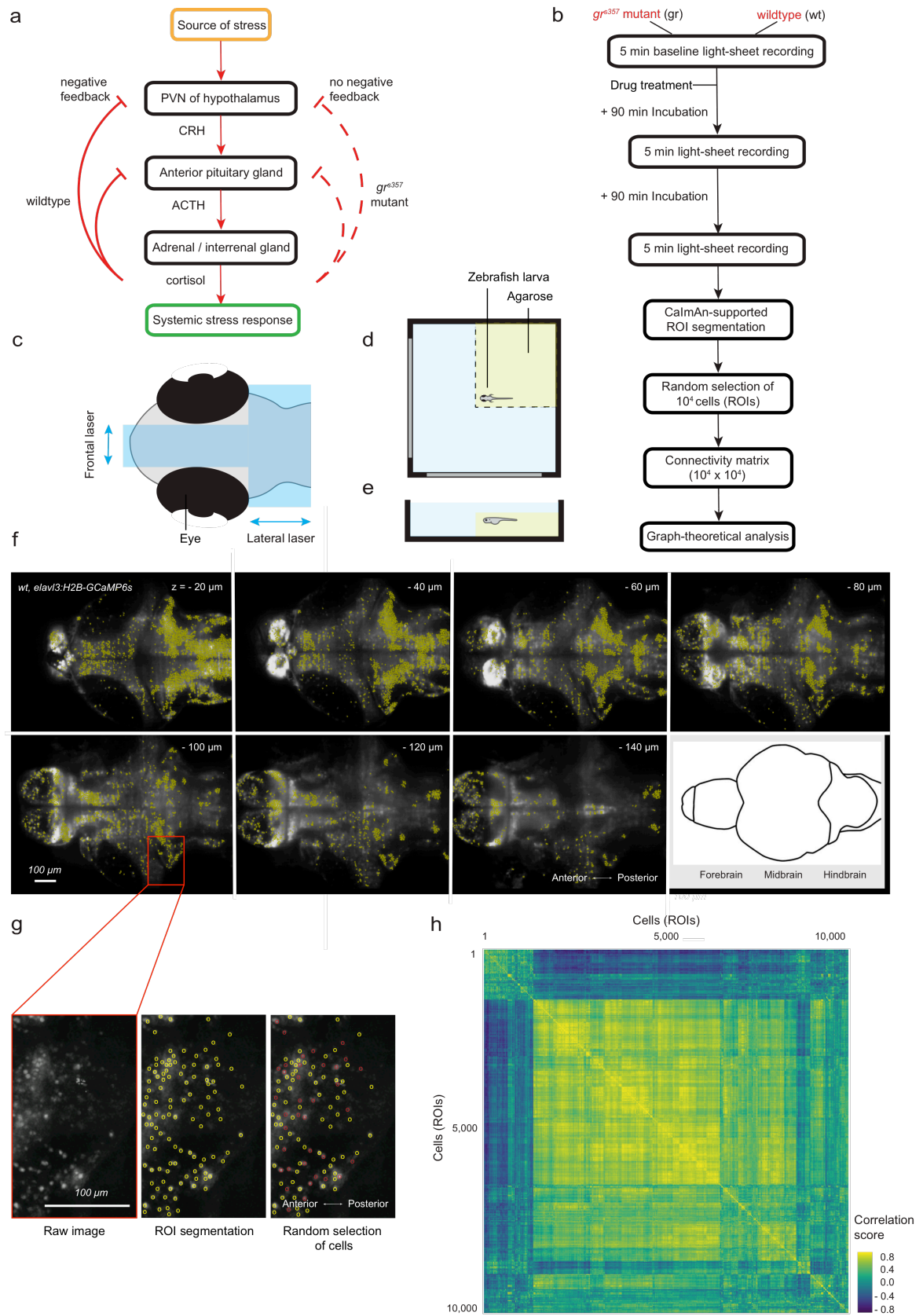


**Figure 1. Experimental workflow.** (a) Dysregulated HPA axis in  $gr^{s357}$  zebrafish mutants. The  $gr^{s357}$  mutation abolishes glucocorticoid receptor transcriptional activity and thus negative feedback on the stress response, which results in a chronically elevated stress axis together with endophenotypes of depression. (b) Experimental workflow. The first light-sheet recording before drug application informs about baseline brain activity of the two genotypes tested ( $gr^{s357}$  mutant, wildtype fish). Thereafter, fish are incubated in the setup for 1.5h with fluoxetine (20 $\mu$ M), ketamine (20 $\mu$ M), or cycloserine (20 $\mu$ M). DMSO serves as vehicle control. Between the second and third recording, fish stay in the setup and incubate for another 1.5h. Graph analysis is applied to all three recordings: 0, 1.5h and 3h drug treatment. (c) Sample preparation in the light-sheet microscope. Laser beam cross (in blue) on head of larva. (d) Top view of embedded larva in a custom chamber. Yellow indicates a block of agarose cut along dashed lines. (e) Side view of larva in chamber. (f) CaImAn-supported ROI detection of neurons in seven representative planes of 30 planes acquired per brain. (g) Close up of cellular resolution before (left) and after ROI detection (middle), and the randomly selected subsample of ROIs in red for further analysis (right). (h) Correlation matrix of functional connectivity. Example of a neuron-to-neuron correlation matrix for fluorescence traces of  $10^4$  randomly selected neurons in one representative fish, as used for network construction and graph analysis of functional connectivity. Neurons were sorted by hierarchical clustering (not shown).



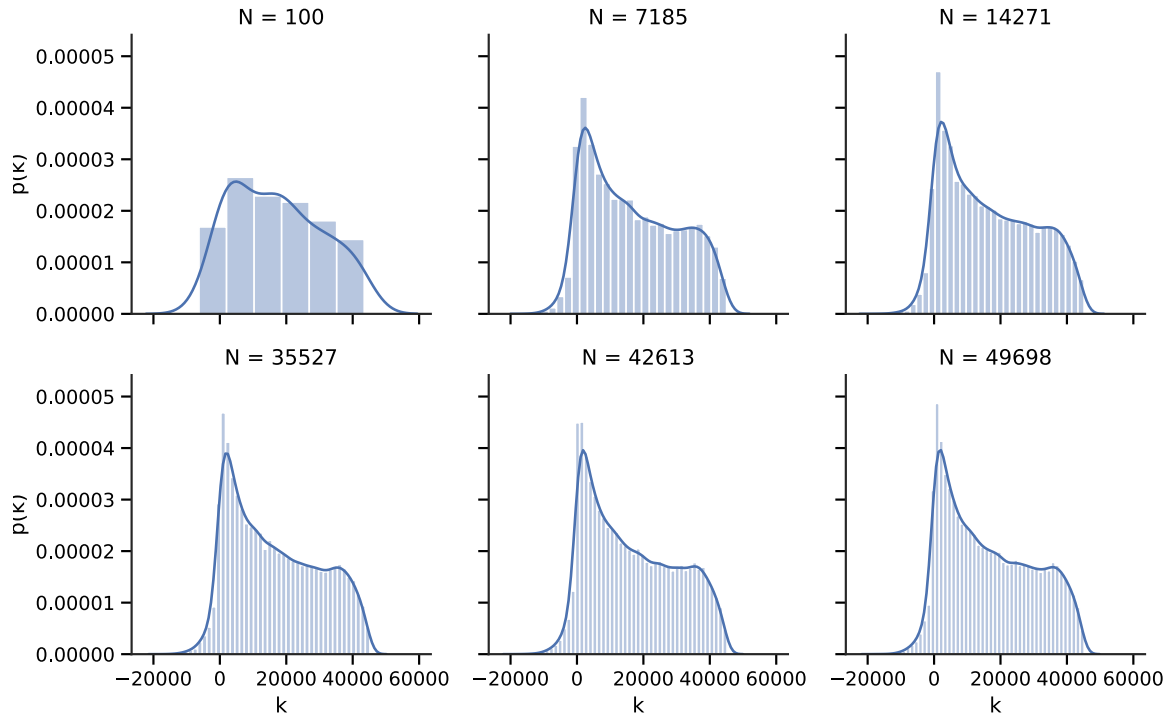


**Figure 2. Degree distribution  $p(k)$  for different numbers of subsampled neurons.** Subsampling and the reduction in the number of cells ( $N$ ) analyzed did not affect the statistics of the overall network structure. (Analysis provided by Chas Nelson, University of Glasgow)

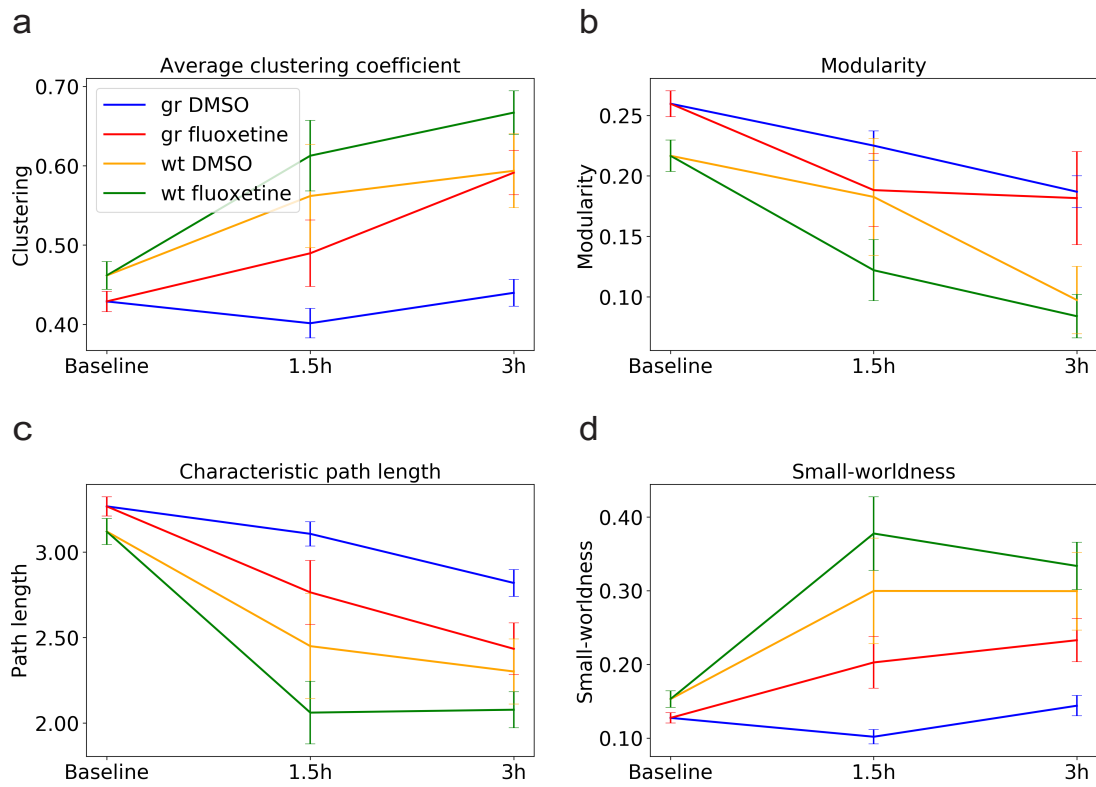
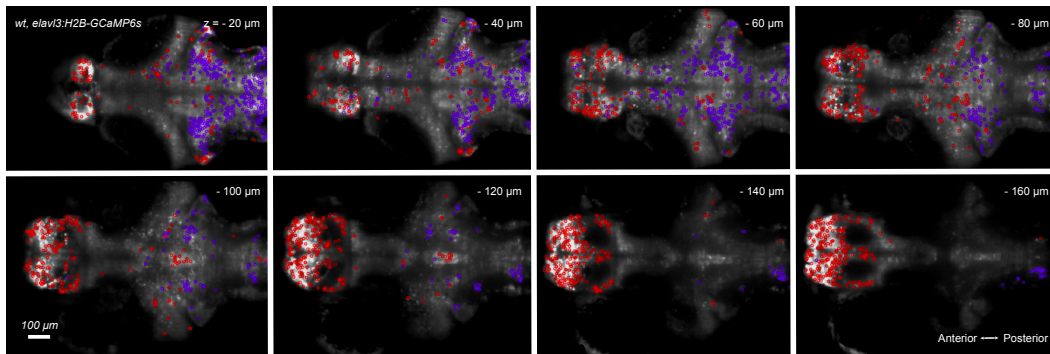


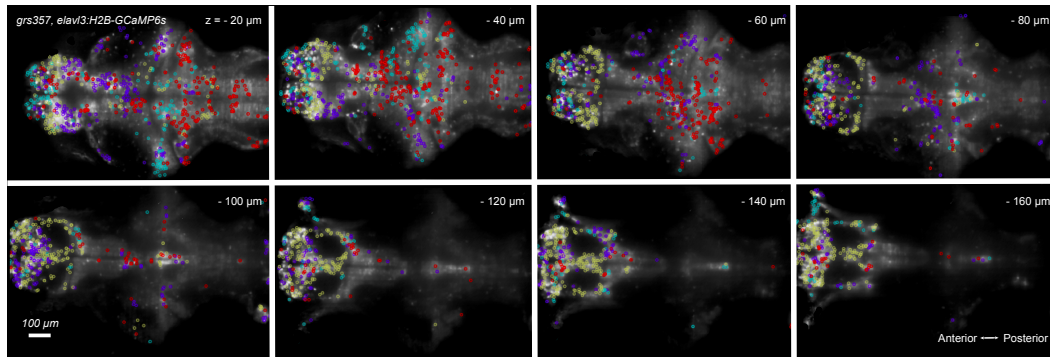
**Figure 3. Effect of genotype and drug treatment with fluoxetine on network parameters.** Mean of the (a) clustering coefficient, (b) modularity, (c) characteristic path length and (d) small-worldness in *gr*<sup>s357</sup> mutant and wildtype (wt) fish before drug treatment (baseline) and after 1.5h and 3h incubation with fluoxetine (20μM) or DMSO. 8 fish were imaged for each combination of genotype (*gr*<sup>s357</sup>, wt) and treatment (fluoxetine, control). Error bars represent the standard error of the mean.

a

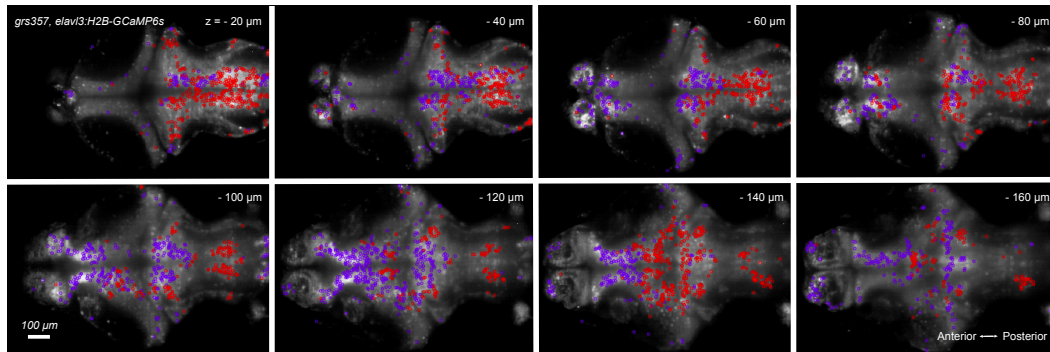
Wildtype (example): 2 modules



b

 $gr^{s357}$  mutant (example): 4 modules

c

 $gr^{s357}$  mutant (example 3h incubation with fluoxetine): 2 modules

**Figure 4. Representative examples of the modular organization of functional brain networks. (a)** Example of a wildtype fish with 2 modules. **(b)** Example of a  $gr^{s357}$  mutant fish with 4 modules. **(c)** Example of a  $gr^{s357}$  mutant fish with 2 modules after 3h incubation with fluoxetine.

**Clustering coefficient:**

The clustering coefficient  $C$  describes the fraction of a node's neighbors that are neighbors of each other. The global level of clustering  $C_g$  in a network is the average of the local clustering coefficients of all the nodes  $n$ .

Clustering on a neuronal level is interpreted as a measure of local efficiency of information transfer.

$$C = \frac{\text{\# of closed triplets}}{\text{total \# of triplets}} ; \quad C_g = \frac{1}{n} \sum_{i=1}^n C_i$$

**Modularity:**

Modularity describes a subdivision of the network into groups of nodes in a way that maximizes the number of within-group edges, and minimizes the number of between-group edges. This metric quantifies the degree to which the network may be subdivided into such groups.

Modules in a neuronal network might correspond to functional circuits that perform certain tasks.

**Characteristic path length:**

The characteristic path length  $l_G$  is the minimum number of edges between two nodes  $v_1, v_2$  in the network. It is a measure of functional integration with shorter paths implying stronger potential for integration. In the brain network it is related to the capability for parallel information propagation.

$$l_G = \frac{1}{n \cdot (n - 1)} \cdot \sum_{i \neq j} d(v_i, v_j)$$

**Small-worldness:**

Small-worldness is a property of networks that are highly clustered, like regular lattices, yet have small characteristic path lengths, like random graphs. Small-world networks possess high local, as well as global, efficiency in signal processing. In our dataset, we calculated small-worldness  $\omega$  as the fraction of the mean clustering coefficient and the mean characteristic path length of the graph. The functional organization of the brain appears to be designed with such small-world network characteristics, because it allows both highly efficient local information processing in specialized modules and global integration at a relatively low wiring cost.

$$\omega = \frac{C_g}{l_G}$$

**Box 1.** Standard metrics for analysis of whole-brain functional connectivity graphs.

	Fluoxetine 1.5h	Fluoxetine 3h	Ketamine 1.5h	Ketamine 3h	Cycloserine 1.5h	Cycloserine 3h
Clustering coefficient	↑↑	↑↑	↓↓	↑↓	↑↓	↓↓
Modularity	↓↓	↓↓	↑↑	↓↑	↓↓	– ↑
Characteristic path length	↓↓	↓↓	↑↑	↓↑	↓↑	– ↑
Small- worldness	↑↑	↑↑	↑↓	↑↓	↑↓	– ↓

**Table 1. Drug-induced changes in  $gr^{s357}$  mutant (left arrow in blue) and wildtype (right arrow in red) network parameters.** Compounds that differentially affected  $gr^{s357}$  mutant and wildtype fish after 1.5h or 3h incubation are highlighted. ↑ indicates an increase in the graph metric; ↓ indicates a decrease; and – indicates no change compared to the genotype-specific DMSO control. Dark arrows indicate statistical significance; light arrows indicate a non-significant trend. Solid green filling indicates a double-sided significant drug x genotype interaction; hatched green indicates a significant interaction in one direction.

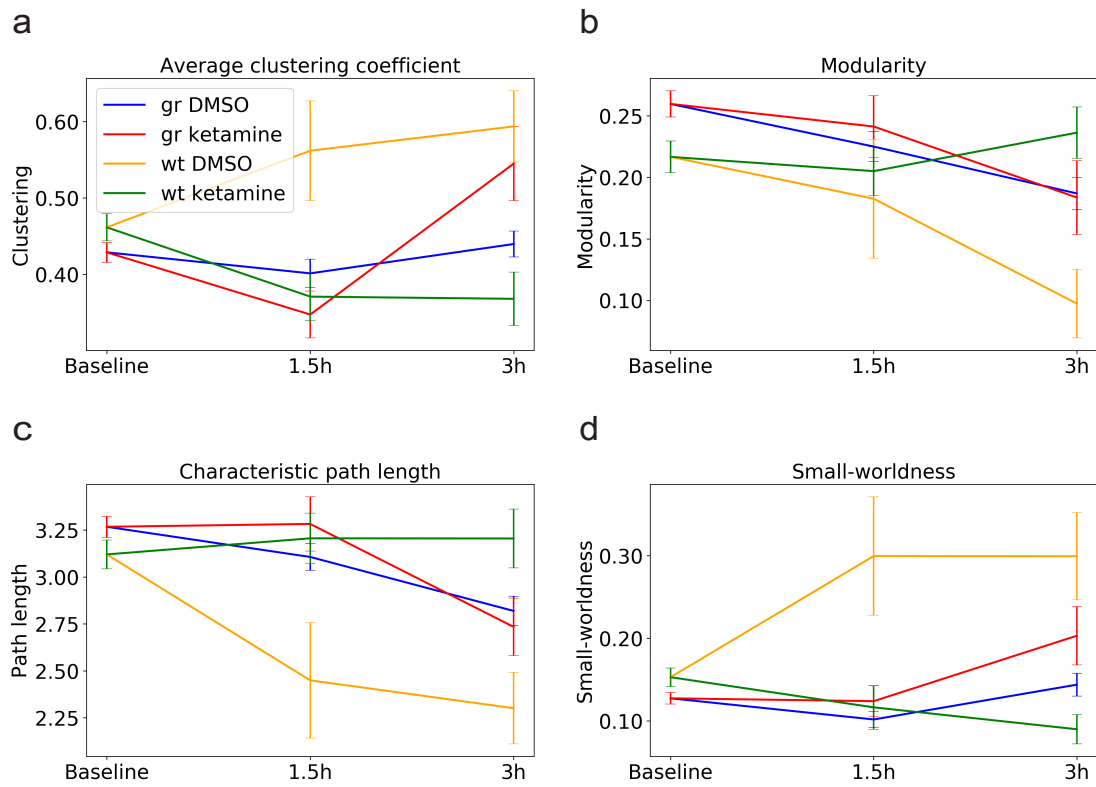


**Figure 5. Effect of genotype and drug treatment with ketamine on network parameters.** Mean of the (a) clustering coefficient, (b) modularity, (c) characteristic path length and (d) small-worldness in *gr*<sup>s357</sup> mutant and wildtype (wt) fish before drug treatment (baseline) and after 1.5h and 3h incubation with ketamine (20μM) or DMSO. 8 fish were imaged for each combination of genotype (*gr*<sup>s357</sup>, wt) and treatment (ketamine, control). Error bars represent the standard error of the mean.

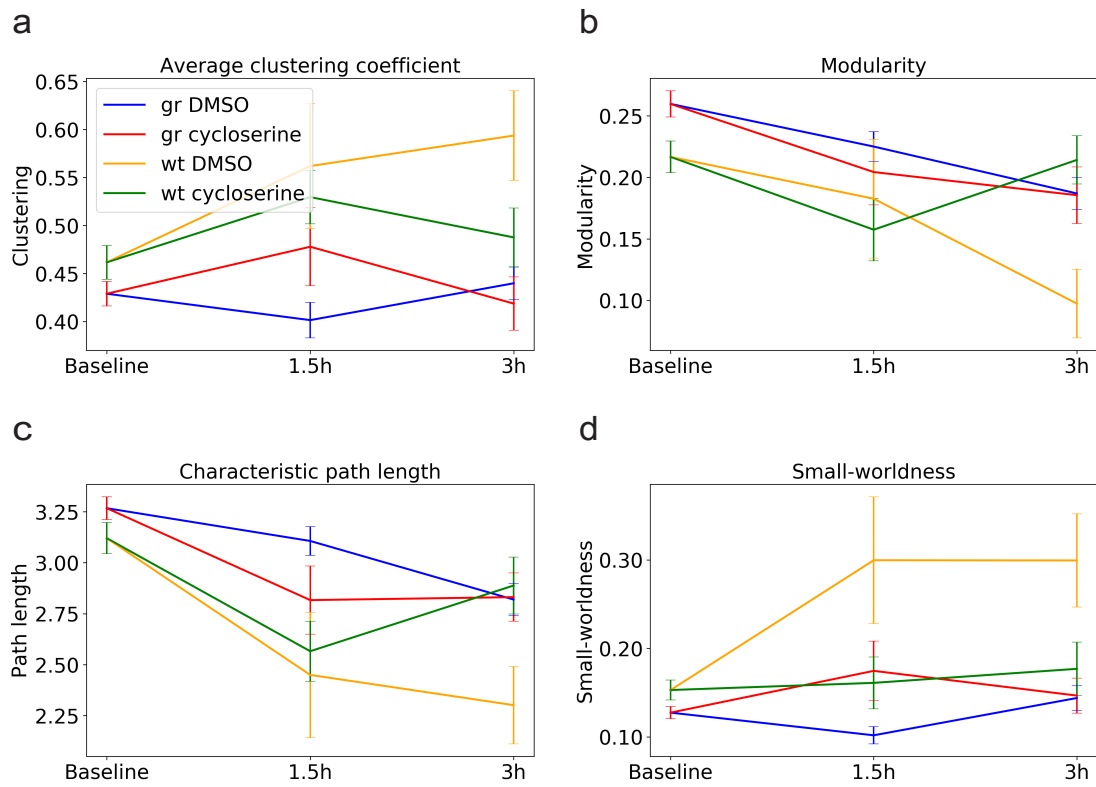


**Figure 6. Effect of genotype and drug treatment with cycloserine on network parameters.** Mean of the (a) clustering coefficient, (b) modularity, (c) characteristic path length and (d) small-worldness in *gr*<sup>s357</sup> mutant and wildtype (wt) fish before drug treatment (baseline) and after 1.5h and 3h incubation with cycloserine (20μM) or DMSO. 8 fish were imaged for each combination of genotype (*gr*<sup>s357</sup>, wt) and treatment (cycloserine, control). Error bars represent the standard error of the mean.

### 3 Discussion and outlook

In the three studies presented in my thesis, I implemented important tools in order to establish the zebrafish as a valuable model organism for drug discovery and testing. In the first (Barber et al, 2016) and second study (Trads et al., 2016), the zebrafish larvae served as a tool to test the effect of a photoswitchable compound on neuronal excitability and its implication in controlling locomotor activity. The developed compound allows optical control of GIRK channels that play a role in balancing excitatory and inhibitory inputs in the brain. The photoswitch is active in the dark and isomerizes to its inactive state upon UV irradiation (Barber et al., 2016). Because UV light is harmful in living organisms, we improved its design to control it with visible light instead (Trads et al., 2016). Using the zebrafish, I performed proof of principle experiments for both compounds and demonstrated their potential to remotely control behavior *in vivo*.

In the third study (Burgstaller et al., 2019), I explored the potential of zebrafish to implement a scalable method to investigate genetic and pharmacological disruptions of whole-brain activity. Performing light-sheet imaging, I recorded spontaneous brain-wide activity (Ahrens et al., 2013) and analyzed its correlational structure with a computational platform based on graph theory (Avitan et al., 2017). Results revealed genotype differences in whole-brain functional connectivity and suggest that, antidepressants differentially affected particular metrics of the activity graphs, with some treatments restoring mutant brain activity to wildtype levels. Importantly, these observations are consistent with the broad expression pattern of the glucocorticoid receptor throughout the brain. With this new scalable approach for studying and quantifying the neural consequences of drug x genotype interactions, the zebrafish presents itself as a powerful model organism to develop drugs and innovative therapies.



### 3.1 Photoswitchable neuroactive compounds in drug discovery

Photopharmacology is an emerging field that focuses on the development of new photoswitchable compounds with two or more isomeric states. Generally, drug development faces many challenges, e.g. poor drug selectivity that results in side effects or drug resistance. Exploration and establishment of selective drugs in pharmacotherapy that can be spatially and temporally controlled in their action is therefore a main goal of clinical research today. Using light to switch between an active and inactive state of specific receptors allows local manipulation of distinct cells in the body. This may circumvent systemic side effects in clinical application. Additionally, these compounds might shed light on biological processes, e.g. enzyme activity, GPCR or functional brain connectivity *in vivo* (Broichhagen et al., 2015; Velema et al., 2014).

In the first publication, we generated a photoswitchable GIRK channel agonist (LOGO), the first synthetic  $K^+$  channel opener that selectively targets GIRK channels. LOGO is active in the dark as its trans-isomer and acts as GIRK channel agonist that efficiently reduces neuronal excitability via hyperpolarization. UV light illumination converts LOGO to its significantly less active cis-isomer which results in membrane potential depolarization of the targeted cell. GIRK channels are ubiquitously expressed throughout the body, especially in the brain. They are an integral part of balancing neuronal excitability and therefore also play a role in psychiatric research, e.g. the study of depression. Because UV irradiation is harmful to living organisms, the second publication was oriented towards improving LOGO in the sense that it can be controlled with less harmful, visible light. This project gave rise to VLOGO, a photoswitchable compound that facilitates further research of GIRK channels *in vivo* because it is active in the dark and rapidly converts to its significantly less active cis-isomer upon green light illumination. In my thesis, I contributed to the development and improvement of these photoswitchable GIRK channel agonists by testing their potential *in vivo*. For both compounds, I was able to show that they successfully allow the control of zebrafish motility in a light dependent manner: in the presence of LOGO or VLOGO, the motility of the zebrafish larvae was significantly reduced in response to activation of GIRK channels with light stimulation. The ability to remotely and non

invasively activate channels, proteins or lipids in the brain of transparent zebrafish allows the study of new potential targets for the treatment of psychiatric diseases in according fish models. Causality of the function of these targets can be inferred from the experimental design because proteins or cell receptors can be switched on and off with these photochemicals. This could spur the development of new classes of drugs with the zebrafish as a powerful model system for drug discovery.

The development and design of photoswitchable compounds that can be controlled in time and space has just started. This procedure comes with a vast amount of molecular structures and a great variety of drug targets to be explored, but also faces many challenges. To begin with, a photoswitchable moiety needs to be present in the compound or it should be possible to incorporate it into the drug of interest without interfering with its biological activity. Additionally, for clinical use, these switches need to be highly selective for the biological target but at the same time thermally and metabolically stable, soluble in water, free of toxins and isomerized in both directions, ideally with harmless light in the range of 600-1200nm. It is also of great interest to consider molecules with two photoisomeric states that differ in their biological activity or target. To guarantee that these molecular switches do not interfere with, e.g. neural processes when in the field of psychiatric research, the development of photocontrolled drugs with fast back-isomerization or isomers with short-lived stability is the route to success (Fehrentz et al., 2011; Velema et al, 2014; Kramer et al., 2013).

The cross-talk between the field of photoswitches and drug development offers a multitude of non-invasive methods to control biological function, e.g. cellular networks and neuronal processes. When reading this thesis the question arises how these compounds can be used in a clinically relevant context in nontransparent organisms. For most applications various studies report efficacy *in vitro*, e.g. diabetes (Broichhagen et al., 2014; Broichhagen et al., 2015; Mehta et al., 2017), pain (Stein et al., 2012; Stein et al., 2013; Mourot et al., 2012) or cancer (Borowiak et al., 2015), yet only very few studies exist on living organisms. Photoswitches have so far most progressed in the field of vision restoration with the advantage of transparency of the human eye. Surprisingly, light delivery through nontransparent tissues is not the greatest challenge in photopharmacology (Gómez-Santacana et al., 2016). Advances in

related fields, e.g. photodynamic therapy approaches or imaging techniques in humans have spurred the development of such photoswitchable compounds. Additionally, new methods in optogenetics with miniaturized wireless and soft optoelectronic systems that can be implanted into the target tissue have greatly contributed to the use of photoswitches *in vivo* (Montgomery et al., 2015; Park et al., 2015; McCall et al., 2017).

The common challenges faced today in drug development should not hinder the attempt to implement photopharmacology in the pharmaceutical industry. For some cases in clinical practice, e.g. when local drug activity without severe side effects is desired, photoswitchable drugs lead the way to numerous new applications and treatment options. For further optimization of the design and spatiotemporal control of photoswitches we have just started to use the zebrafish. It serves as a valuable tool with a bright future to implement photopharmacology in the light of novel therapeutic applications in the clinic.

### **3.2 Emerging roles of light-sheet microscopy combined with graph-theoretical analysis in health and disease**

The main project of my dissertation (Burgstaller et al., 2019) was to explore functional connectivity of the whole-brain in healthy and diseased fish. For this, I performed light-sheet microscopy recordings in combination with application of drugs, which are currently used in stress therapy. Furthermore, I applied the graph-theoretical analysis of neuronal network parameters in different genotypes and response to these treatments. The aim was to demonstrate the potential of the zebrafish as vehicle for investigating mechanism of known pharmaceuticals and to lead the way for discovery of new drugs. For that purpose, I used a combined approach of *in vivo* brain imaging and graph-theoretical analysis.

First, I evaluated the potential of the  $gr^{s357}$  mutant fish to address the research goals mentioned above. This fish line carries a mutation in the glucocorticoid receptor ( $gr^{s357}$ ) and shows a chronically elevated HPA axis together with high levels of cortisol (see Fig. 2). The behavioral phenotype of the  $gr^{s357}$  mutant has been described

by studies previously performed in our laboratory (Griffith et al., 2012; Ziv et al., 2013). These studies have shown that mutants swim less, but show an increased startle response to unknown auditory stimuli compared to wildtype larvae. The fact that their behavior can be normalized by treatment with the SSRI fluoxetine and by commonly prescribed anxiolytics (Griffith et al., 2012; Ziv et al., 2013) gave rise to the questions addressed in my project. The neuroendocrinological parameters and behavioral profile of the  $gr^{s357}$  mutant have been dissected, but what remains to be elucidated is how this mutation affects brain activity. Is there a behavioral correlate in the sense of altered brain function in these fish? And how do the neuroactive compounds that display promising therapeutic effects in the fish act on a neuronal level?

In the first set of *in vivo* imaging experiments, I recorded the brain activity of the  $gr^{s357}$  mutant and wildtype fish at baseline condition (i.e. in absence of external stimuli or pharmacological treatment). Extracting network properties revealed baseline differences in modularity, with  $gr^{s357}$  mutant brains being organized in a greater number of functional modules than wildtype brains. These modules have dense within-connections and sparse between-connections and might correspond to neuronal circuits with specific functions in the brain. These results are consistent with studies performed in human subjects suffering from major depression, where a greater number of modules was found in diseased individuals compared to healthy controls (Ye et al., 2015).

For pharmacological experiments, fish were incubated in the setup for 3h with fluoxetine, ketamine or cycloserine. Additionally, incubation in DMSO for 3h was performed as vehicle control, to quantify the impact of the experimental procedure on functional brain connectivity in  $gr^{s357}$  mutant and wildtype fish. Analysis of the data suggests that  $gr^{s357}$  mutant clustering and small-worldness of the functional connectivity network is reduced while the characteristic path length is increased compared to wildtype fish after 3h. I assume that different effects in both genotypes arise because mutant fish have a chronically elevated level of stress hormones, while wildtype fish might naturally respond during the time course of the experiment by activating their stress axis, which in turn affects network properties. Additionally, ceiling effects of the cortisol level on functional connectivity in the  $gr^{s357}$  mutant fish brain might play a role.

The next set of experiments was performed to explore the potential of fluoxetine to normalize disrupted network properties in  $gr^{s357}$  mutant fish. At baseline measurement, modularity was higher in the  $gr^{s357}$  fish and all parameters describing functional connectivity revealed genotype differences after 3h in the setup. I could show that after treatment with fluoxetine for 1.5h and 3h, network parameters of the functional organization in  $gr^{s357}$  fish were not different from wildtype fish. The results suggest that fluoxetine has the potential to normalize disrupted whole-brain functional connectivity and processing in the diseased fish brain. Despite the increasing number of publications and advances in the study of antidepressants, the exact mechanism of action remains to be elucidated. Furthermore, I did not observe differential effects of the drug in the two genotypes. It has been shown that serotonin acts downstream of signals from the HPA axis activity (Fox & Lowry, 2013; Ziv et al., 2013). Therefore, I assume that fluoxetine action on whole-brain functional connectivity may be independent of the animals' baseline level of stress.

In addition to exploring the SSRI fluoxetine, I focused on the rapid-acting antidepressant ketamine that exerts its antidepressant effect by acting as NMDA receptor antagonist that has been shown to modulate zebrafish behavior (Michelotti et al., 2018). Analysis of the imaging data revealed that brain networks of ketamine treated  $gr^{s357}$  fish show similar clustering as wildtype fish. At baseline measurements with vehicle control this was not the case. This suggests that ketamine increases the clustering coefficient and thereby reduces segregation in the  $gr^{s357}$  fish network structure. In humans ketamine affects glutamatergic and dopaminergic signaling accompanied by transient psychotic symptoms. Thus, the interaction among different neurotransmitters in response to treatment with ketamine seems to be highly complex (Aalto et al., 2005). Because the drug acts as NMDA receptor antagonist, I assume that reduced inhibition in the brain might be the underlying cause for the effects observed in the mutant fish brain (Trullas et al., 1990). Interestingly, in wildtype fish ketamine reduced clustering compared to the vehicle control. There seems to be a drug x genotype interaction that needs to be further defined in future experiments.

Further experiments were performed with cycloserine, a natural antibiotic product of *Streptomyces orchidaceus* and *Streptomyces garyphalus* that acts as NMDA receptor agonist at low and antagonist at high dosages. The drug has previously been

used in tuberculosis therapy. Studies reporting its effect on long-term potentiation, a neuronal mechanism thought to be relevant for learning (Watanabe et al., 1992), triggered the exploration of its potential for the treatment of neurological and psychiatric conditions, e.g. major depression. Incubation with the drug for 1.5h showed similar effects on network parameters as treatment with fluoxetine. After application of the drug for 1.5h, network parameters were not significantly different between  $gr^{s357}$  mutant and wildtype control fish. 3h Incubation however revealed that this effect is not stable over time. Results suggest that after incubation for 1.5h, cycloserine concentration in the fish is at its peak and the compound affects functional connectivity by acting as a NMDA receptor antagonist. Its antidepressant potential however vanishes after 3h. This is in line with paradoxical effects reported about cycloserine facilitating consolidation and retrieval of memory only after acute application of high dosages. Chronic exposure to the drug however leads to desensitization of receptors in the brain and drug effects disappear (Quartermain et al., 1994). I assume, after exposure to the drug for 3h, the fish brain has desensitized or the compound has, at least to some extent, washed out of the fish system and might act as NMDA receptor agonist. In both cases cycloserine might lose its antidepressant potential. Moreover, I observed a drug x genotype interaction over the course of the 3h experiment. Results suggest that incubation for 1.5h with cycloserine leads to a highly clustered functional network with augmented local and global efficiency in information processing and integration in  $gr^{s357}$  mutant fish. I assume that decreased inhibition in the brain due to cycloserine blocking NMDA receptors is responsible for these observations. This effect was not present in wildtype fish. However, after 3h treatment, this effect disappeared in the  $gr^{s357}$  mutant fish. Results suggest that cycloserine has washed out after 3h and might act as NMDA agonist at such low dosages. In contrast, wildtype fish functional connectivity seems to be affected after 3h incubation and network parameters are shifted, interestingly in the opposite direction as in mutants after 1.5h incubation. This might be due to cycloserine's effect as receptor agonist and is only present in the wildtype fish because in the  $gr^{s357}$  mutant, the level of inhibition in the brain is already high at baseline.

Despite the detailed analysis of genotype differences and drug effects on whole-brain functional connectivity presented in this thesis, further investigation is

still necessary for a more detailed analysis of changes in network parameters extracted from the recordings. There are several open questions that remain to be solved. Two limitations of this project however attracted by far the most attention: a) This project investigated functional connectivity of brain networks but did not address any issues concerning structural or anatomical correlates, and b) the experimental protocol was designed to explore resting state whole-brain activity without using a stimulus and therefore does not allow a more concise, regression based analysis of stimulus dependent differences in brain activity between genotypes or treatments.

The first issue raises questions about how these differences manifest on a structural level. Are they confined to overall brain activity, or do regional differences exist? If the latter is the case, can these be defined anatomically, or is only the functional activity and/or coupling affected? To test this, I propose to perform the following: To allow averaging of groups, the individual light-sheet recordings can be registered to a template brain using the Computational Morphometry Toolkit (CMTK), CMTK employs non-rigid transformation followed by morphing algorithms, with 3-4 $\mu$ m accuracy (Randlett et al., 2015). Modules and clustering between functional units can then be mapped back to a standard brain, which allows anatomical localization of differences in functional connectivity and comparison between groups of genotypes or drug treatments.

The other major question concerns the experimental procedure. Here, I acquired resting-state data without a stimulus protocol. Can we observe differences in resting state, and even if so, would a stimulus protocol that induces neural responses reveal further genotype or treatment differences? It is likely and the data also shows that differences in resting state are rather subtle, yet would the addition of a stimulus (visual, auditory, mechanosensory) enhance or suppress those characteristics? We assume the latter, and have thus, for the meantime, concentrated on probing the neural networks involved in resting state. But to test this in the future, we could perform experiments with the *gr*<sup>s357</sup> mutant and wildtype fish that incorporate visual stimuli to identify specific regions in the brain that might show genotype specific activation in response to the environment. These regions could then, in a next step, be optogenetically stimulated and behavior could simultaneously be recorded to establish causal relationships between neuronal activity and its behavioral implementation.

The scalability of light-sheet microscopy for drug discovery has already been successfully demonstrated. Lin et al. (2018) describe an *in vivo* drug screening strategy that combines high-throughput technology to generate large-scale brain activity maps (BAMs) with machine learning for predictive analysis. In their approach, drug effects and potential therapeutic uses can be evaluated based on information-rich BAMs derived from drug-treated zebrafish larvae. From a screen of clinically used drugs, they identified coherent drug clusters that are associated with known therapeutic categories (Lin et al., 2018). However, different incubation times or dosages were not included and analysis was constrained to a projection of whole-brain cell activity in one 2D plane. Our analysis platform provides a valuable complementation of this approach because it allows a much more detailed analysis of functional brain-wide activity and the study of individual drug action beyond simply clustering compounds based on similarity in their effects.

### 3.3 Outlook

I conclude that with my work I could demonstrate the graph-theoretical analysis approach applied to whole-brain data as a successful method to determine changes in functional network connectivity after drug treatment. The identification of a zebrafish model with a mutation in the glucocorticoid receptor has provided an opportunity to study the pathogenesis of depression. Construction of graphs from cells and their functional connections allows the analysis of complex changes in whole-brain network parameters. I propose that exploring genotype x drug interactions in imaging assays with graph-theoretical characterization of functional whole-brain connectivity opens up new possibilities for understanding the depressed brain state and for identifying novel therapeutic avenues for the treatment of stress-related disorders. In the future, this scalable approach with the zebrafish as promising vehicle for drug discovery can be applied to a variety of disease genotypes and compounds to accelerate our understanding of drug action in neurobiology.



## 4 References

- Aalto, S., Ihalainen, J., Hirvonen, J., Kajander, J., Scheinin, H., Tanila, H., ... & Hietala, J. (2005). Cortical glutamate–dopamine interaction and ketamine-induced psychotic symptoms in man. *Psychopharmacology*, 182(3), 375–383.
- Ahrens, M. B., & Engert, F. (2015). Large-scale imaging in small brains. *Current Opinion in Neurobiology*, 32, 78–86.
- Ahrens, M. B., Orger, M. B., Robson, D. N., Li, J. M., & Keller, P. J. (2013). Whole-brain functional imaging at cellular resolution using light-sheet microscopy. *Nature Methods*, 10, 413–420.
- Amaral, L. A. N., Scala, A., Barthelemy, M., & Stanley, H. E. (2000). Classes of small-world networks. *Proceedings of the National Academy of Sciences*, 97(21), 11149–11152.
- Ansorge, M., Hen, R., & Gingrich, J. (2007). Neurodevelopmental origins of depressive disorders. *Current Opinion in Pharmacology* 7, 8–17.
- Artigas, F. (2001). Limitations to enhancing the speed of onset of antidepressants—are rapid action antidepressants possible?. *Human Psychopharmacology: Clinical and Experimental*, 16(1), 29–36.
- Avitan, L., Pujic, Z., Mölter, J., Van De Poll, M., Sun, B., Teng, H., ... & Goodhill, G. J. (2017). Spontaneous activity in the zebrafish tectum reorganizes over development and is influenced by visual experience. *Current Biology*, 27(16), 2407–2419.
- Barabási, A. L., & Albert, R. (1999). Emergence of scaling in random networks. *Science*, 286(5439), 509–512.
- Barber, D. M., Schönberger, M., Burgstaller, J., Levitz, J., Weaver, C. D., Isacoff, E. Y., Baier, H., & Trauner, D. (2016). Optical control of neuronal activity using a light-operated GIRK channel opener (LOGO). *Chemical Science*, 7(3), 2347–2352.

## REFERENCES

---

- Belmaker, R., & Agam, G. (2008). Major Depressive Disorder. *New England Journal of Medicine*, 358, 55–68.
- Bennett, D. V., & Ahrens, M. B. (2016). A practical guide to light sheet microscopy. In *Zebrafish* (pp. 321-331). Humana Press, New York, NY.
- Berton, O., Hahn, C.-G., & Thase, M. E. (2012). Are We Getting Closer to Valid Trans- lational Models for Major Depression? *Science*, 338, 75–79.
- Boccaletti, S., Latora, V., Moreno, Y., Chavez, M., & Hwang, D. U. (2006). Complex networks: Structure and dynamics. *Physics Reports*, 424(4-5), 175-308.
- Borowiak, M., Nahaboo, W., Reynders, M., Nekolla, K., Jalinot, P., Hasserodt, J., ... & Trauner, D. (2015). Photoswitchable inhibitors of microtubule dynamics optically control mitosis and cell death. *Cell*, 162(2), 403-411.
- Broichhagen, J., Frank, J. A., & Trauner, D. (2015). A roadmap to success in photopharmacology. *Accounts of Chemical Research*, 48(7), 1947-1960.
- Broichhagen, J., Schönberger, M., Cork, S. C., Frank, J. A., Marchetti, P., Bugliani, M., ... & Trauner, D. (2014). Optical control of insulin release using a photoswitchable sulfonylurea. *Nature Communications*, 5, 5116.
- Broichhagen, J., Podewin, T., Meyer-Berg, H., Von Ohlen, Y., Johnston, N. R., Jones, B. J., ... & Trauner, D. (2015). Optical control of insulin secretion using an incretin switch. *Angewandte Chemie International Edition*, 54(51), 15565-15569.
- Burgess, H. A., Schoch, H., & Granato, M. (2010). Distinct Retinal Pathways Drive Spatial Orientation Behaviors in Zebrafish Navigation. *Current Biology*, 20(4), 381–386.

## REFERENCES

---

Burgstaller, J., Hindinger, E., Donovan, J., Dal Maschio, M., Kist, A. M., Gesierich, B., Nelson, C., Portugues, R. & Baier, H. (2019). Light-sheet imaging and graph analysis of antidepressant action in the larval zebrafish brain network. *BioRxiv*.

Callaway, D. S., Newman, M. E., Strogatz, S. H., & Watts, D. J. (2000). Network robustness and fragility: Percolation on random graphs. *Physical Review Letters*, 85(25), 5468.

Clauset, A., Moore, C., & Newman, M. E. (2008). Hierarchical structure and the prediction of missing links in networks. *Nature*, 453(7191), 98.

Cohen, R., Erez, K., Ben-Avraham, D., & Havlin, S. (2000). Resilience of the internet to random breakdowns. *Physical Review Letters*, 85(21), 4626.

Cornelisse, L. N., van der Harst, J. E., Lodder, J. C., Baarendse, P. J., Timmerman, A. J., Mansvelder, H. D., ... & Brussaard, A. B. (2007). Reduced 5-HT<sub>1A</sub>- and GABA<sub>B</sub> receptor function in dorsal raphe neurons upon chronic fluoxetine treatment of socially stressed rats. *Journal of Neurophysiology*.

Cruz, H. G., Berton, F., Sollini, M., Blanchet, C., Pravetoni, M., Wickman, K., & Lüscher, C. (2008). Absence and rescue of morphine withdrawal in GIRK/Kir3 knock-out mice. *Journal of Neuroscience*, 28(15), 4069-4077.

Easter, Jr., S. S., & Nicola, G. N. (1996). The Development of Vision in the Zebrafish (*Danio rerio*). *Developmental Biology*, 180(2), 646–663.

Euler, L. (1741). Solutio problematis ad geometriam situs pertinentis. *Commentarii Academiae Scientiarum Petropolitanae*, 128-140.

Euler, L. (1953). Leonhard Euler and the Königsberg bridges. *Scientific American*, 189(1), 66-72.

## REFERENCES

---

- Fehrentz, T., Schönberger, M., & Trauner, D. (2011). Optochemical genetics. *Angewandte Chemie International Edition*, 50(51), 12156-12182.
- Fox, J. H., & Lowry, C. A. (2013). Corticotropin-releasing factor-related peptides, serotonergic systems, and emotional behavior. *Frontiers in Neuroscience*, 7, 169.
- Giovannucci, A., Friedrich, J., Gunn, P., Kalfon, J., Koay, S. A., Taxidis, J., ... & Chklovskii, D. B. (2018). CaImAn: An open source tool for scalable Calcium Imaging data Analysis. *BioRxiv*.
- Gómez-Santacana, X., Pittolo, S., Rovira, X., Lopez, M., Zussy, C., Dalton, J. A., ... & Goudet, C. (2016). Illuminating phenylazopyridines to photoswitch metabotropic glutamate receptors: from the flask to the animals. *ACS Central Science*, 3(1), 81-91.
- Griffiths, B. B., Schoonheim, P. J., Ziv, L., Voelker, L., Baier, H., & Gahtan, E. (2012). A zebrafish model of glucocorticoid resistance shows serotonergic modulation of the stress response. *Frontiers in Behavioral Neuroscience*, 6.
- Harkins, A. B., & Fox, A. P. (2002). Cell death in weaver mouse cerebellum. *The Cerebellum*, 1(3), 201.
- He, Y., & Evans, A. (2010). Graph theoretical modeling of brain connectivity. *Current Opinion in Neurology*, 23(4), 341-350.
- Hibino, H., Inanobe, A., Furutani, K., Murakami, S., Findlay, I. A. N., & Kurachi, Y. (2010). Inwardly rectifying potassium channels: their structure, function, and physiological roles. *Physiological Reviews*, 90(1), 291-366.
- Holsboer, F. (2000). The corticosteroid receptor hypothesis of depression. *Neuropsychopharmacology*, 23(5), 477.

## REFERENCES

---

- Huang, C. L., Slesinger, P. A., Casey, P. J., Jan, Y. N., & Jan, L. Y. (1995). Evidence that direct binding of G $\beta\gamma$  to the GIRK1 G protein-gated inwardly rectifying K<sup>+</sup> channel is important for channel activation. *Neuron*, 15(5), 1133-1143.
- Inanobe, A., Morishige, K. I., Takahashi, N., Ito, H., Yamada, M., Takumi, T., ... & Kurachi, Y. (1995). G $\beta\gamma$  directly binds to the carboxyl terminus of the G protein-gated muscarinic K<sup>+</sup> channel, GIRK1. *Biochemical and Biophysical Research Communications*, 212(3), 1022-1028.
- Jeanneteau, F. D., Lambert, W. M., Ismaili, N., Bath, K. G., Lee, F. S., Garabedian, M. J., & Chao, M. V. (2012). BDNF and glucocorticoids regulate corticotrophin-releasing hormone (CRH) homeostasis in the hypothalamus. *Proceedings of the National Academy of Sciences*, 109, 1305–1310.
- Kobayashi, T., Washiyama, K., & Ikeda, K. (2004). Inhibition of G protein-activated inwardly rectifying K<sup>+</sup> channels by various antidepressant drugs. *Neuropsychopharmacology*, 29(10), 1841.
- Koyrakh, L., Luján, R., Colón, J., Karschin, C., Kurachi, Y., Karschin, A., & Wickman, K. (2005). Molecular and cellular diversity of neuronal G-protein-gated potassium channels. *Journal of Neuroscience*, 25(49), 11468-11478.
- Kramer, R. H., Mourot, A., & Adesnik, H. (2013). Optogenetic pharmacology for control of native neuronal signaling proteins. *Nature Neuroscience*, 16(7), 816.
- Krapivinsky, G., Gordon, E. A., Wickman, K., Velimirović, B., Krapivinsky, L., & Clapham, D. E. (1995). The G-protein-gated atrial K<sup>+</sup> channel I KACH is a heteromultimer of two inwardly rectifying K<sup>+</sup>-channel proteins. *Nature*, 374(6518), 135.

## REFERENCES

---

- Kubo, F., Hablitzel, B., Dal Maschio, M., Driever, W., Baier, H., & Arrenberg, A. B. (2014). Functional architecture of an optic flow-responsive area that drives horizontal eye movements in zebrafish. *Neuron*, 81(6), 1344-1359.
- Labouèbe, G., Lomazzi, M., Cruz, H. G., Creton, C., Luján, R., Li, M., ... & Boyer, S. B. (2007). RGS2 modulates coupling between GABA B receptors and GIRK channels in dopamine neurons of the ventral tegmental area. *Nature Neuroscience*, 10(12), 1559.
- Lesage, F., Duprat, F., Fink, M., Guillemare, E., Coppola, T., Lazdunski, M., & Hugnot, J. P. (1994). Cloning provides evidence for a family of inward rectifier and G-protein coupled K<sup>+</sup> channels in the brain. *FEBS Letters*, 353(1), 37-42.
- Liao, X., Vasilakos, A. V., & He, Y. (2017). Small-world human brain networks: perspectives and challenges. *Neuroscience & Biobehavioral Reviews*, 77, 286-300.
- Liao, Y. J., Jan, Y. N., & Jan, L. Y. (1996). Heteromultimerization of G-protein-gated inwardly rectifying K<sup>+</sup> channel proteins GIRK1 and GIRK2 and their altered expression in weaver brain. *Journal of Neuroscience*, 16(22), 7137-7150.
- Lin, X., Duan, X., Jacobs, C., Ullmann, J., Chan, C. Y., Chen, S., ... & Haggarty, S. J. (2018). High-throughput brain activity mapping and machine learning as a foundation for systems neuropharmacology. *Nature communications*, 9(1), 5142.
- Logothetis, D. E., Kurachi, Y., Galper, J., Neer, E. J., & Clapham, D. E. (1987). The  $\beta\gamma$  subunits of GTP-binding proteins activate the muscarinic K<sup>+</sup> channel in heart. *Nature*, 325(6102), 321.
- Luján, R., de Velasco, E. M. F., Aguado, C., & Wickman, K. (2014). New insights into the therapeutic potential of Girk channels. *Trends in Neurosciences*, 37(1), 20-29.
- Luján, R., Maylie, J., & Adelman, J. P. (2009). New sites of action for GIRK and SK channels. *Nature Reviews Neuroscience*, 10(7), 475.

## REFERENCES

---

- Lüscher, C., Jan, L. Y., Stoffel, M., Malenka, R. C., & Nicoll, R. A. (1997). G protein-coupled inwardly rectifying K<sup>+</sup> channels (GIRKs) mediate postsynaptic but not presynaptic transmitter actions in hippocampal neurons. *Neuron*, 19(3), 687-695.
- Marcus, M., Yasamy, M. T., van Ommeren, M., & Chisholm, D. (2015). Depression: A Global Public Health Concern. Technical report WHO Department of Mental Health and Substance Abuse.
- Marker, C. L., Luján, R., Colón, J., & Wickman, K. (2006). Distinct populations of spinal cord lamina II interneurons expressing G-protein-gated potassium channels. *Journal of Neuroscience*, 26(47), 12251-12259.
- Mazarati, A., Lundström, L., Sollenberg, U., Shin, D., Langel, Ü., & Sankar, R. (2006). Regulation of kindling epileptogenesis by hippocampal galanin type 1 and type 2 receptors: the effects of subtype-selective agonists and the role of G-protein-mediated signaling. *Journal of Pharmacology and Experimental Therapeutics*, 318(2), 700-708.
- McCall, J. G., Qazi, R., Shin, G., Li, S., Ikram, M. H., Jang, K. I., ... & Rogers, J. A. (2017). Preparation and implementation of optofluidic neural probes for in vivo wireless pharmacology and optogenetics. *Nature Protocols*, 12(2), 219.
- Mehta, Z. B., Johnston, N. R., Nguyen-Tu, M. S., Broichhagen, J., Schultz, P., Larner, D. P., ... & Hodson, D. J. (2017). Remote control of glucose homeostasis in vivo using photopharmacology. *Scientific Reports*, 7(1), 291.
- Meloni, E. G., Reedy, C. L., Cohen, B. M., & Carlezon, W. A. (2008). Activation of Raphe Efferents to the Medial Prefrontal Cortex by Corticotropin-Releasing Factor: Correlation with Anxiety-Like Behavior. *Biological Psychiatry*, 63, 832-839.
- Michelotti, P., Quadros, V. A., Pereira, M. E., & Rosemberg, D. B. (2018). Ketamine modulates aggressive behavior in adult zebrafish. *Neuroscience Letters*, 684, 164-168.

## REFERENCES

---

- Montgomery, K. L., Yeh, A. J., Ho, J. S., Tsao, V., Iyer, S. M., Grosenick, L., ... & Poon, A. S. (2015). Wirelessly powered, fully internal optogenetics for brain, spinal and peripheral circuits in mice. *Nature Methods*, 12(10), 969.
- Mourot, A., Fehrentz, T., Le Feuvre, Y., Smith, C. M., Herold, C., Dalkara, D., ... & Kramer, R. H. (2012). Rapid optical control of nociception with an ion-channel photoswitch. *Nature Methods*, 9(4), 396.
- Mukamel, E. A., Nimmerjahn, A., & Schnitzer, M. J. (2009). Automated Analysis of Cellular Signals from Large-Scale Calcium Imaging Data. *Neuron*, 63, 747–760.
- Muto, A., Orger, M. B., Wehman, A. M., Smear, M. C., Kay, J. N., Page-McCaw, P. S., Gahtan, E., Xiao, T., Nevin, L. M., Gosse, N. J., Staub, W., Finger-Baier, K., & Baier, H. (2005). Forward Genetic Analysis of Visual Behavior in Zebrafish. *PLoS Genetics*, 1, e66.
- Naumann, E. A., Kampff, A. R., Prober, D. A., Schier, A. F., & Engert, F. (2010). Monitoring neural activity with bioluminescence during natural behavior. *Nature Neuroscience*, 13(4), 513.
- Neuhauss, S. C., Biehlmaier, O., Seeliger, M. W., Das, T., Kohler, K., Harris, W. A., & Baier, H. (1999). Genetic disorders of vision revealed by a behavioral screen of 400 essential loci in zebrafish. *Journal of Neuroscience*, 19(19), 8603-8615.
- Newman, M. E. (2002). Assortative mixing in networks. *Physical Review Letters*, 89(20), 208701.
- Orger, M. B., & Portugues, R. (2016). Correlating whole brain neural activity with behavior in head-fixed larval zebrafish. In *Zebrafish* (pp. 307-320). Humana Press, New York, NY.
- Orger, M. B., Smear, M. C., Anstis, S. M., & Baier, H. (2000). Perception of Fourier and non- Fourier motion by larval zebrafish. *Nature Neuroscience*, 3(11), 1128–1133.



## REFERENCES

---

- Pariante, C. M., & Lightman, S. L. (2008). The HPA axis in major depression: classical theories and new developments. *Trends in Neurosciences*, 31, 464–468.
- Park, S. I., Brenner, D. S., Shin, G., Morgan, C. D., Copits, B. A., Chung, H. U., ... & Yoon, J. (2015). Soft, stretchable, fully implantable miniaturized optoelectronic systems for wireless optogenetics. *Nature Biotechnology*, 33(12), 1280.
- Pastor-Satorras, R., Vázquez, A., & Vespignani, A. (2001). Dynamical and correlation properties of the Internet. *Physical Review Letters*, 87(25), 258701.
- Pfaffinger, P. J., Martin, J. M., Hunter, D. D., Nathanson, N. M., & Hille, B. (1985). GTP-binding proteins couple cardiac muscarinic receptors to a K channel. *Nature*, 317(6037), 536.
- Pnevmatikakis, E., & Giovannucci, A. (2017). Normcorre: An online algorithm for piecewise rigid motion correction of calcium imaging data. *BioRxiv*.
- Portugues, R., Feierstein, C., Engert, F., & Orger, M. (2014). Whole-Brain Activity Maps Reveal Stereotyped, Distributed Networks for Visuomotor Behavior. *Neuron*, 81, 1328–1343.
- Quartermain, D., Mower, J., Rafferty, M. F., Herting, R. L., & Lanthorn, T. H. (1994). Acute but not chronic activation of the NMDA-coupled glycine receptor with D-cycloserine facilitates learning and retention. *European journal of Pharmacology*, 257(1-2), 7-12.
- Randlett, O., Wee, C. L., Naumann, E. A., Nnaemeka, O., Schoppik, D., Fitzgerald, J. E., Portugues, R., Lacoste, A. M. B., Riegler, C., Engert, F., & Schier, A. F. (2015). Whole-brain activity mapping onto a zebrafish brain atlas. *Nature Methods*, 12, 1039–1046.
- Ravasz, E., & Barabási, A. L. (2003). Hierarchical organization in complex networks. *Physical Review E*, 67(2), 026112.

## REFERENCES

---

- Reuveny, E., Slesinger, P. A., Inglese, J., Morales, J. M., Iñiguez-Lluhi, J. A., Lefkowitz, R. J., ... & Jan, L. Y. (1994). Activation of the cloned muscarinic potassium channel by G protein  $\beta\gamma$  subunits. *Nature*, 370(6485), 143.
- Schweitzer, F., Fagiolo, G., Sornette, D., Vega-Redondo, F., Vespignani, A., & White, D. R. (2009). Economic networks: The new challenges. *Science*, 325(5939), 422-425.
- Siarey, R. J., Carlson, E. J., Epstein, C. J., Balbo, A., Rapoport, S. I., & Galdzicki, Z. (1999). Increased synaptic depression in the Ts65Dn mouse, a model for mental retardation in Down syndrome. *Neuropharmacology*, 38(12), 1917-1920.
- Signorini, S., Liao, Y. J., Duncan, S. A., Jan, L. Y., & Stoffel, M. (1997). Normal cerebellar development but susceptibility to seizures in mice lacking G protein-coupled, inwardly rectifying K<sup>+</sup> channel GIRK2. *Proceedings of the National Academy of Sciences*, 94(3), 923-927.
- Simon, G. E. (2003). Social and economic burden of mood disorders. *Biological Psychiatry*, 54, 208–215.
- Slesinger, P. A., Stoffel, M., Jan, Y. N., & Jan, L. Y. (1997). Defective  $\gamma$ -aminobutyric acid type B receptor-activated inwardly rectifying K<sup>+</sup> currents in cerebellar granule cells isolated from weaver and Girk2 null mutant mice. *Proceedings of the National Academy of Sciences*, 94(22), 12210-12217.
- Stein, M., Breit, A., Fehrentz, T., Gudermann, T., & Trauner, D. (2013). Optical control of TRPV1 channels. *Angewandte Chemie International Edition*, 52(37), 9845-9848.
- Stein, M., Middendorp, S. J., Carta, V., Pejo, E., Raines, D. E., Forman, S. A., ... & Trauner, D. (2012). Azo-propofols: photochromic potentiators of GABAA receptors. *Angewandte Chemie International Edition*, 51(42), 10500-10504.

## REFERENCES

---

- Streisinger, G., Walker, C., Dower, N., Knauber, D., & Singer, F. (1981). Production of clones of homozygous diploid zebra fish (*Brachydanio rerio*). *Nature*, 291(5813), 293.
- Torrecilla, M., Marker, C. L., Cintora, S. C., Stoffel, M., Williams, J. T., & Wickman, K. (2002). G-protein-gated potassium channels containing Kir3. 2 and Kir3. 3 subunits mediate the acute inhibitory effects of opioids on locus ceruleus neurons. *Journal of Neuroscience*, 22(11), 4328-4334.
- Trads, J. B., Burgstaller, J., Laprell, L., Konrad, D. B., Weaver, C. D., Baier, H., ... & Barber, D. M. (2017). Optical control of GIRK channels using visible light. *Organic & Biomolecular Chemistry*, 15(1), 76-81.
- Trevelyan, A. J., & Watkinson, O. (2005). Does inhibition balance excitation in neocortex?. *Progress in Biophysics and Molecular Biology*, 87(1), 109-143.
- Trullas, R., & Skolnick, P. (1990). Functional antagonists at the NMDA receptor complex exhibit antidepressant actions. *European Journal of Pharmacology*, 185(1), 1-10.
- Urani, A., Chourbaji, S., & Gass, P. (2005). Mutant mouse models of depression: Candidate genes and current mouse lines. *Neuroscience & Biobehavioral Reviews*, 29, 805–828.
- Ustun, T. B. (2004). Global burden of depressive disorders in the year 2000. *The British Journal of Psychiatry*, 184, 386–392.
- Velema, W. A., Szymanski, W., & Feringa, B. L. (2014). Photopharmacology: beyond proof of principle. *Journal of the American Chemical Society*, 136(6), 2178-2191.
- Watts, D. J., & Strogatz, S. H. (1998). Collective dynamics of ‘small-world’ networks. *Nature*, 393(6684), 440.

## REFERENCES

---

- Wickman, K. D., Iñiguez-Lluhi, J. A., Davenport, P. A., Taussig, R., Krapivinsky, G. B., Linder, M. E., ... & Clapham, D. E. (1994). Recombinant G-protein  $\beta\gamma$ -subunits activate the muscarinic-gated atrial potassium channel. *Nature*, 368(6468), 255.
- Willner, P., Scheel-Krüger, J., & Belzung, C. (2013). The neurobiology of depression and antidepressant action. *Neuroscience & Biobehavioral Reviews*, 37, 2331–2371.
- Yamada, M., Inanobe, A., & Kurachi, Y. (1998). G protein regulation of potassium ion channels. *Pharmacological Reviews*, 50(4), 723-757.
- Ye, M., Yang, T., Qing, P., Lei, X., Qiu, J., & Liu, G. (2015). Changes of functional brain networks in major depressive disorder: a graph theoretical analysis of resting-state fMRI. *PloS one*, 10(9), e0133775.
- Ziv, L., Muto, A., Schoonheim, P. J., Meijsing, S. H., Strasser, D., Ingraham, H. A., Schaaf, M. J. M., Yamamoto, K. R., & Baier, H. (2013). An affective disorder in zebrafish with mutation of the glucocorticoid receptor. *Molecular Psychiatry*, 18, 681–691.

## 5 APPENDIX

## Acknowledgements

First of all, I thank Herwig for being the first supervisor of my PhD thesis, for his inspiring broad knowledge and the freedom he gave me, to follow my curiosity and to work on a project that I am deeply passionate about. Thanks for your guidance and for constantly challenging and motivating me. Further, I express my appreciation to Jason and Chadi, my TAC members, for their scientific advice and constructive supervision during my PhD project. Special thanks goes to Swantje and Anja for carefully reading my thesis. Moreover, I very much thank Krasimir for guiding me through the first years of my PhD and introducing me to the zebrafish model system. I also very much thank Robert for all the time he spent with me setting up the light-sheet microscope and Thomas for our very special breaks and your scientific input. Irene, thanks for your open ears and your open heart. I admire your positive attitude and very much enjoyed every day with you in the lab. Thank you for all your help and the great moments and fun we had as partners in crime in our drug business!

I am very grateful for all my friends who always support me. There is the whole family: Ibi, Lisa, Julia, Conny, Miri, Anja, Tine...just to name a few. There would be no thesis without you always reminding me of what is really important in life. #liebeundbier

I very much thank my brother Domi for being someone I can always look up to. Lisa, thank you so much for your support during highs and lows in the final phase of my PhD and for clearing my mind, helping me to stay focused and motivated. Thanks for the warmhearted home, the beautiful life that we share and the awesome meals you always prepare for me. My deepest gratitude belongs to Isabel. Thank you for your sincere friendship. You are my best companion, you mean the world to me and I don't know what I'd do without you in my life.

*“Wie ermutigend, dir zu begegnen. Worte mit dir zu wechseln,  
die eine Tiefe haben in der die ganze Welt Platz hat”*

Mam, without you, I wouldn't be who I am or where I am today. You inspire me. Thank you for your endless love, support and your everlasting belief and trust in me. I hope that one day I can be as good of a mom as you are.

## Curriculum vitae

### Jessica Burgstaller

Born in Munich, Germany

#### Education

10/2013 – 12/2019	Fast-Track PhD program at the Graduate School of Systemic Neurosciences (GSN)
10/2013 – 08/2015	Master of Science in Clinical Psychology and Cognitive Neuroscience (LMU) Degree: Master of Science (1.15)
10/2010 – 08/2013	Bachelor of Science in Psychology (LMU) Degree: Bachelor of Science (1.28)
10/2008 – 08/2011	Bachelor of Pharmaceutical Sciences (LMU) Degree: Bachelor of Science (1.53)
09/1999 – 06/2008	Oskar-Maria-Graf Gymnasium, Neufahrn Graduation Certificate: Allgemeines Abitur (1.3)

#### Research experience

10/2014 – 10/2019	Max-Planck-Institute for Neurobiology, Martinsried PhD Student in the department: Genes-Circuits-Behavior Evaluation of the use of a zebrafish model with mutation in the glucocorticoid receptor for research into the pathogenesis of depression
05/2014 – 09/2014	Max-Planck Institute for Psychiatry, Munich Investigation of acute and long-lasting consequences of early life stress in a mouse model with special emphasis on ultrasonic pup vocalizations
07/2013 – 09/2013	Campus Charité Mitte, Berlin Introduction to psychological investigation procedures at the Department of Psychiatry and Psychotherapy. Diagnostic procedures in the fields of personality disorders, autism spectrum disorders and neuropsychological disorders
03/2012 – 04/2012	Max-Planck Institute for Psychiatry, Munich Investigation of the neuronal circuits impaired in depressive diseases and searching for new putative molecular targets for the development of more effective antidepressant therapies

## List of publications

McIlwrick, S., Rechenberg, A., Matthes, M., **Burgstaller, J.**, Schwarzbauer, T., Chen, A., & Touma, C. (2016). Genetic predisposition for high stress reactivity amplifies effects of early-life adversity. *Psychoneuroendocrinology*, 70, 85-97.

Barber, D. M., Schönberger, M., **Burgstaller, J.**, Levitz, J., Weaver, C. D., Isacoff, E. Y., ... & Trauner, D. (2016). Optical control of neuronal activity using a light-operated GIRK channel opener (LOGO). *Chemical Science*, 7(3), 2347-2352.

Trads, J. B., **Burgstaller, J.**, Laprell, L., Konrad, D. B., Weaver, C. D., Baier, H., ... & Barber, D. M. (2017). Optical control of GIRK channels using visible light. *Organic & Biomolecular Chemistry*, 15(1), 76-81.

**Burgstaller, J.**, Paulus, M., & Pfundmair, M. (2019). Oxytocin promotes action prediction. *Hormones and Behavior*, 107, 46-48.

Pfundmair, M., Schindler, S., & **Burgstaller, J.** (2019). The role of oxytocin in terror management processes. *Psychoneuroendocrinology*.

**Burgstaller, J.**, Hindinger, E., Donovan, J., Dal Maschio, M., Kist, A. M., Gesierich, B., Nelson, C., Portugues, R. & Baier, H. (2019). Light-sheet imaging and graph analysis of antidepressant action in the larval zebrafish brain network. *BioRxiv*.



## Affidavit

### Eidesstattliche Versicherung

Hiermit versichere ich an Eides statt, dass ich die vorliegende Dissertation “Neuroactive drug discovery in the larval zebrafish” selbstständig angefertigt habe, mich außer der angegebenen keiner weiteren Hilfsmittel bedient und alle Erkenntnisse, die aus dem Schrifttum ganz oder annähernd übernommen sind, als solche kenntlich gemacht und nach ihrer Herkunft unter Bezeichnung der Fundstelle einzeln nachgewiesen habe.

I hereby confirm that the dissertation “Neuroactive drug discovery in the larval zebrafish” is the result of my own work and that I have only used sources or materials listed and specified in the dissertation.

München, den 3. Mai 2019

---

Jessica Burgstaller

## Author contributions

Barber, D. M., Schönberger, M., **Burgstaller, J.**, Levitz, J., Weaver, C. D., Isacoff, E. Y., Baier, H. & Trauner, D. (2016). Optical control of neuronal activity using a light-operated GIRK channel opener (LOGO). *Chemical Science*, 7(3), 2347-2352.

## Author contributions

D.T. supervised the research. D.M.B, M.S. and D.T. conceived and designed the study. D.M.B performed the chemical synthesis and the UV-Vis spectroscopy. D.M.B and M.S. performed the HEK cell electrophysiology experiments. J.L. and E.Y.I. performed the dissociated hippocampal neuron electrophysiology experiments. **J.B.** and H.B. performed the zebrafish motility experiments. B.N. performed the rat in vivo electrophysiology experiments. C.D.W. performed the thallium flux assays. D.M.B and D.T. wrote the manuscript with input from all of the authors.

Trads, J. B., **Burgstaller, J.**, Laprell, L., Konrad, D. B., Weaver, C. D., Baier, H., ... & Barber, D. M. (2017). Optical control of GIRK channels using visible light. *Organic & Biomolecular Chemistry*, 15(1), 76-81.

## Author contributions

D.M.B. and D.T. conceived, designed and supervised the study. J.B.T., D.M.B. and D.B.K. performed the chemical synthesis. J.B.T. and D.M.B. performed the HEK293T cell electrophysiology experiments. L.O.R. performed the cell culture work and the HEK293T transfections. L.L. performed electrophysiology experiments in acute brain slice preparations. **J.B.** performed and H.B. supervised the zebrafish motility experiments. C.D.W. performed the thallium flux assays. D.M.B. and D.T. wrote the manuscript with input from all of the authors.

**Burgstaller, J.**, Hindinger, E., Donovan, J., Dal Maschio, M., Kist, A. M., Gesierich, B., Nelson, C., Portugues, R. & Baier, H. (2019). Light-sheet imaging and graph analysis of antidepressant action in the larval zebrafish brain network. *BioRxiv*.

The version presented here was published in BioRxiv on 26.04.2019.

### **Author contributions**

**J.B.** and H.B. conceived and designed the project. J.D., M.D.M., A.M.K. and R.P. set up the light-sheet microscope. **J.B.** and E.H. performed imaging experiments. **J.B.** performed graph analysis. B.G. provided MATLAB scripts. **J.B.** and C.N. performed data analysis. **J.B.**, E.H. and H.B. wrote the manuscript.

---

Jessica Burgstaller

---

Prof. Herwig Baier